# CALCIUM PHOSPHATE CEMENT COMPOSITES IN REVISION HIP REPLACEMENT

by

## ANDREW DAVID SPEIRS

B.Sc.E., Queen's University, 1996

A THESIS SUBMITTED IN PARTIAL FULFILMENT OF
THE REQUIREMENTS FOR THE DEGREE OF

MASTER OF APPLIED SCIENCE

in

THE FACULTY OF GRADUATE STUDIES

DEPARTMENT OF MECHANICAL ENGINEERING

We accept this thesis as conforming
to the required standard

THE UNIVERSITY OF BRITISH COLUMBIA

February 2001

© Andrew Speirs, 2001

Department of _MECHANICAL ENGINEERING_

The University of British Columbia
Vancouver, Canada

Date _5 APRIL 2001_

# Abstract

Loosening and failure of hip implants can cause extensive bone loss, and revision of the implant can pose a challenge to the surgeon. Impaction allografting has gained popularity as a method to treat the bone loss. However, significant rates of complications have been seen, including massive subsidence of the implant and perioperative fractures. Subsidence may be due to graft layer consolidation or failure. It is hypothesized that the addition of an interstitial, resorbable cement may improve the clinical outcome of this procedure while reducing the impaction forces and simplifying the surgery. The goal of this thesis was to evaluate the handling characteristics and mechanical properties of a bone particle-cement composite material.

Mixtures of bone particles with a commercially-available calcium phosphate cement were made with 25% to 100% cement by volume. Viscosity of the composite paste was tested in a capillary rheometer to quantify the handling characteristics, and compared to PMMA. Composite cylindrical specimens were moulded and set for 24 hours in a 37°C water bath. Specimens were tested in uniaxial compression, diametral tension and shear. The composites were also tested in confined compression along with 100% bone specimens.

The viscosity of pure cement paste was similar to PMMA, but showed a large increase due to the addition of bone particles. The paste did not flow at bone fractions higher than 25%, so the surgical procedure for these compositions may require hand packing.

Compressive and tensile ultimate strengths were 1.35-2.47MPa and 0.25-0.67MPa, respectively. Compressive modulus increased from 15MPa for 75% bone specimens to 270MPa for 100% cement specimens. There was an associated large decrease in ductility. The confined compression modulus was 6MPa for bone particles and 50MPa for 25% cement. Above 25% cement, the modulus ranged from 163 to 316 MPa.

The composite material showed improved strength and stiffness compared to bone particles alone. Further testing is required with more realistic loading models as well as assessment of the biological characteristics, however results indicate the composite material may be appropriate for use in treating extensive bone loss in revision hip arthroplasty.

# Table of Contents

# List of Tables

# List of Figures

# Acknowledgements

I would first like to thank my thesis committee for their input into the development of this thesis.

Special thanks to my supervisor, Dr. Tom Oxland, who has given me valuable advice and supported me throughout my time at UBC and during my biomechanics career.

The clinical knowledge and input of Drs. Masri and Duncan was greatly appreciated, and helped me maintain some perspective on the overall goals of this research.

I would also like to acknowledge the help I received from various people in the Department of Metals and Materials Engineering, especially Drs. Anoush Poursartip and Göran Fernlund.

Thank you to NSERC and the George W. Bagby Research Fund for their financial support.

# 1.0 Introduction

The purpose of this study was to evaluate the mechanical properties of a potential bioresorbable cement to supplement morsellized allograft bone in revision hip arthroplasty. Aseptic loosening of a hip implant is a common cause of failure, and may lead to massive bone loss in the femur or acetabulum. Revision of the implant in such a scenario can pose a challenge to the surgeon because the bone may be unable to support another implant due to the structural defects. A technique known as impaction allografting makes use of morsellized bone chips, packed into the defects, in an attempt to restore the patient's bone stock. While this has shown some promising results, studies have found significant rates of complications, possibly due to the weakness of the graft layer. The addition of an interstitial cement may provide sufficient strength and stiffness to the graft layer to improve the clinical results of this technique.

## 1.1 Overview of Chapters

The remainder of this chapter gives some general background information on hip implants, failure of hip implants, and what options are available to the surgeon after a failure. The specific hypothesis as well as the scope of this study are outlined at the end of the chapter.

Chapter 2 describes the testing apparatus and protocol used to assess the mechanical characteristics of the composite material. Detailed drawings of the apparatus are in Appendix A.

The results of the tests are given in Chapter 3. Flow tests of the composite material in its handling phase will measure the workability. Standard material properties will be evaluated to determine the effect of bone-cement ratio in uniaxial tests, as well as confined compression.

Chapter 4 discusses the results and implications for clinical use. Problems encountered in testing are also discussed. Failure mechanisms of the composite

material are analysed and compared to similar composite materials such as concrete. Comparison to other experimental and finite element studies is given to assess the suitability of the material for use in revision hip arthroplasty.

Chapter 5 gives conclusions based on the findings of the study, as well as recommendations for future work.

## *1.2 Background*

### 1.2.1 Anatomy and biology

The hip is a ball-and-socket joint: the head of the femur is approximately hemispherical, and articulates with a congruent acetabulum, as shown in Figure 1.1. At the bearing surface is a thin layer of hyaline cartilage, a special tissue adapted to allow smooth articulation under large loads.
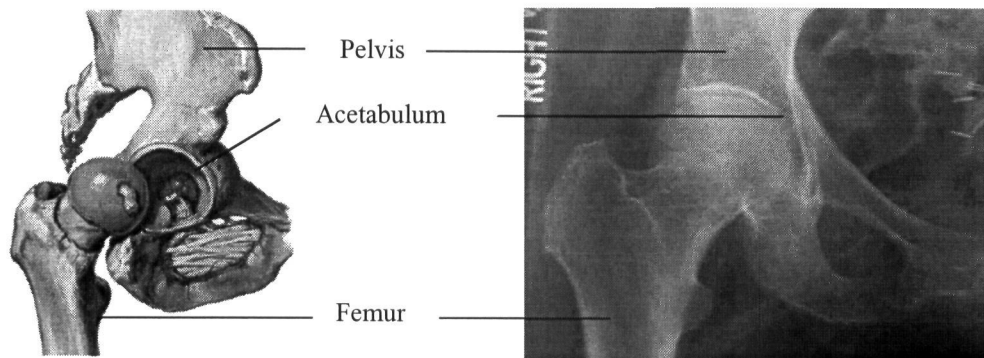


**Figure 1.1:** Anatomy of a hip joint. The diagram on the left shows a lateral view of the hip joint with the femur rotated posteriorly to show the acetabulum; from Netter (1997). On the right is an anterior-posterior radiograph of a hip joint; from Wheeless (2001); used with permission.

The bones of the pelvis consist primarily of highly porous cancellous bone, with a thin shell of denser cortical bone, as shown in Figure 1.2. The femur is a typical long bone, with a hollow cylindrical shaft of hard, dense cortical bone, called the diaphysis. The bone flares towards the ends, where the cortical bone thins, and is filled with porous cancellous bone (see Figure 1.2), a region called the metaphysis. At the end of the bone is the epiphysis, similar in structure to the metaphysis, demarcated by the growth plate. The epiphysis of the femoral head is covered by articular cartilage.
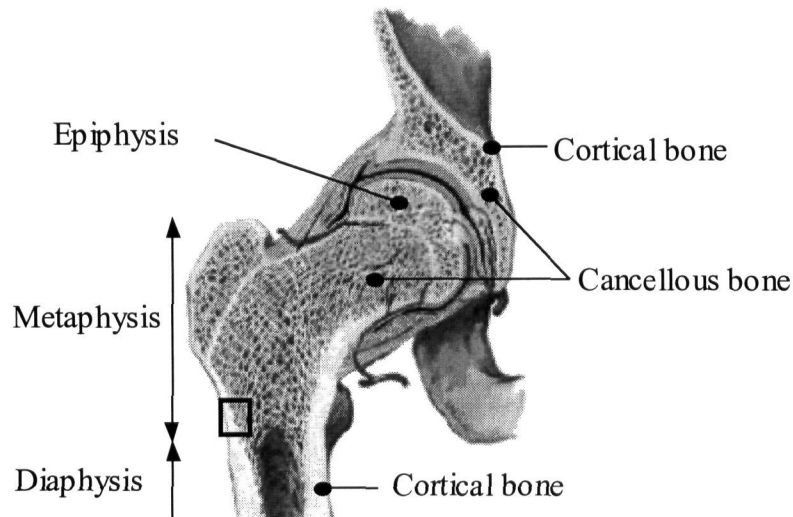
**Figure 1.2:** Coronal-plane cross-section of a hip joint showing the internal structure of the bones. The box is shown enlarged in Figure 1.3. From Netter (1997).

The joint is controlled and stabilized by large muscles crossing the joint, such as the glutei, iliopsoas and adductor muscles. Activity in these muscles can create large loads at the joint surface, as will be described later.

There are two principal types of bone in the hip, cortical and cancellous, also called compact and trabecular, respectively. Figure 1.3 shows a section of bone, with the outer cortical shell on the left, transforming to cancellous bone towards the right. In practice, the main distinction between the two is the porosity, where typically bone of greater than 30% porosity is called trabecular bone. As can also be seen in the figure, cortical bone has an obvious microscopic structure. Concentric lamellae surround a central blood supply, called the Haversian canal. These cylindrical Haversian systems, or osteons, are glued together by interstitial lamellae. The low porosity of cortical bone provides it with its characteristic high strength and stiffness.
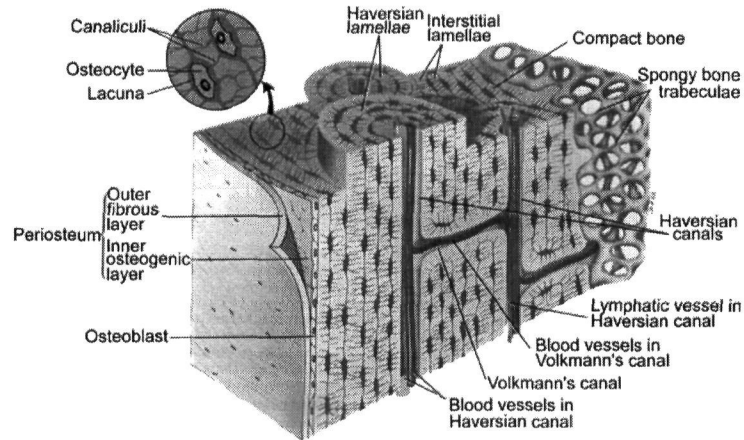
**Figure 1.3:** Structure of bone. Cortical bone (left) is strong, dense bone. Cancellous bone (right) is highly porous and much weaker. From Tartora (1984).

Bone material is comprised of two phases, an organic matrix called osteoid and a mineral phase. Osteoid makes up approximately 50% of bone by volume, and consists of collagen, glycosaminoglycans and glycoproteins. The mineral phase is mostly calcium phosphate in the form of hydroxyapatite [$Ca_{10}(PO_4)_6(OH)_2$] and amorphous calcium phosphate, but also includes calcium carbonate, sodium, magnesium and fluoride.

Unlike most structural materials, bone is 'alive' and can self-repair and adapt to the loads placed on it. It does this through the activity of osteoblast and osteoclast cells, which are specific to bone. Osteoblasts create new bone by laying down osteoid on the surface of old bone or compatible implant materials, which is then infiltrated by the minerals mentioned above. Osteoclasts are responsible for resorbing bone, by attaching to the surface of the bone and creating an acidic microclimate in which bone minerals are soluble, then enzymatically breaking down the organic phase (Teitelbaum, 2000). In addition to these are cells called osteocytes (see Figure 1.3), which are actually dormant osteoblasts found in cavities within the bone. Osteoblastic and osteoclastic activity are regulated by biochemical mediators such as growth factors and cytokines which are produced by various different sources. This is a very active area of research, but is beyond the scope of this thesis. Some aspects of the mediators will be discussed in relation to failure of hip implants and the use of bone grafts and substitutes, below.

## 1.2.2 Mechanical aspects of bone

Cortical bone exhibits slight viscoelastic behaviour, however the two- to three-fold increase in strength and modulus is seen over a six-order-of-magnitude increase in strain rate (Wright, 1976). More importantly, the properties are highly direction-dependent. Cortical bone is generally considered orthotropic, the axis of highest strength and stiffness is aligned with the osteons (the longitudinal direction), which in long bones such as the femur, is approximately aligned with the anatomic axis. The strength is lower in tension than compression, but the elastic modulus is approximately the same. Representative strength and modulus values are shown in Table 1.1 and Table 1.2, respectively.

The material properties of bone also show an age-related decline, approximately 2% per decade between the ages of 25 and 85 (Burstein, 1976).

| Loading Direction | Tension | Compression | Shear |
|---|---|---|---|
| Longitudinal | 133 | 193 | 68 |
| Transverse | 51 | 133 | |

**Table 1.1:** Ultimate strengths (MPa) of femoral cortical bone in various directions. Shear strength was determined from torsion tests about the longitudinal axis. From Reilly (1975).

| Loading Direction | Modulus (GPa) |
|---|---|
| Longitudinal | 17.0 |
| Transverse | 11.5 |
| Shear | 3.3 |

**Table 1.2:** Elastic moduli of femoral cortical bone (GPa). Cortical bone exhibits highest stiffness in the direction parallel to the osteons, which is approximately aligned with the axis of the femur. From Reilly (1975).

In contrast to dense cortical bone, trabecular bone is highly porous, making it much weaker. Trabecular bone has an open pore structure, i.e. the pores are interconnected. Porosity in trabecular bone ranges from 30% to 95%, and has a large influence on the mechanical properties. Apparent density of trabecular bone forms a power law relationship with ultimate strength and modulus, as shown in Figure 1.4. The above

porosities correspond to apparent densities of approximately 1.3 g/cm$^3$ to 0.1 g/cm$^3$, compared to 1.8 g/cm$^3$ for cortical bone. The approximate relationships are:

$$\sigma = 60\rho^2$$

$$E = 2915\rho^3$$

for density in g/cm$^3$, strength in MPa and modulus in GPa (Hayes, 1997).
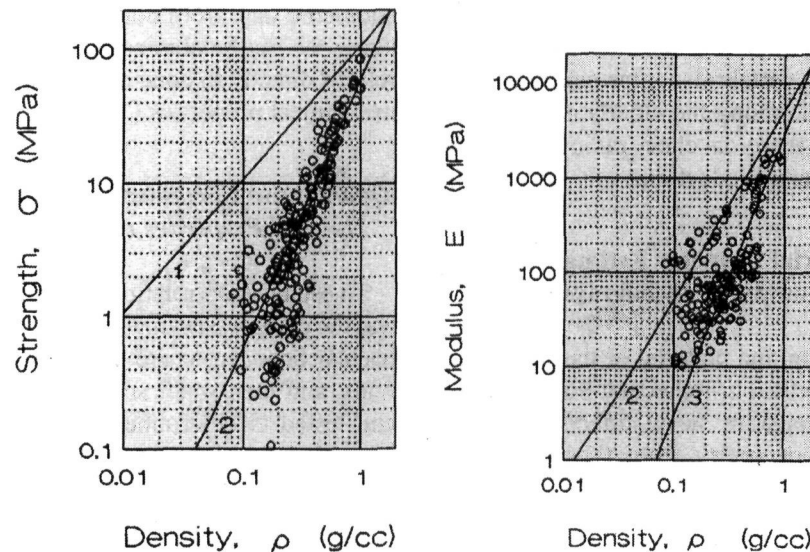


**Figure 1.4:** Material property relationships for trabecular bone. Measurements were made in compression, but tensile behavior is similar. From Hayes (1991); used with permission.

The adaptation of bone to external loads, mentioned above, is loosely referred to as Wolff's Law (Wolff, 1892). The precise mechanism of how external loads affect the activity of bone cells is unknown, however its effects are apparent. Trabecular bone in the proximal femur has an identifiable architecture, and it has been suggested that this architecture mimics the lines of principal strain, as shown in Figure 1.5. If the stress state in the proximal femur is altered, for example in hip deformities or by insertion of a hip implant, the bone will alter its form through osteoclastic resorption followed by osteoblastic bone formation. Silva et al. (1999) showed that in post-mortem-retrieved cemented implants, the decrease in cortical bone mass was correlated with the decrease in bone stress predicted by beam theory. Even under normal, healthy conditions, the bone turns over by the same processes, however osteoblastic and osteoclastic activity are balanced, and bone mass is maintained. In some pathological conditions this state of

equilibrium is disturbed and bone mass increases e.g. osteopetrosis, or decreases e.g. osteoporosis.
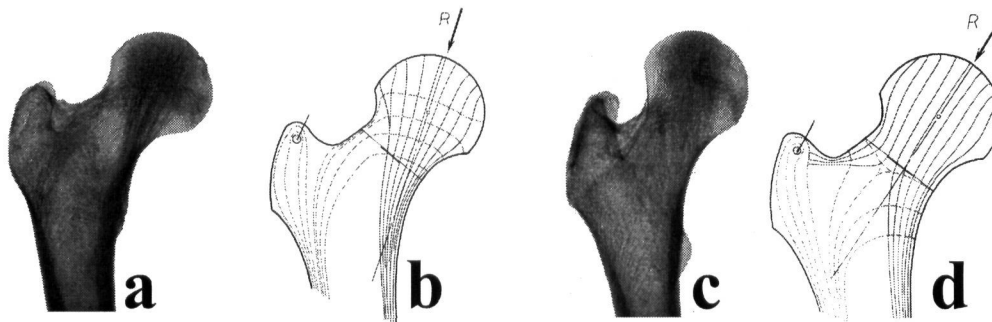


**Figure 1.5:** Inverted radiograph of a normal femur (a). Note the two main bands of trabeculae, and compare to the lines of principal strains (b). The solid and dashed lines are minimum (compression) and maximum (tension) principal strains, respectively. In a valgus deformity (c), the femoral neck is more vertical, creating more compression (d). Note that the trabecular architecture in (c) has changed. From Pauwels (1976); Figures 41 and 42, pp34-5; © Springer-Verlag, 1976; used with permission.

### 1.2.3   Total hip arthroplasty

There are a number of pathological conditions in the hip that are best treated with total hip arthroplasty (THA). By far the most common reason for THA is osteoarthritis, a painful, debilitating condition resulting from the breakdown of the articular cartilage. Osteoarthritis accounts for about 70% of all THA patients (Ritter, 1987). Other indications for THA include rheumatoid arthritis, osteonecrosis and ankylosing spondylitis. The main goal of the operation is immediate pain relief as well as restoration of joint mobility and function. It is widely considered a very successful procedure, especially for short-term relief of pain and restoration of function, and an estimated one million THA procedures are performed per year world-wide (Malchau, 1993).

Total hip arthroplasty involves two components, a stem in the femur and a cup in the acetabulum, shown in Figure 1.6. The head and neck of the femur are removed and a stem is inserted into the reamed canal of the femur, with or without polymethylmethacrylate cement (PMMA). For cemented designs, the stem is made of cobalt-chrome or stainless-steel. In uncemented designs, a titanium alloy stem is press-fit into the femur and relies on bone on-growth for fixation. The acetabular component is usually an ultra-high molecular-weight polyethylene cup that may use a metal backing, and can also be inserted with or without cement. Some designs also make use of all-

metal or all-ceramic bearings, but are less common. So-called hybrid THA consists of a cemented femoral stem with a non-cemented acetabular cup.
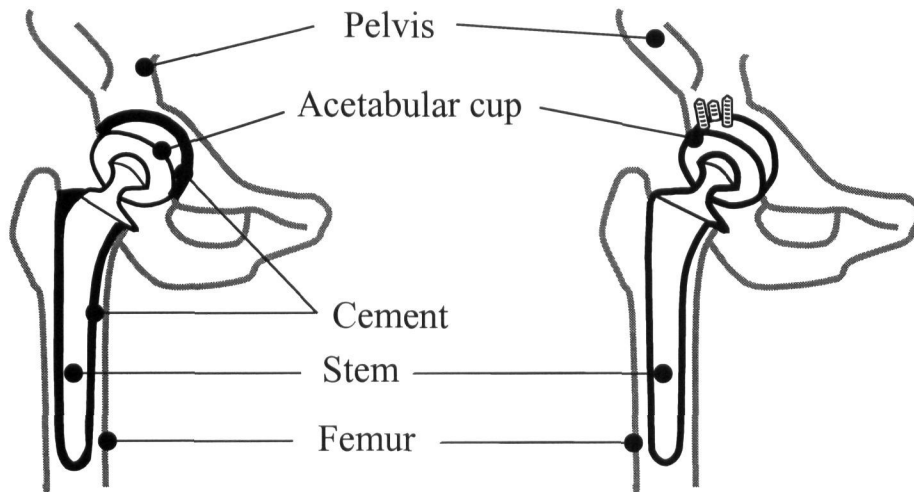


**Figure 1.6:** Components of a hip implant. Cemented designs (left) are typically CoCr or stainless steel stems inserted with acrylic cement. Uncemented designs (right) are usually made from titanium alloy. The acetabular cup is usually polyethylene.

The hip joint, and thus hip implants, are subjected to large loads, even during normal walking. A simplified frontal-plane free-body analysis demonstrates the significant role of the muscles in producing these large loads. Figure 1.7 shows a person in 'one-leg stance', a situation that occurs with each step. The pelvis structure is modelled as a rigid body. The femoral head acts as a fulcrum, with the weight of the torso and unsupported leg balanced by the force of the hip abductor muscles . A simple two-dimensional static analysis, shown in the figure with multiples of body-weight, yields a force on the femoral head of about three-times body weight. Gait studies, which use a ground contact force and measured accelerations of limb segments, modelled as rigid bodies, have also been used to estimate the force at the hip. The resultant joint force is about four to five times the subjects' body-weight (4xBW to 5xBW) for normal walking (Rohrle, 1984; Crowninshield, 1978; Brand, 1986). Femoral stems containing strain gauges in the implant neck have been used to measure the forces and moments by telemetry during daily activities. A peak force of 2.7 to 2.8xBW was measured during normal walking, but can increase to as much as 5.5xBW during fast walking (Bergmann, 1993). Also significant are the high torques measured, a result of anterior- or posterior-directed forces on the femoral head. Peak torque measured during normal walking ranged from 24 Nm

to 40 Nm (Bergmann, 1993), but can double during stair-climbing, and is felt to be a significant factor in loosening of implants (Bergmann, 1995). Hip implants are subjected to these large loads, for approximately one million cycles per year, throughout their service life.



W=0.83xBW

R=3.0xBW

M=2.3xBW
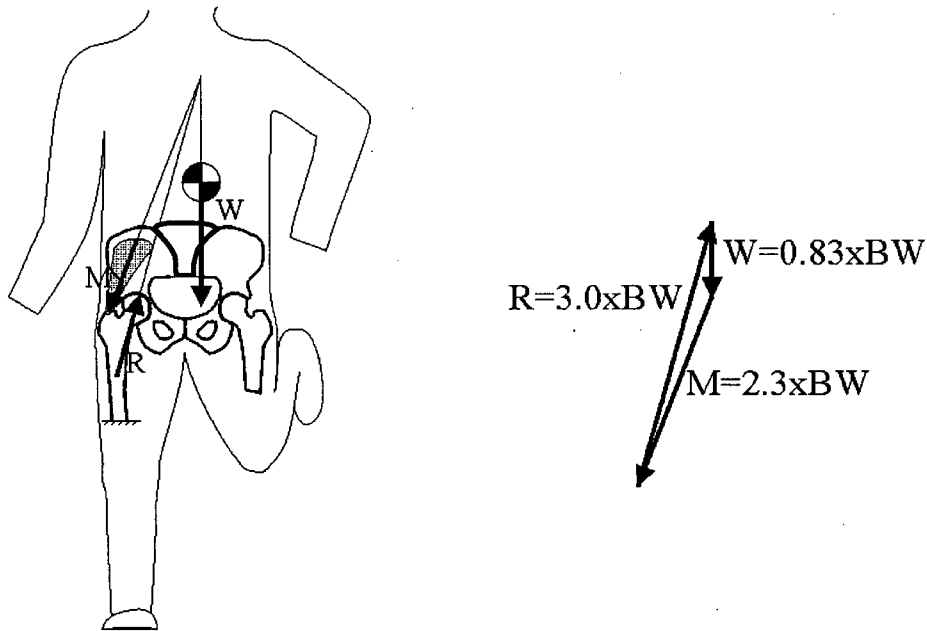
**Figure 1.7:** Hip joint loads during one-leg stance. The femoral head acts as a fulcrum and the pelvis is modeled as a rigid structure. The moment from the torso and unsupported leg (W=0.83xBW) is balanced by the muscle force M, which is large due to the small moment-arm. The two forces M and W are balanced by the joint reaction force, R.

These loads have been incorporated into *in vitro* and finite element models of the implant, femur (Lee, 1993; Manley, 1985; Mann, 1995; Mann, 1997b; Rohlmann, 1983; Verdonschot, 1997a; Verdonschot, 1997b) and acetabulum (Hedia, 2000; Mantell, 1998) to understand the effect of different implant design parameters. Minimum and maximum principal stresses in the cement surrounding the femur are generally reported to be about 10 MPa, depending on interface conditions, stem geometry, cement thickness and many other factors. Stresses in the cement under the acetabular cup are in the same range, although tend to be more compressive. A more detailed review will be given in Section 4.4.2.

Despite these high service demands, THA is considered a successful operation, and may provide good function and pain relief for 20 years or more (Callaghan, 2000). Survival curves of some commonly-used implants are shown in Figure 1.8, which may be

considered 'good' long-term results. Some implants have been introduced to the market that show much higher failure rates (Swedish National Hip Arthroplasty Registry, 2000).

**All diagnosis**
Male Patients of Any Age

**All diagnosis**
Female Patients of Any Age
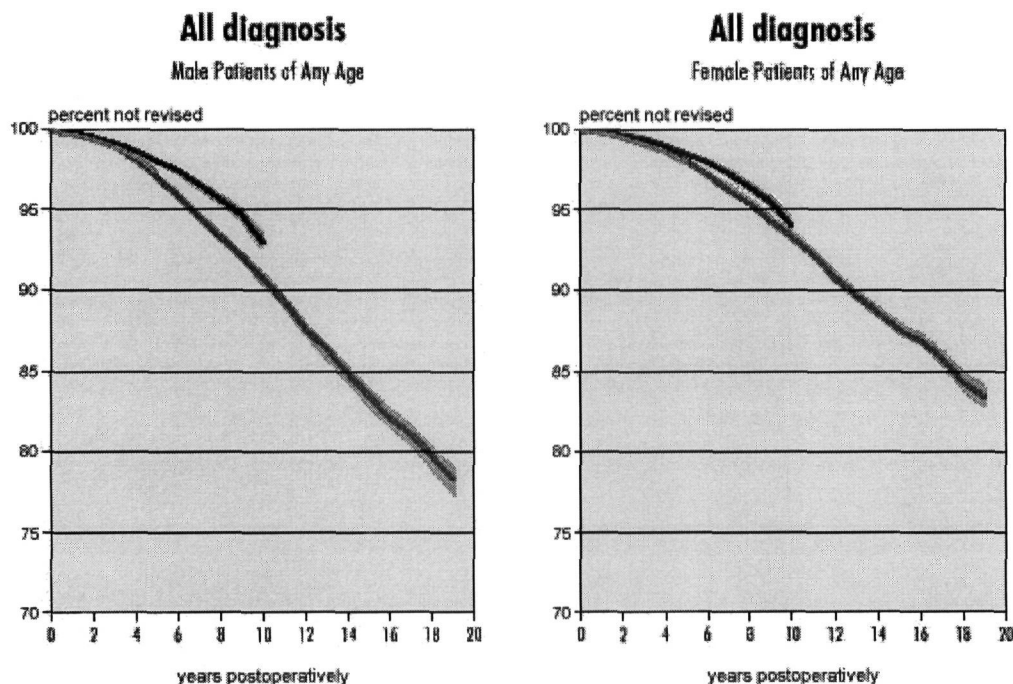


**Figure 1.8:** Survival curves of implants from the Swedish Hip Registry for different time periods. Note that 13-17% of implants have failed after 15 years. From The Swedish National Hip Arthroplasty Registry (2000). The darker line represents the patient series that used a more modern cementing technique.

### 1.2.4 Failure and revision of THA

It has been shown that approximately 13-20% of primary THAs fail after 17 years of service (Swedish National Hip Arthroplasty Registry, 2000). Actual failure rates depend on many factors, including patient age, weight, and activity level, implant design and surgical technique. Aseptic loosening is by far the most common cause of failure, accounting for 76% of all failures (Swedish National Hip Arthroplasty Registry, 2000). Other causes include infection, fracture, dislocation and surgical error, but are much less common. Aseptic loosening is attributed mainly to osteolysis, an inflammatory response to wear or corrosion particles, and to fatigue failure of the acrylic cement or implant interfaces, termed mechanical loosening.

In long-term follow-up studies of commonly-used implants, osteolysis was found to occur in approximately 15% of cemented primary THA (Joshi, 1998; Smith, 1997) and 23% of uncemented primary THA (Learmonth, 1996), although reported rates can vary

widely (Leopold, 1999). Complicating revision surgery following osteolytic loosening is the accompanying loss of bone in the femur.

The process of osteolytic loosening begins with the generation of particles through wear processes or corrosion. Wear particles are most commonly polyethylene from the bearing surface, but may also be PMMA or metallic particles from the implant i.e. titanium alloy, stainless steel or cobalt-chrome. The particles can migrate into the femur or pelvis where they can produce an inflammatory response. Macrophage cells recognise the particles as foreign bodies and attempt to remove them by digestion, termed phagocytosis. This process causes the macrophages to secrete mediators that stimulate osteoclast formation and activation. Research continues into these signalling pathways, but it is believed that the most important mediators are prostaglandine $E_2$ ($PGE_2$), tumour necrosis factor $\alpha$ (TNF-$\alpha$) and the interleukins IL-1 and IL-6 (Archibeck, 2000). The increased osteoclastic activity creates large defects in the periprosthetic tissues, destabilising the implant construct. Examples of failed implants with bone loss can be seen in Figure 1.9.
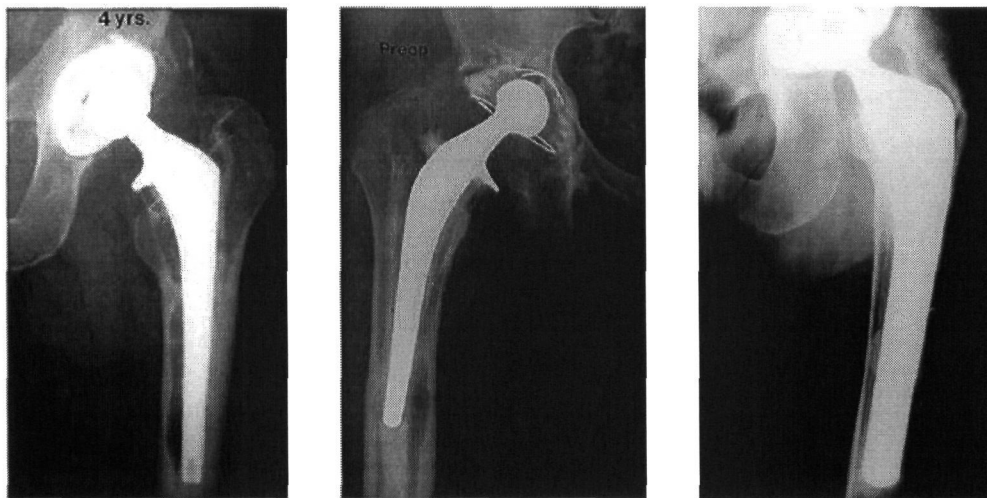


**Figure 1.9:** Examples of osteolytic bone loss. The osteolytic cysts appear as obvious defects around the implant, and the implant becomes loose in the weakened bone. From Livingston et al., J. Bone Joint Surg.Am. 79:1533, 1997; Bourne et al., J. Bone Joint Surg.Am., 80:1777, 1998; and Ragab et al., J. Bone Joint Surg.Am., 81:215, 1999. All figures © The Journal of Bone and Joint Surgery; used with permission.

The degree of biological response to particulate debris depends on the composition, size and concentration of the particles. Not all combinations of materials, particle size and concentration have been studied, but the general trend is that higher concentrations and

larger particles invoke a more severe response. There is a threshold size above which the particles can be considered bulk material and biologically inert, which is in the range of 15 μm, depending on the material. A more detailed review is found elsewhere (Archibeck, 2000).

Osteolysis has been described as an asymptomatic (Learmonth, 1996; Roberson, 1992) and progressive (Learmonth, 1996; Joshi, 1998; Maloney, 1990) condition. The osteolytic lesions grow until the periprosthetic tissues can no longer support the implant and a revision becomes necessary. Care must be taken when removing the implant to minimise additional bone loss, but the bone stock deficiency is often exacerbated by this procedure. In the femur, patterns of bone loss may be erosion of the internal surface of the diaphysis, partial or complete loss of metaphyseal cancellous bone, or a combination of both. In the case of osteolytic loosening with bone loss, the surgeon has several options, such as ordinary cemented revision (Buchholz, 1988; Jasty, 1992), proximal structural graft (Haddad, 2000), and impaction allografting (Eldridge, 1997; Elting, 1995; Gie, 1993; Leopold, 1999; Malkani, 1996; Masterson, 1997a; Masterson, 1997c; Meding, 1997; Nelissen, 1995).

If bone loss is minimal, it can be treated with a straight-forward cemented (Buchholz, 1988) or uncemented (Paprosky, 1999) revision with standard components. However, failure rates of revision implants are typically higher than for primary implants (Kershaw, 1991; Stromberg, 1992), and implant survival decreases with increasing bone loss (Buchholz, 1988; Paprosky, 1999). Failure rates may be as high as 35% after five years for severe cases of bone loss (Buchholz, 1988), and it has been shown that successive revisions show an increasing failure rate (Retpen, 1992). Due to the loss of cancellous bone, the internal surface of the femur in the revision scenario is often smooth and provides a poor surface for cement fixation. Dohmae et al. (1988) found that the cement-bone interface shear strength decreased from primary to revision surgery. Some have advocated the use of uncemented designs, but the remaining endosteal bone may be sclerotic and unable to achieve ingrowth fixation (Paprosky, 1999). Proximal structural grafts have been used on the femoral side to treat massive defects (Haddad, 2000); however, graft incorporation is slow and incomplete (Enneking, 1991), and the surgery is complex.

Impaction allografting is a technique that was introduced to address the problem of bone loss in revision THA. It was first used on the acetabular side for acetabular protrusion (Slooff, 1984), and later to treat bone defects in revision of the femoral component (Gie, 1993).

The technique involves morsellizing allograft bone, usually femoral heads from a bone bank, and impacting the chips into place to rebuild the natural anatomy. The process for the femoral side is shown in Figure 1.10. Ideally this provides a stable graft layer into which an implant can be cemented. The femur is sometimes reinforced with metal mesh, plates or cortical struts with cerclage wires to prevent fracture during the impaction procedure, or to contain the graft particles if the cortical walls have been perforated. This process has gained popularity because it is a biological solution, restoring the patient's bone stock through a creeping substitution of graft with host bone, similar to bone remodelling processes (Schreurs, 1994).
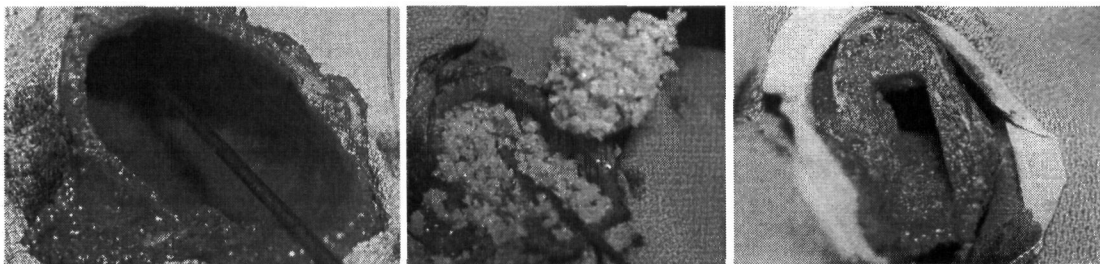


**Figure 1.10:** Impaction grafting procedure. After the loose stem is removed, the femur is merely a thin shell of cortex (left). Morsellized bone is inserted into the cavity (middle), and impacted to form a neo-medullary canal (right). From Mikhail (1998).

The procedure works well on the acetabular side (Schreurs, 1998), and has shown promise on the femoral side (Gie, 1993). Gie et al. expressed "cautious optimism" due to the good clinical results, and were especially encouraged by the apparent graft remodelling and incorporation noted on follow-up x-rays (Gie, 1993). The series reported in this study had relatively minor bone loss, and subsequent studies have failed to reproduce the success of Gie et al., especially if bone loss was more extensive (Eldridge, 1997; Elting, 1995; Masterson, 1997b; Meding, 1997; van Biezen, 2000). A significant rate of complications has been seen in these later studies, including intra-operative or early post-operative femoral fracture, dislocation, and large distal migrations. See Table 1.3 for a summary. Meding et al. expressed concern about the

high rates and unpredictable nature of stem subsidence and about the number of fractures associated with this technique (Meding, 1997).

| Study | Hips | Bone loss | Fractures | Subsidence | Failures |
|---|---|---|---|---|---|
| Gie (1993) | 56 | mild | 3 (5%) | >2 mm: 24<br>>8 mm: 4 | 0 |
| Elting (1995) | 60 | mild | 3 (5%) | >2mm: 10<br>>8mm: 2 | 0 |
| van Biezen (2000) | 21 | severe | 2 (10%) | 1-6mm: 13<br>15-32mm: 4 | 0 |
| Eldridge (1997) | 79 | n/s | n/s | >5mm: 18 | 8 (10%) |
| Masterson (1997b) | 35 | moderate | 6 (17%) | >10mm: 7 | 1 (3%) |
| Meding (1997) | 34 | moderate | 6 (18%) | >4mm: 13 | 2 (6%) |
| Leopold (1999) | 25 | mild | 6 (24%) | >1mm: 2 | 2 (8%) |

**Table 1.3:** Results of femoral component revision with impacted allograft. n/s = not stated; subsidence: number of hips subsiding indicated distance; Failure defined as revision for aseptic loosening. All studies used a polished, collarless, tapered cemented stem except Leopold et al. who used a precoated stem.

The poor results reported by Masterson et al. (1997b) were attributed to undersized impactors which did not create sufficient space for cement between the graft and implant. Massive subsidence, if it occurs, is typically seen in the first year after the operation (van Biezen, 2000; Eldridge, 1997; Meding, 1997). In the study by Eldridge et al. (1997), nine stems subsided more than 10 mm, all within the first three months. Although the number of failures stated are relatively low, the high incidence of subsidence is a concern since the patients may develop pain or abnormal gait, and may be at risk for future failure. The high incidence of perioperative fractures is also troubling, as it often leads to poor clinical results (Meding, 1997).

### 1.2.5 Bone graft and substitutes

#### 1.2.5.1 Mechanics of morsellized graft

In noting the high rate of complications with impaction allografting, Duncan et al. identified a need for "graft layer optimisation" (Duncan, 1998), although they did not

suggest how this may be achieved. High rates of subsidence in the early post-operative period may be due to the low strength and stiffness of the graft layer or consolidation of the bone graft particles. Subsidence rates usually decrease with time, possibly due to the implant settling into an equilibrium position or the bone graft particles being incorporated into the host bone structure. Some work has been done to characterise the mechanical properties of the morsellized graft alone or within an *in vitro* revision implant structure.

Brewster et al. studied the shear characteristics of morsellized bone using soil mechanics theory (Brewster, 1999). Soil mechanics defines two important parameters to define the resistance to shear: cohesion, (c), and the angle of internal friction ($\phi$). Cohesion is determined by the interlocking of particles, and is low for friable aggregates such as morsellized bone. Once the particles break, resistance to shear is purely by friction, and thus depends on any normal stress. The relationship between shear strength, cohesion, internal friction and applied normal stress is given by the Mohr-Coulomb equation $\tau = c + \sigma\tan\phi$, which is also the failure envelope in the Coulomb-Mohr failure theory (Craig, 1993). The study found a cohesion coefficient of 6 kPa and angle of internal friction of 38°. They also found that after impaction of the particle specimens, the peak shear stress increased by approximately 35% compared to unimpacted specimens at the same strain level; doubling this 'impaction energy' could increase the peak shear stress a further 15%. The corollary to this is that under a given load (the *in vivo* situation may be considered under 'load control'), the impacted graft will deform less than unimpacted graft. As this test may be similar to the *in vivo* stress state i.e. both shear and compressive loads on the graft layer, the results suggest that failure of the implant by graft-layer subsidence may be due to the quality of the packing.

Brewster et al. (1999) hypothesized that graft layer shear strength could be improved by achieving an 'optimal' grading of particle sizes. The optimal grading may be defined by Fuller's curve, which achieves the highest theoretical packing density for spherical particles:

$$p = 100\left(\frac{d}{D}\right)^{0.5} \tag{1.1}$$

Where $p$ is the percent of particles finer than size $d$, with maximum particle size $D$. This may be modified to a log-linear grading for irregular particles, which is a straight line on

a $p$ vs. log($d$) chart between the maximum and minimum sizes (Brewster, 1999). Brewster et al. (1999) achieved optimal grading by adding small bioactive glass spheres. There was only a small change in shear resistance for unimpacted specimens, however impacted specimens showed improved shear resistance when the bioactive glass was added. However, as noted in clinical studies, the femur may be too weak to withstand the impaction forces required for optimal packing, and intra-operative or early post-operative fractures may result (Meding, 1997).

Brodt et al. also identified limitations in the mechanical properties of morsellized graft in multiaxial compression testing (Brodt, 1998). Specimens exhibited bilinear behaviour, with an initial modulus ranging from 52 to 152 MPa, depending on the confining pressure, which dropped to less than 6 MPa at higher deformations. The initial stiffness was due to interlocking of the irregularly shaped bone particles. As the load increased the particles began to break, reducing the interlocking and allowing the particles to slip relative to each other, resulting in a reduced stiffness. The transition occurred at 0.17 to 0.27MPa of axial compressive stress.

Other approaches to characterising morsellized graft have used biphasic theory (viscoelastic) and porous material theory. Giesen et al. (1999) and Voor et al. (2000) suggested that time-dependent deformation of the morsellized graft is responsible for implant subsidence. In confined compression tests, deformation of the graft material occurred due to both fluid (fat and water) exudation under load, as well as movement of the solid particles. This implies that immediate post-operative subsidence could be due to outflow of marrow and water under the loads imposed by walking. Continued subsidence, although slower, could occur due to particles rolling and sliding past each other, and would only cease if and when graft incorporation occurred. Voor et al. (2000) found that reducing the moisture content of the graft allowed better packing, resulting in lower fluid-constrained and solid phase strains. In a similar approach, Verdonschot et al. (2000) showed that morsellized graft undergoes unrecoverable deformation when subjected to dynamic loads in confined compression. Figure 1.11 shows the strain of the graft during dynamic loading (0 to 900s) and unloaded (900 to 1800s) periods. If the dynamic loads are considered an extension of the impaction procedure, the effect of the amount of compaction is apparent. In Figure 1.11, point A would represent the behaviour

16

of a specimen with only minor impaction. Once the loading begins, an immediate large deformation of the material occurs, resulting in implant subsidence. If the graft is moderately packed (point B) the initial consolidation would be less, resulting in less overall subsidence. Further impaction would produce a specimen at point C that is closer to equilibrium for the given load. Obviously optimal packing would minimise initial subsidence and result in less unrecoverable strain. This graft consolidation mechanism is also illustrated by the large difference between the modulus reported by Giesen et al. (1999), who used preconditioning cycles, and Voor et al. (2000), who did not, and therefore measured a much lower confined compression modulus. The implications are, again, that subsidence of the implant is dependent on the quality of packing. This would mean that graft-layer consolidation, and therefore implant subsidence, would be mainly seen in the early post-operative period, before the graft can be incorporated into the structure of the bone. In fact, if large subsidence does occur, it is usually in this period (Eldridge, 1997; Meding, 1997; van Biezen, 2000)
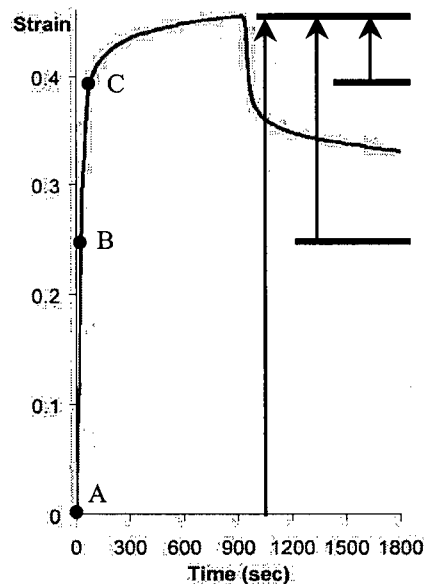


**Figure 1.11:** Consolidation of graft particles in cyclic confined compression testing results in unrecoverable strain. Specimens were loaded cyclically for 900s and allowed to recover for 900s. Cyclic loading results in packing of the graft, so that increasing the initial impaction (points A to C) would be expected to reduce initial subsidence and unrecoverable strain. The initial subsidence for each specimen is indicated by the arrows. From Verdonschot (2000).

Studies using *in vitro* models of revision hip surgery support the claim that the graft layer may be unable to prevent subsidence of the implant (Schreurs, 1994; Berzins, 1996;

Malkani, 1996). Using a stereo x-ray technique, Schreurs (1994) showed that slippage and compaction of the graft allowed the implant to subside into the femur. After step loading to 800N, the cemented stems with impacted graft had subsided 0.5 mm compared to 2.9 mm seen with uncemented stems with impacted graft. The lower migrations with cemented stems may be due to penetration of the PMMA into the morsellized bone, helping to stabilise the graft layer. The loading in this study was quasistatic, however, so more migration would be expected under physiologic cyclic loading. Berzins et al. (1996) studied the motions of cemented and uncemented stems with impacted allograft, as well as primary cemented THA, under cyclic loading. The loads were high (5xBW), representing stair climbing, and only applied for 60 cycles. For implants with impacted allograft, cemented stem subsidence was 22 µm compared to 451 µm for uncemented stems; primary cemented stems subsided only 3 µm. Malkani et al. (1996) found that primary cemented implants subside less over the first 5000 cycles compared to revision cemented implants with impacted graft. Much of this subsidence occurred during the first five cycles. There was no significant difference in failure torques between the primary and revision implants, although the difference may have been obscured by the large standard deviations and low number of specimens. These studies illustrate that the *in vitro* performance of simulated revision cemented implants with impacted graft is considerably poorer than primary cemented stems.

Incomplete remodelling of the graft layer may also be responsible for failure of the revision implant, although over the longer term. Nelissen et al. (1995) performed a biopsy of the graft layer one to two years after revision surgery. They identified three zones: an outer layer of viable cortical bone, a middle layer of viable trabecular bone with few cement particles, and an inner layer of little viable trabecular bone with fibrous tissue, necrotic bone (unremodelled graft) and cement. Similarly, Johnson et al. (1996) found that new bone showed limited penetration into graft materials in the absence of osteoinductive materials. These findings suggest that the remodelling process may not be able to penetrate the full thickness of the graft layer, leaving dead bone tissue adjacent to the implant and making the patient vulnerable to failure. Furthermore, in an animal model, Tägil et al. (2000) found that impaction delayed incorporation of morsellized bone graft.

Evidently, further work is required to improve the stability of the revision implant construct by modifying the graft layer, as stated by Duncan et al. (1998).

### 1.2.5.2 Bone graft substitutes

It is possible that this graft layer optimisation may be achieved by the use of bone graft substitutes. The role of bone graft materials is to form a scaffold into which new bone can grow, while providing structural support if necessary. The 'gold standard' for bone graft material is autologous bone, also known as autograft (Goldberg, 1987; Bauer, 2000). Autograft serves as a good scaffold and can also induce new bone formation due to the presence of osteoblastic and osteoclastic mediators, as well as form new bone directly if the contained cells survive the operation. However, the quantity of tissue available is limited and the extra surgical procedure may cause pain and inhibit patient recovery. Allograft is available in larger quantities from bone banking, but its use may add significant costs to a revision procedure (Barrack, 1999), and quantities are limited. Incorporation of allograft into the host bone is slower and the tissue may invoke local or systemic immune responses that interfere with the incorporation process (Goldberg, 1987). Allograft has also been shown to induce a cellular immune response due to mismatched donor antigens, leading to rejection of the graft (Dijkers, 1999), although the clinical significance is unknown, but probably minor. The shortcomings of using bone as a graft material has led to much effort being applied in the development of bone graft substitutes that can be incorporated/remodelled as well as autograft and are more readily available than allograft.

It is important to define two terms when discussing incorporation/remodelling of bone grafts and substitutes: osteoinduction and osteoconduction. The former refers to the biological stimulation of bone formation by inducing local or transplanted osteogenic precursor cells to differentiate into osteoblasts, leading to bone formation. Osteoconductive materials promote bone apposition directly to their surface, and serve as a passive scaffold for bone formation. A third term, osteogenic, refers to a material containing viable cells that can form new bone, but is applicable only to fresh, vascularized autograft or grafts and implants containing cell cultures specifically for that purpose.

Bone graft substitutes may be derived from natural materials e.g. demineralized bone matrix, bovine collagen mineral composites and processed coralline hydroxyapatite, or they may be completely synthetic, typically based on ceramics or polymers. Of the synthetic bone graft substitutes, the most active area of research and development is in the area of calcium-phosphate-based materials, although calcium sulphate, bioactive glasses and polymer-matrix materials are also being examined. Some of the natural materials may have some osteoinductive potential, but the majority of bone graft substitutes are osteoconductive only. The following is a brief review of the most common bone graft substitute materials, but is not exhaustive.

**Demineralized bone matrix**

Demineralized human bone matrix (DBM) is simply bone processed to remove all of the mineral phase, leaving the osteoid. The remaining material is "rubber-like" when set, lacking stiffness and strength in compression (Ladd, 1999). It was first available as a gel (Grafton, Osteotech Inc, Eatontown NJ), but other manufacturers have recently released similar products. DBM is osteoinductive, (Urist, 1967) due to the presence of proteins in the matrix. The osteoinductive potential of each commercially available batch of DBM can be measured using a commercially available assay.

**Bovine collagen**

Bovine collagen is available commercially (Collagraft, Zimmer Inc, Warsaw, IN) as granules, which also contain hydroxyapatite and tricalcium phosphate minerals. On its own it is osteoconductive, but is meant to be used with aspirated autologous bone marrow, which makes the mixture osteoinductive. The manufacturer claims it offers no structural support, and one study suggested it evokes an immune response due to the presence of bovine collagen-specific antibodies (Chapman, 1997).

**Coralline Hydroxyapatite**

Materials derived from coral have been used as granules or blocks. Naturally occurring coral is largely calcium carbonate, which can be processed to convert a thin layer on the surface to osteoconductive calcium phosphate e.g. ProOsteon, Interpore Cross

International. The material is highly porous, resembling cancellous bone, and in its bulk form offers high compressive strength (Martin, 1989). However, the mechanism and time of resorption are not well characterised, and it may not undergo osteoclastic resorption (Jensen, 1996).

## Calcium Sulphate

Calcium sulphate, better known as Plaster of Paris, is a biocompatible, osteoconductive material that has long been used for treating bone defects (Peltier, 1959). However, using it as a paste can produce variable results because the setting proceeds randomly, producing crystals of variable size and shape with many defects in the crystal structure (Tay, 1999). A commercially available form of calcium sulphate is OsteoSet (Wright Medical Technology) in which pellets are produced in a strictly controlled environment, resulting in a more uniform, crystalline material that is less soluble and slower to resorb (Tay, 1999).

## Bioactive Glass

Bioactive glasses have been introduced to promote implant-tissue bonding (Hench, 1998). They are composed of $MgO$-$CaO$-$SiO_2$-$P_2O_5$-$CaF_2$ glass or glass ceramic, or closely related materials that form a biologically active hydroxycarbonate apatite surface layer *in vivo*. This surface layer can form direct bonds with bone, and it has been suggested that these materials may also be osteoinductive (Hench, 1998), which may be due to bonding of osteoinductive signal proteins to the surface layer (Ladd, 1999). Use of Bioglass® particles in a rabbit femoral defect model showed faster trabecular bone regeneration than similar hydroxyapatite particles (Oonishi, 1997). MgO-free glass has been shown to be at least partially resorbable, however the material was developed primarily for incorporation into a polymer matrix to replace PMMA, and is not resorbable. Tamura et al. (1997) showed that a composite cement consisting of the bioactive glass powder and bisphenol-a-glycidyl methacrylate (BIS-GMA) has superior material properties compared to PMMA. More importantly, however, is the bone-bonding ability of the cement due to the presence of the bioactive glass. Following 25 weeks *in vivo*, tensile failure loads of the bone-bioactive cement interface were two-

orders-of-magnitude higher than for the bone-PMMA interface. Additionally, some specimens containing PMMA contained an intervening fibrous tissue layer which has also been noted in revision surgery (Elting, 1995; Meding, 1997; Nelissen, 1995), but was absent in the bioactive cement specimens.

**Calcium Phosphate**

There are many calcium phosphate-materials either on the market or under development. Synthetic materials based on calcium phosphate ceramics generally mimic natural bone mineral and are well tolerated (Johnson, 1996). They are typically not passively resorbable (Driessens, 1995), requiring osteoclastic activity to break down, although for some forms of calcium phosphate even this is insufficient. Materials reported in the literature include monocalcium phosphate, dicalcium phosphate dihydrate, tricalcium phosphate, tetracalcium phosphate, octocalcium phosphate, calcium deficient hydroxyapatite, hydroxyapatite, amorphous calcium phosphate, carbonated hydroxyapatite (dahllite), as well as mixtures of the above (Driessens, 1995; Frankenburg, 1998; Hamanishi, 1996; Ikenaga, 1998; Ishikawa, 1999; Knaack, 1998; Knabe, 2000). Many of these materials show some phase transformation to bone mineral-like apatite (Driessens, 1995). Driessens et al. (1995) found the compressive strength of selected calcium phosphates to range from 4 to 40 MPa and diametral tensile strengths of 1 to 8 MPa.

The most common forms under investigation are tricalcium phosphate ($Ca_3[PO4]_2$) and hydroxyapatite ($Ca_{10}[PO4]_6[OH]_2$). Bone attaches to these materials *in vivo* through a strong bond (Johnson, 1996), then ingrowth may occur if the surface pores are at least 100-150 $\mu$m or osteoclasts can resorb the material (Johnson, 1996).

Many of the commercially available forms of calcium phosphate materials are particulates or porous blocks (Ladd, 1999), however some cements have also been developed. These calcium phosphate cements are osteoconductive and show a range of resorption characteristics, but they also simplify the surgical technique, allowing the material to be shaped for the specific purpose. Table 1.4 shows the characteristics of three commercially available calcium phosphate cements, as reported by the manufacturers.

| Material | Composition (set) | Compressive Strength (MPa) | Resorbable | Working time |
|---|---|---|---|---|
| Bone Source | HA | 36 | possibly | 10 minutes |
| SRS, Norian | carbonated apatite | 55 | >78 wks in dogs | 10 minutes |
| α-BSM, Etex | amorphous CaP | 10 | 14 wks in dogs | 20 minutes* |

**Table 1.4:** Selected properties of FDA-approved calcium phosphate cements. *Note: setting time in 37°C environment; the cement does not set appreciably for one day at room temperature.

The first commercially-available calcium phosphate-based cement is marketed as BoneSource (Howmedica). It is a mixture of tetracalcium phosphate (TTCP) and dicalcium phosphate dihydrate (DCPD), which sets to form hydroxyapatite. It was originally thought to be non-resorbable, but more recent work indicated that it may be partially resorbable (Driessens, 1995).

A carbonated hydroxyapatite, SRS, Norian Corp., was introduced because it showed better resorption characteristics. SRS implanted in canine tibial metaphyseal defects was only approximately 50% resorbed after 78 weeks (Frankenburg, 1998). Histological examinations revealed osteoclastic resorption with associated osteoblastic new bone formation, indicating that the material is remodelled in the same process as natural bone. The torsional strength of the bone-SRS composite returned to 100% of intact contra-lateral controls within eight weeks. Incorporation of graft and restoration of mechanical properties of the tibia was slightly faster for allograft bone, although differences were not significant.

The most recent calcium phosphate cement to be introduced to the market is α-BSM from Etex Corp. The material is mixed to form a paste and undergoes an endothermic reaction *in vivo* to form an amorphous non-carbonated apatite. X-ray diffraction patterns indicate a strong similarity between the final set material and bone (Knaack, 1998). Canine femoral slot defects filled with α-BSM showed restored normal bone morphology with less than 4% remaining cement after only four weeks (Knaack, 1998). Dogs that received autograft bone showed more new bone formation in the first four weeks, although differences disappeared after 12 weeks. The remodelling rate of α-BSM

appears to be much faster than that of SRS, but age and breed of the dogs and defect size and location may account for some of the difference. It should be noted that all strengths reported above are those from the manufacturer, and have not been independently verified.

Use of a calcium phosphate cement for filling bone defects has many advantages over particulates or porous-solid blocks. The cement can be injected to easily fill a defect of any size and shape, and the mechanical strength and stiffness of the final set material is expected to be superior to that of particulates.

## 1.3   Hypothesis

Impaction allografting has shown potential for treatment of bone loss in the revision hip scenario. However, high rates of complications have been shown. Studies of morsellized allograft suggest that the mechanical properties of the graft layer may be insufficient to support an implant. Thus there is a need to improve the strength and stiffness of the graft layer. The general hypothesis of this research is that the allograft layer may be improved by the addition of synthetic materials, specifically resorbable cements. The objective of this thesis is to evaluate the effects on the handling and mechanical properties of adding different amounts of cement to the allograft particles. Handling characteristics will be quantified by flow tests in a capillary rheometer. Mechanical properties will be evaluated by standard material properties in uniaxial compression, tension and shear, as well as confined compression.

## 1.4   Scope

There are three requirements that must be considered for the composite material: it must be able to withstand in vivo stresses and support the implant during the remodelling process by providing adequate strength and stiffness; it must be moldable/injectable such that the surgeon can easily implant it into the bone defects; and it must be resorbable in the same manner that bone tissue is resorbable, such that it does not significantly impede remodelling of the graft layer.

This thesis is primarily concerned with the mechanical properties of the graft (consideration #1), and will also evaluate the handling characteristics (#2). Biological characteristics of the composite material is beyond the scope of this thesis.

The goal of this study is to evaluate the effect on the mechanical properties of adding different amounts of calcium phosphate cement to morsellized allograft. The first two requirements will be addressed by measuring the flow characteristics of the composite during the working phase, and determining standard material properties of the set composite. Although the biological properties (the third requirement) of the composite material are important for clinical success, they will not be evaluated in this study, but remain as future work.

# 2.0 Materials and Methods

## 2.1 Specimen Preparation

Fresh-frozen human cadaveric femurs were obtained and allowed to thaw. Specimen details are given in Table 2.1. Donors generally had no known skeletal pathologies, although in a separate study osteoporosis was noted in the vertebrae of donors 1012, 1017 and 1021 based on bone mineral density from DEXA scans (Grant, 2000). Vertebrae from donors 1008 and 1018 were also used in the same study, but had normal bone mineral density. Donor 1018 was known to have been a smoker. Visual analysis of x-rays did not reveal any abnormalities.

| Donor | Gender | Age | Weight (kg) | Height (cm) | Cause of Death |
|-------|--------|-----|-------------|-------------|----------------|
| 1001-R | M | | | -unknown- | |
| 1005-L | M | 70 | 70 | 170 | -unknown- |
| 1008-RL | F | 58 | 52 | 163 | End stage liver disease |
| 1012-R | M | 62 | 54 | 168 | Liver cancer (metastasis) |
| 1017-R | M | 84 | 59 | 191 | Alzheimers |
| 1018-RL | F | 72 | 54 | 157 | Leukemia |
| 1021-R | M | 90 | 70 | 170 | Myocardial infarction |
| 1025-L | M | | | -unknown- | |

**Table 2.1:** Details of donors of femurs used in this thesis. Mean age was 73 years (range 58 - 90). In the donor column, R and L indicate side of femur; note that both femurs were used from two donors.

All soft tissues, except for the articular cartilage, were removed, and the head resected at the head-neck junction. The heads were then cut into pieces approximately 15 x 15 x 40 mm, and morsellized in a pneumatic bone mill (Depuy, Warsaw, IN), shown in Figure 2.1. The chips were passed through the mill a second time using a finer blade. The bone chips were placed in acetone for 72 hours to remove the fat and marrow; the acetone was changed once, after the first 24 hours. After removal from the acetone, the bone chips were rinsed in alcohol then distilled water. A sample of the cleaned and dried particles is shown in Figure 2.2.

**Figure 2.1:** Pneumatic bone mill used to morsellize the femoral heads. The course blade is mounted and the fine blade is shown below the mill.
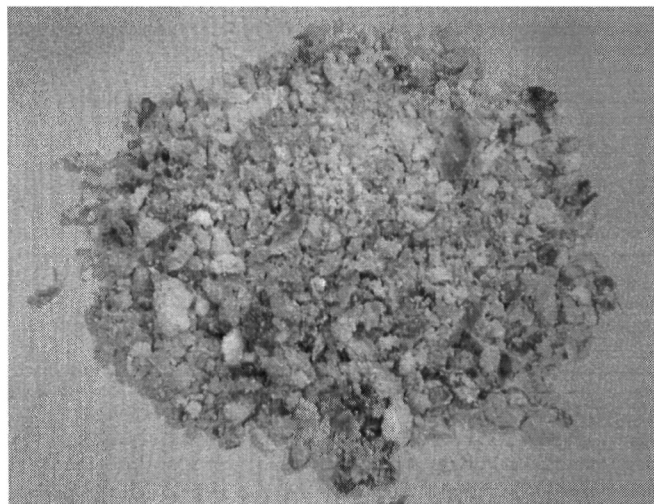


**Figure 2.2:** Morsellized bone from three femoral heads. Bone chips have been defatted, cleaned and dried.

To characterise the bone chips, particle size distribution was determined by sieve analysis. The bone chips were passed through sieves with successively smaller pores, using mesh sizes 5, 6, 8, 10, 18, and 30 (Fisher Scientific, Nepean, ON). The sieves were shaken by hand for three minutes which resulted in minimal further passage of the particles through the sieves. Particles that passed through the #30 mesh and particles that did not pass through the #5 mesh were discarded, to give particles ranging in size from 4.00 mm to 600 μm. The contents of each sieve were weighed to determine the weight-

proportion of each particle size. The chips were then recombined for later use with the calcium phosphate cement.

The calcium phosphate cement, α-BSM (Etex Corp., Boston, MA), was prepared according to the manufacturer's instructions. The product is supplied as a powder of amorphous calcium phosphate, which is mixed with saline solution in a mixing bulb (see Figure 2.3). The powder was mixed with 0.9% unbuffered NaCl solution in the ratio 0.8 mL saline per gram of powder. The powder was weighed on an analytical balance (Model AB-104, Mettler-Toledo Inc., Columbus OH; resolution: 0.1mg). It was determined that 10.75g of powder resulted in $10.86cm^3$ of final, set material (four complete cylindrical specimens). Saline was measured in a micropipette (Model 5000DG-1000, Nichiryo America Inc., Flanders NJ; resolution: 1 μL). Mixing was done in a bulb by kneading by hand for 90 seconds to create a paste. For specimens containing bone graft, the particles were mixed with the powder before adding the saline solution, and the same saline:powder ratio was used throughout. Mixtures of 75%, 50%, 25% and 0% bone, by volume, were prepared[1]. Bone particle volume was measured by water displacement in a 10 mL graduated cylinder with 2 mL graduations. Each batch of 10.86cc was prepared adjusting bone particle and cement proportions to give the desired bone volume fraction.
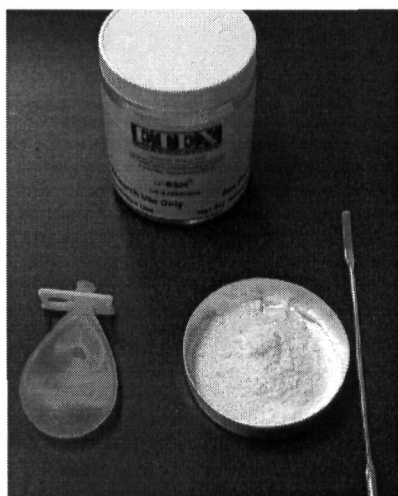


**Figure 2.3:** Calcium phosphate from Etex Corp. The powder (lower-right) is mixed by hand with 0.9% saline in the bulb shown (lower-left).

---

[1] Throughout this thesis, all references to bone and cement fractions in the composite material are by volume.

## 2.2 Experimental Apparatus

### 2.2.1 Viscosity Measurement

A capillary rheometer, similar to that used by Liu et al. (1987), was machined from aluminum stock, and can be seen in Figure 2.4. The reservoir was 24.90mm dia. *x* 24.90mm deep; the capillary was 9.50mm dia. *x* 55.25mm long. The plunger, shown to the left of the rheometer in Figure 2.4, was machined from aluminum bar stock to 24.86mm, allowing sufficient clearance in the reservoir for easy sliding but preventing significant backflow. The plunger face was milled to a smooth, flat surface. Design drawings can be found in Appendix A.
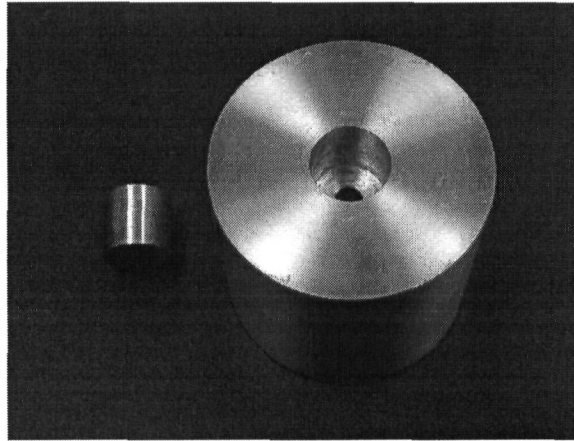


**Figure 2.4:** Capillary rheometer used for measuring viscosity. The bore is 25mm dia. x 25mm deep. The capillary is 9.5mm dia. x 55mm long. The plunger is shown to the left.

### 2.2.2 Material Properties Measurement

**Specimen Moulds**

Eight cylindrical moulds, 12mm dia. *x* 24mm long, were machined from two aluminum plates clamped together, as shown in Figure 2.5. This allowed the moulds to be parted after the specimens had set. The final inside surface of each mould was machined with a boring bar to achieve a good finish, allowing easy specimen removal. A specimen holder and clamp were made from Delrin® and aluminum channel, respectively, and are also shown in Figure 2.5.
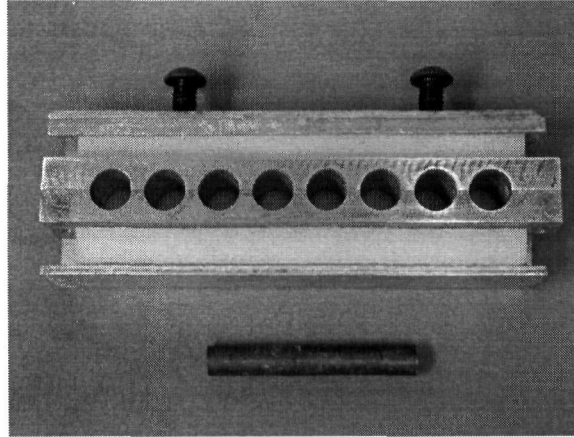
**Figure 2.5:** Moulds used to create specimens. Moulds were drilled from aluminum plate, and clamped together with a Delrin and aluminum clamp. The rod shown below was used for packing the material into the moulds.

## Water Bath

A water bath (Serological Bath, Fisher Scientific Ltd., Nepean ON) was used for the setting environment of the specimens. The bath was set to 37°C and was monitored periodically with a standard pool thermometer (generic; range –20° to +50°C, 2° increments).

## Platens

Two platens were fabricated for compression testing. The lower platen was machined from 1" aluminum bar. The testing surface was first milled with a standard end mill, then ground and polished with an Exakt Micro Grinding System (Exakt 400CS, Exakt Technologies, Inc., OK, USA). Final polishing was performed with 2000-grit polish paper. Two flat surfaces were milled on the side at the opposite end to allow clamping in a vice. The upper platen was made from aluminum plate and milled to 1" square. The testing surface was milled, ground and polished in the same method as for the lower platen. A small indentation was drilled in the middle of the opposite side to allow seating of a 3/8" ceramic ball. See Figure 2.6 for the test setup.

## Materials Testing Machine

All testing was performed on a biaxial materials testing machine (Instron 8874, Instron Corporation, Canton, MA). The Instron controller was connected to a PC by a general

purpose interface bus. Instron-supplied software, FastTrak Console and SAX, were used to control each test. All data was acquired by the Instron controller using a 12-bit data acquisition card, sampled at 50 Hz.

Force measurements were made using a biaxial load cell (Model 211-113, SensorData Technologies Inc., Sterling Heights, MI; serial number 97533). Original calibration showed that accuracy of the load cell was less than 0.1% of rated output (certified by Instron, 27/11/98). Application of a 75N dead-weight indicated the calibration was valid. A shunt calibration was performed at the beginning of each day, and the load cell output was balanced before each test.

Displacement measurements were made using the Instron-supplied LVDT ($\pm$50mm; serial number 0291). The LVDT calibration was verified with a Vernier calliper; positions agreed within 0.3mm over a range of 62mm.

## 2.3 Experimental Methods

### 2.3.1 Viscosity Measurement

The handling characteristics of the composite material as a paste were quantified by the viscosity determined in a flow test. Flow tests were carried out according to Liu et al. (1987) using the capillary rheometer and plunger described above, shown in Figure 2.4.

The test is based on ASTM Standard F451, a test standard for acrylic bone cements. The portion of the standard related to flow is based on ASTM Standard D3835, a flow test specification for thermoplastics. Liu et al. (1987) did not follow the standard exactly since the reservoir:capillary diameter was 2.6, slightly below the range of 3 to 15 specified in ASTM Standard D3835. Corrections are required for ratios above the specified range due to irregular flow into the capillary (Tordella, 1957), but ratios at the low end and slightly below the range specified should give reasonable uncorrected results. A paste of the composite material, with 75%, 50%, 25% or 0% bone particles by volume, was prepared as described above, and packed into the reservoir for immediate testing.

Traditional bone cement, polymethylmethacrylate (Simplex P, Howmedica International Inc., Ireland), was also tested for comparison. One 20 mL ampoule of liquid monomer was added to the 40g package of powder and stirred by hand for 90 seconds at

approximately 2 revolutions per second. The dough was poured into the reservoir, and the test began at 135 seconds after the start of mixing. Two samples of PMMA were tested.

The plunger was placed in the reservoir on top of the paste, and force was applied until paste emerged from the bottom before the test began. The plunger was then moved at 0.3 mm/s until it reached the bottom of the reservoir. This gave a shear rate of $4Q/\pi r^3 = 0.25$ $s^{-1}$. The viscosity was calculated at 5 second intervals throughout the test, according to the formula:

$$\mu = \frac{Fr^4 t}{8R^2 LV} \tag{2.1}$$

where $F$ is the measured force, $R$ and $r$ are the radius of the reservoir and capillary, respectively, $t$ is the time interval, $L$ is the length of the capillary and $V$ is the volume extruded from the capillary in time $t$. The extruded volume can be calculated from the reservoir diameter and plunger displacement using the principle of conservation of mass and assuming constant density.

This value is the apparent viscosity and is valid for a particular strain rate. Corrections can be made to account for non-Newtonian flow of the pastes, and will be performed for PMMA in order to compare to other studies. For all fluids, the relationship between viscosity and shear rate is:

$$\mu = K(\dot{\gamma})^{n-1} \tag{2.2}$$

Where K and n are derived from experiment. The power index, n, indicates how close a fluid is to being Newtonian. For Newtonian fluids, n=1, and viscosity is independent of shear rate. For pseudoplastic fluids, 0<n<1. Thus the measured viscosity $\mu_o$ can be adjusted from the experimental shear rate $\gamma_o$ to any desired shear rate $\gamma$:

$$\mu = \mu_o \left( \frac{\dot{\gamma}}{\dot{\gamma}_o} \right)^{n-1} \tag{2.3}$$

Corrections can also be made for the aspect ratios of the rheometer used, but were omitted in this study.

## 2.3.2 Material Properties Measurement

A paste of $\alpha$-BSM and bone particles was mixed as described above, using 75%, 50%, 25% or 0% bone particles by volume. The material was packed into cylindrical moulds, 12mm diameter $x$ 24mm long, creating four specimens per batch. The moulds were incrementally filled, packing the material by hand using the rod shown at the bottom of Figure 2.5, applying a static force of approximately 50N for each quantity. The moulds were immersed in a distilled water bath at 37°C for 24 hours while the cement set.

After 24 hours, the mould was removed from the bath, and the ends of the specimens were sanded with 150-grit sandpaper until flush with the moulds. Specimens were removed from the mould and the dimensions were measured with a micrometer (Digimatic 293-761-30, Mitutoyo America Corp., Aurora, IL; resolution: 0.0001 mm).

For compressive properties, platens compression tests were performed. Preliminary tests with Plaster of Paris specimens showed failures occurred close to the specimen ends, indicating significant 'end artefacts'. The platens were sprayed with graphite (Crown Dry Graphite Lubricant #68078) followed by a thin layer of silicone (Dow Corning 510 Fluid). Subsequent failures occurred in the middle of the specimen.

For compression, the lower platen was aligned in a vice with matched parallels so that the surface was parallel with the base of the test machine; this was verified with a dial gauge (Products Engineering Corp.; resolution: 0.001"/0.025mm). The specimen was centred on the lower platen with the aid of Vernier calipers, with the axis of the cylinder perpendicular to the platen. The upper platen and 3/8" ceramic ball were placed on top of the specimen and aligned with the lower specimen with a set-square. The setup is shown in Figure 2.6. The cross-head of the Instron was lowered at 0.1 mm/s until failure occurred. Ultimate compressive strength and compressive modulus were determined from the test.
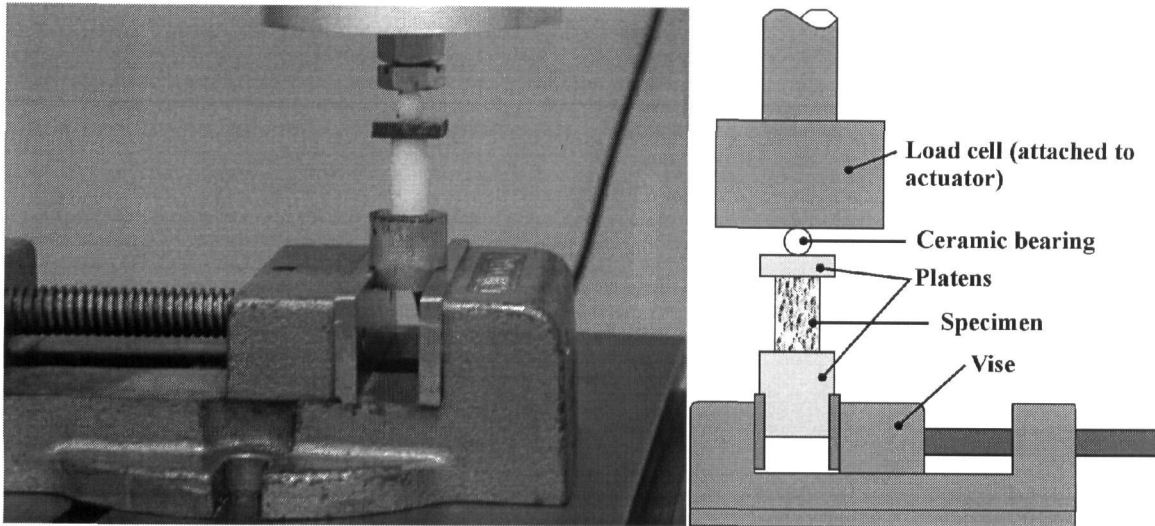
**Figure 2.6:** Uniaxial compression testing setup. Left: photograph of specimen in loading apparatus. Right: schematic representation of loading. Loads were applied by a hydraulic actuator with the load cell attached. A ceramic bearing between the actuator and upper platen corrected any misalignment of the actuator axis.

Additional parameters calculated were strain at failure (ultimate strain) and strain energy to failure, defined as the area under the stress-strain curve, up to the ultimate strain, shown in Figure 2.7.
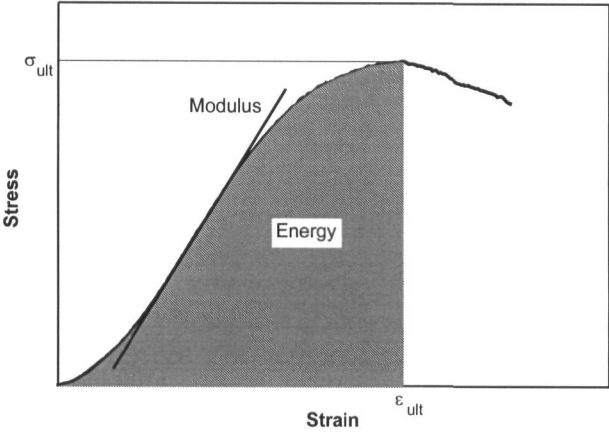


**Figure 2.7:** Definition of parameters obtained from compression tests. Modulus was calculated by regression over the steepest portion of the stress-strain curve. The failure point was defined by the maximum load. At this point, ultimate strength, ultimate strain and strain energy were calculated.

For tensile testing, a diametral tension test was performed similar to ASTM Standard C496, developed for concrete. The test setup was similar to the compression test, although the upper 1" square platen and ceramic bearing were omitted. The specimen

was placed on the platen with the cylinder axis parallel to the platen surface, shown in Figure 2.8. The cross-head was used to load the specimen directly, and was lowered at 0.1 mm/s until failure. This test uses the geometry of the specimen to create tensile stresses across the diameter of the specimen. Ultimate tensile strength was calculated according to the standard:

$$S_{ut} = \frac{2F}{\pi l d} \tag{2.4}$$

Where $F$ is the maximum measured load, $l$ and $d$ are specimen length and diameter, respectively.
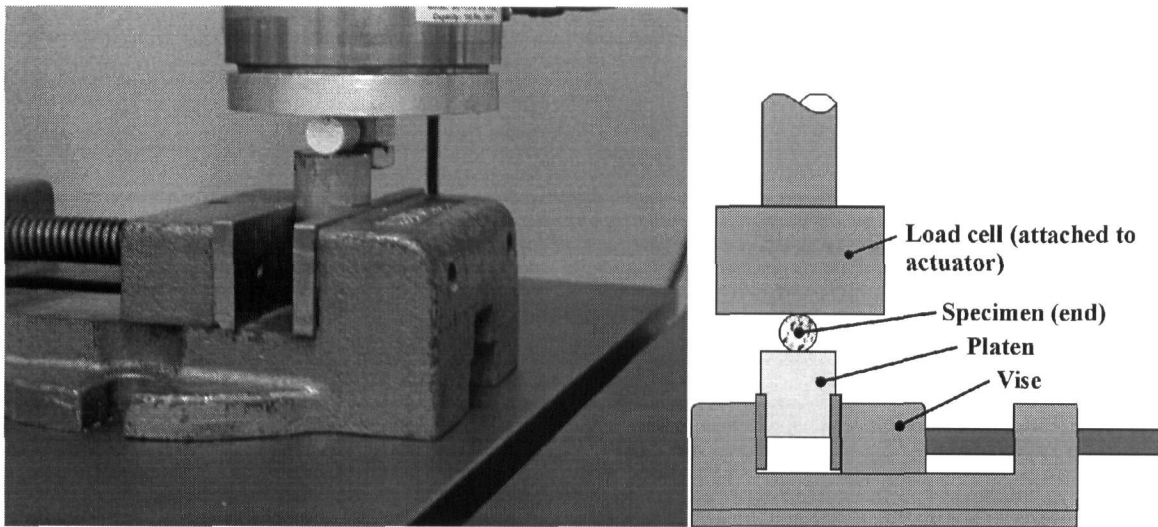


**Figure 2.8:** Diametral tensile testing setup. Left: photograph of specimen in the loading apparatus. Right: schematic representation of loading. Loads were applied parallel to the specimen diameter; the upper platen and ceramic bearing were omitted.

Shear testing consisted of a simple shear test in which both ends of the specimen were gripped, and one grip was moved perpendicular to the cylinder axis, as shown in Figure 2.9. The grips were contained inside a cylinder, with no intervening space to minimise bending moments on the specimen. The ultimate shear strength was determined from the test.
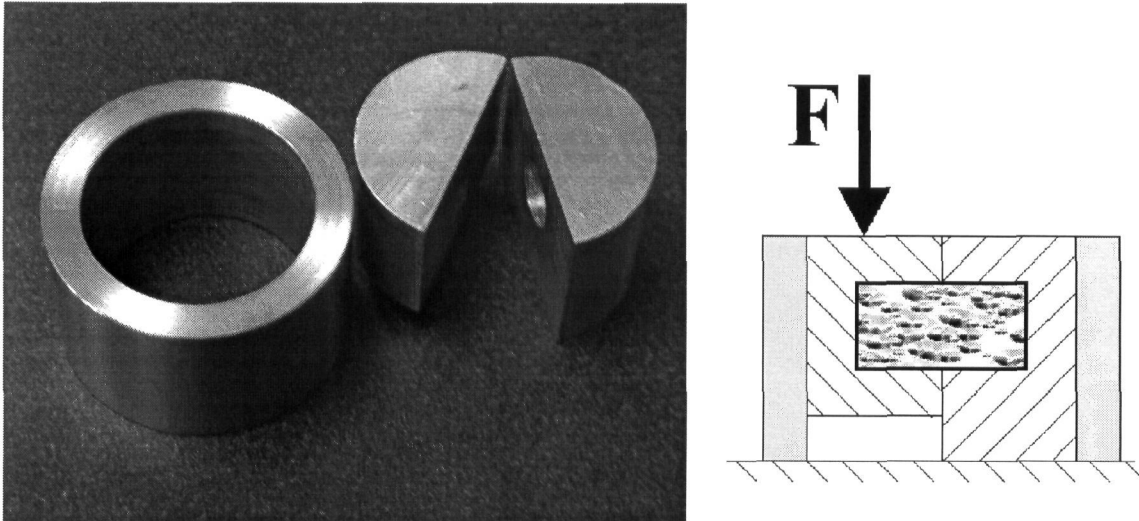
**Figure 2.9:** Shear testing apparatus. Left: the specimen was held between the two brass grips which were confined by the steel housing to prevent bending moments on the specimen. Right: schematic representation of loading. The specimen grips are shown in cross-section (hatched area) within the confining cylinder (shaded). The specimen is shown in the middle.

A confined compression test was carried out because it gives a stress state closer to what is found *in vivo*. Specimens were moulded as for the previous tests, creating specimens 12mm diameter and approximately 20mm long, capped with a 2mm-thick aluminum disc. Specimens of 100% bone were also tested. Specimens of all compositions were left in the water bath at 37°C for 24 hours. Once set, the specimens were tested in the mould by loading the cap until failure occurred. Four specimens of each cement-bone mixture and six specimens of 100% bone were tested.

Parameters calculated were stress and modulus at 5%, 10% and 15% strain. Modulus was calculated by a linear regression at each strain level over the interval $\varepsilon\pm0.001$ e.g. 0.049 to 0.051 for the 5% strain level; the interval was expanded to $\varepsilon\pm0.002$ for 100% bone specimens due to the larger influence of signal noise at lower forces.

Many specimens displayed long toe-regions in the force-displacement relationship. This region was eliminated by assuming that loading began once the slope of force vs. displacement exceeded and remained above 10N/mm. This was calculated by numerical differentiation (first-order, central difference approximation); a five-point moving average was performed on force and position data first since numerical differentiation is extremely sensitive to noise. Since the signal-to-noise ratio was very high for 100% bone specimens, loading was assumed to begin once the force exceeded and remained above

1N. The first strain level, 5%, was chosen because some specimens displayed yield-type behaviour at low strain levels. The stress level at which this occurred corresponded approximately to the uniaxial ultimate compressive strength. This phenomenon may have occurred due to shrinkage of the cement during setting, resulting in uniaxial, unconfined behaviour. The specimen expanded radially under compressive load until it was constrained by the mould. This occurred below 5% strain for all specimens. Subsequent strain levels were analysed to examine strain-hardening of the material.

## 2.4 Data Analysis

### 2.4.1 Statistical Analysis

For the uniaxial tests, specimens of each composition were prepared as two batches of four specimens. Thus a two-factor ANOVA, with bone fraction (0%, 25%, 50% and 75%) and batch (1 vs. 2) as factors, was performed to determine the effects of cement:aggregate ratio on compressive strength, modulus, strain-to-failure and strain energy-to-failure; tensile strength; and shear strength. A Student Neuman-Keuls (SNK) post-hoc test was then performed to detect specific differences between each composition with pooled data from both batches. SNK post-hoc tests were also performed to examine batch-batch differences for each composition.

### 2.4.2 Failure Envelope Analysis

In vivo, the material will experience complex, three-dimensional stress states. The material is brittle and behaves differently in tension than in compression. A Coulomb-Mohr failure analysis was therefore performed to predict *in vivo* performance. Briefly, Mohr's circles can be constructed from the tensile, shear and compressive strengths. A line tangent to these circles defines the failure envelope, and any stress state outside this envelope produces failure in the material (see Figure 2.10). If the envelope is assumed to be a straight line, as in the Coulomb-Mohr theory, it can be defined as a slope and an intercept:

$$\tau = c + \sigma \tan \phi \qquad (2.5)$$

This is the same as the shear strength-normal stress relationship in soil mechanics used to characterise morsellized bone graft. Thus the Coulomb-Mohr failure theory was used to

compare morsellized graft characteristics with the uniaxial strengths of the composite specimens. Confidence limits were estimated by constructing failure envelopes using compressive and tensile Mohr's circles of the mean strength ± one standard deviation. ANOVA was performed to examine the effect of bone fraction on the intercept and angle $\phi$ of the envelope for 0%, 25%, 50% and 75% bone. SNK post-hoc tests were performed to detect specific differences. Since Brewster et al. (1999) did not provide confidence limits for 100% bone, each composition tested was compared to the reported parameter value with a t-test, with a Bonferoni correction for multiple comparisons.
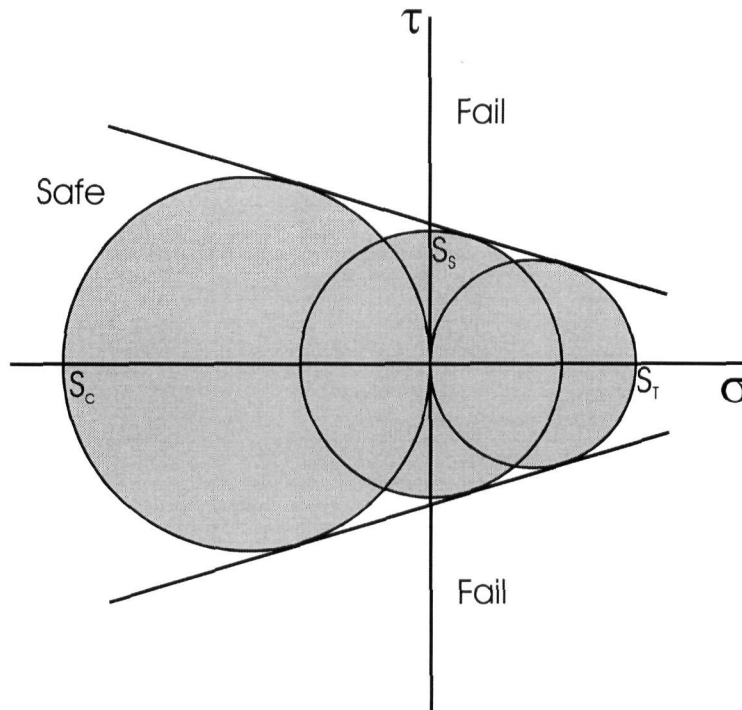


**Figure 2.10:** Graph for the Coulomb-Mohr analysis. Three Mohr's circles are constructed using the compressive (Sc), shear (Ss) and tensile (St) strengths obtained from uniaxial tests. The lines tangent to these circles define the failure envelope. Inside the envelope are all 'safe' stress states.

Confined compression tests allow direct comparison of the composite specimens with morsellized graft alone. The impetus for adding cement is to prevent excessive subsidence of the implant from graft layer consolidation. Thus stress and modulus were analysed at low strain levels, i.e. 5%. Due to the small number of specimens, a non-parametric Kruskal-Wallis ANOVA was performed to examine the effect of bone fraction (0%, 25%, 50%, 75% and 100%). If bone fraction was found to have a significant effect (p<0.05), Mann-Whitney U-tests, the non-parametric equivalent of the

unpaired t-test, were performed to detect specific differences between groups for each increment of cement fraction. Bonferoni corrections were made based on four comparisons. Unlike uniaxial tests, only one batch of each composition was prepared, so batch-to-batch variability could not be assessed. Data for 10% and 15% strain levels are presented in graph form, but were not analysed statistically.

# 3.0 Results

## 3.1 Bone Particle Size

Bone particles were produced in a wide range of sizes, as shown in Figure 3.1. Values in the figure above each quantity of bone indicate the size of mesh through which the particles could not pass. In the order of decreasing particle size (Mesh #5 being the largest), this resulted in particles larger than 4.00, 3.35, 2.36, 2.00, 1.00, and 0.600 mm. The last quantity, labelled '<#30' contains particles that passed through the smallest sieve. Both the largest and smallest particles in Figure 3.1 were discarded, to give particles ranging from 0.600 up to 4.00 mm.
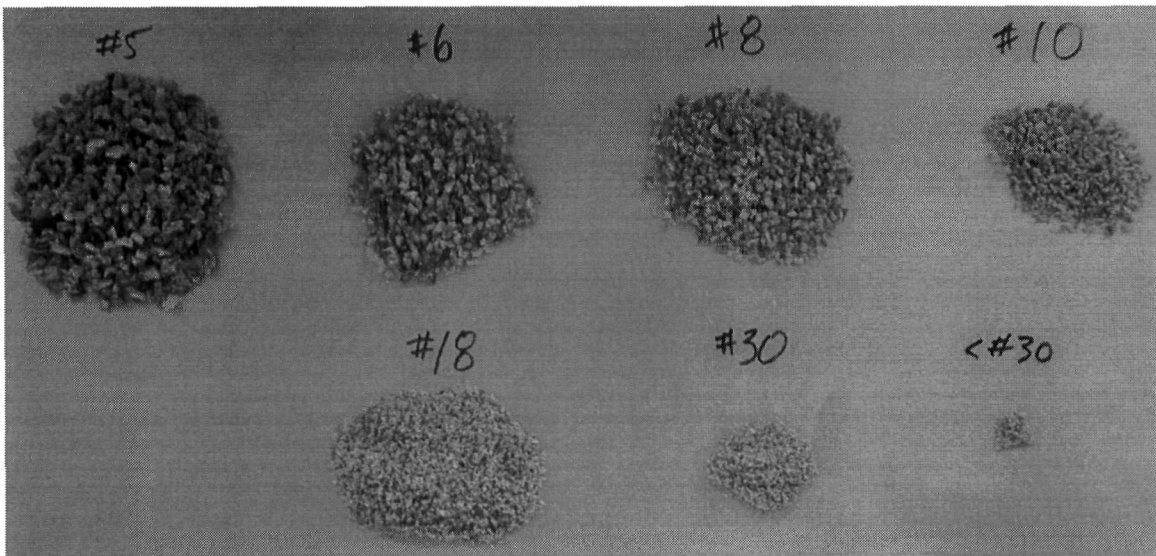


**Figure 3.1:** Particles produced by the bone mill following defatting, cleaning and sieving. See text for details of particle sizes indicated.

Figure 3.1 shows the chips produced from one batch of three femoral heads, but two subsequent batches of similar quantity were processed to produce all the bone particle material required for this study. The cumulative quantity of particles of a specified size is shown in Figure 3.2 for the three different batches. Note that the cumulative quantity includes particles that are *finer* than a specified size, a standard classification method for soils. Two 'optimal' particle gradings are shown for comparison: Fuller's curve for spherical particles and the log-linear curve for irregular particles. These will be further discussed in Section 4.1.
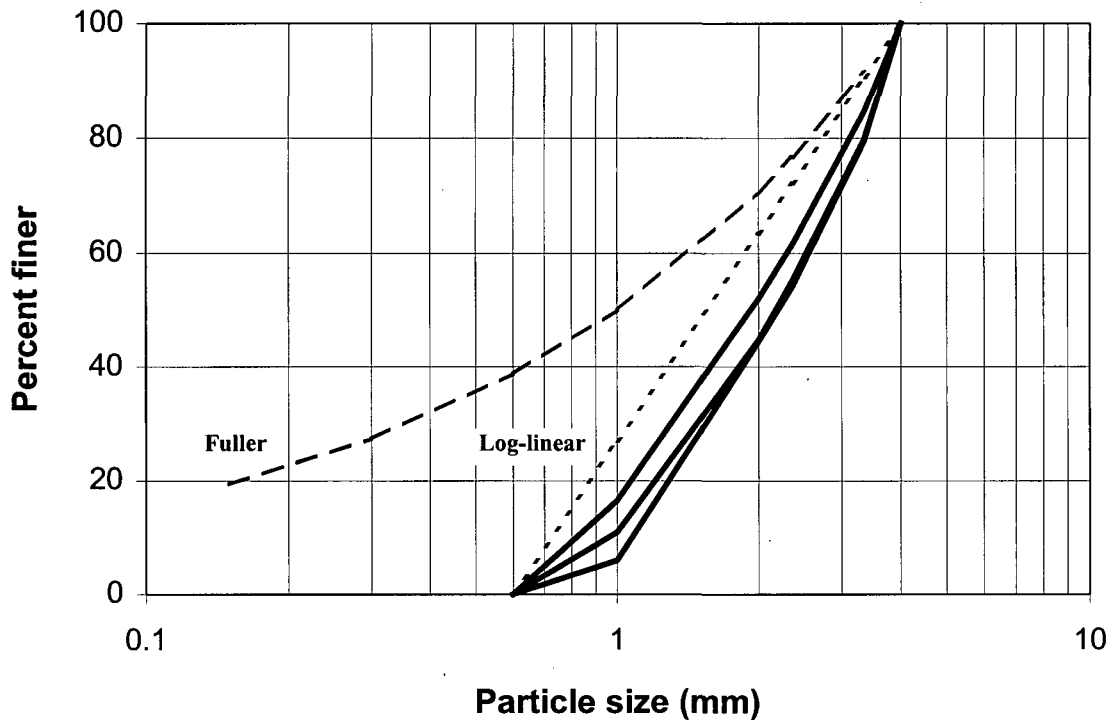
**Figure 3.2:** Particle size distribution of bone chips used in this thesis, after the largest and smallest particles had been discarded. Fuller's curve (dashed line) and the log-linear curve (dotted line) are shown for comparison. These give the theoretical optimum shear strength for spherical and irregular particles, respectively.

## 3.2  Flow Characteristics

The apparent viscosity was determined for pastes of 0% and 25% bone as well as for PMMA. Pastes of higher bone composition did not flow through the rheometer, so viscosity values could not be determined. Apparent viscosity values, calculated at five second intervals according to equation 2.1, are shown in Figure 3.3 for the materials tested. The average apparent viscosity at each interval for each material is shown for clarity, and are based on two samples for PMMA, two samples for 0% bone, and three samples for 25% bone. Curves for all tests can be found in Appendix B.

The apparent viscosity of PMMA increases exponentially with time according to the equation $\mu=973\exp(0.024t)$ for viscosity in Pa·s and time in seconds.

The calcium phosphate cement behaved quite differently during flow testing. Initial apparent viscosity values were comparable to that of PMMA, but increased much more rapidly after about 30 seconds. This was probably due to the plunger nearing the bottom

of the reservoir. This did not occur with the PMMA since there was more material in the reservoir at the start of the test.

Addition of bone particles, accounting for 25% by volume of the paste material, resulted in a large increase in initial apparent viscosity compared to pure cement and PMMA, as shown in Figure 3.3. The test was performed under position control so that flow continued throughout the test. However, the measured force increased very rapidly, and the test was stopped when the force reached 5000N (4000N for one specimen) at approximately 10-15 seconds.
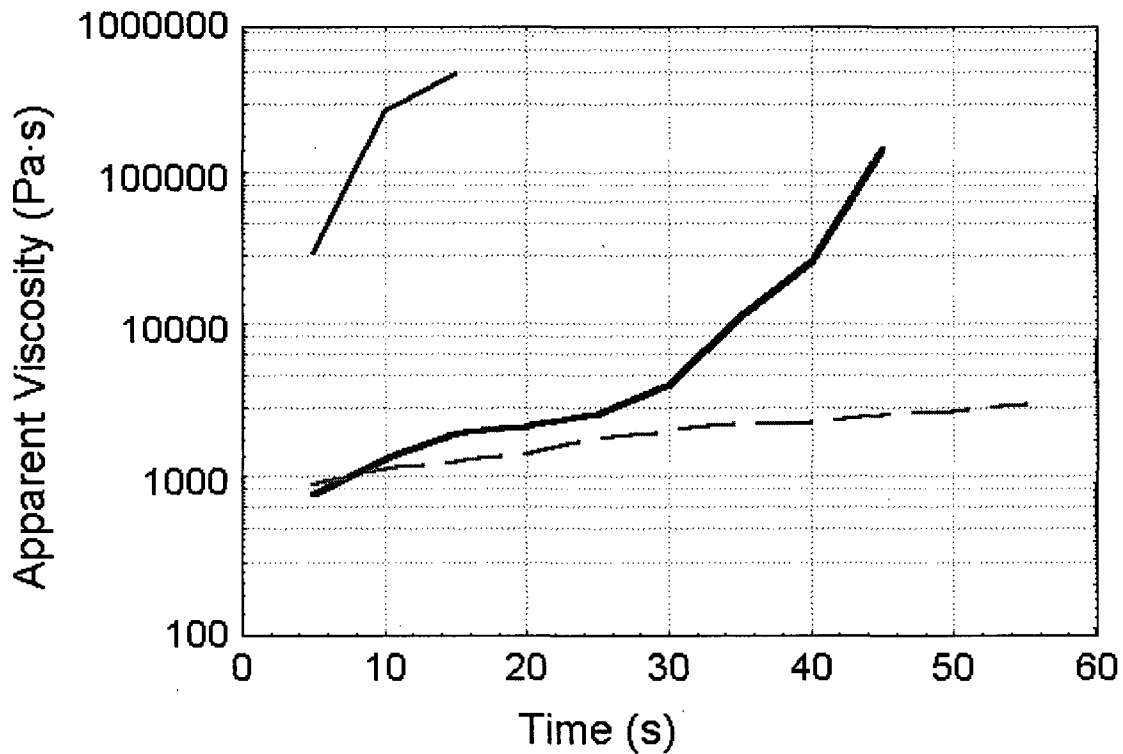


**Figure 3.3:** Flow characteristics. Paste of 0% bone (thick solid line) is slightly more viscous than PMMA (dashed line). The addition of 25% bone particles caused a large increase in viscosity (thin solid line). Viscosity is plotted on a log scale due to the wide range in values obtained.

### 3.3 Mechanical Properties

3.3.1 Compression

Figure 3.4 shows the compressive stress-strain curve from a typical specimen from each composition. As expected, specimens of pure cement behaved in a brittle manner, with relatively high modulus but low ductility. As the bone content increases, the modulus decreases and the ductility increases. The ultimate compressive strength exhibited only

small changes with no consistent trend. Specimens were prepared in two batches of four, resulting in eight specimens per composition. Only seven specimens were tested for 25% bone due to insufficient material in the first batch; nine specimens were tested for 75% bone because extra material was prepared.
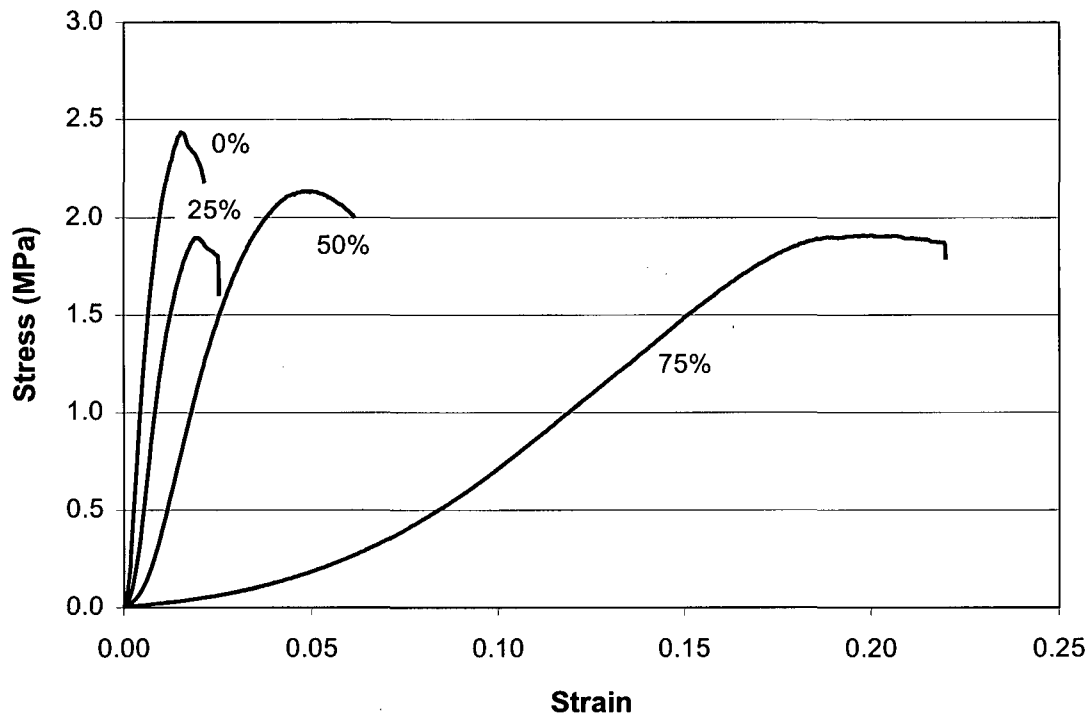


**Figure 3.4:** Compressive characteristics of the calcium phosphate-bone composite. Increasing the bone composition decreases the stiffness but increases the ductility.

The effect of bone:cement ratio on individual mechanical properties can be seen in the figures below. Figure 3.5 shows the axial compressive strength for the various compositions tested and results are presented in Table 3.1. ANOVA indicated that bone composition had a significant effect on the ultimate compressive strength ($p < 0.001$). The data appeared to show large variances, which could be due to batch-batch variability. A two factor ANOVA, with composition and batch as the independent variables indicated that there were differences between batches for specimens of 50% and 75% bone ($p < 0.0005$, SNK post-hoc). This can be seen as two distinct groups for 75% bone specimens in Figure 3.5. For 50% bone specimens, all strengths for one batch lie below the mean and all strengths from the other batch lie above the mean.
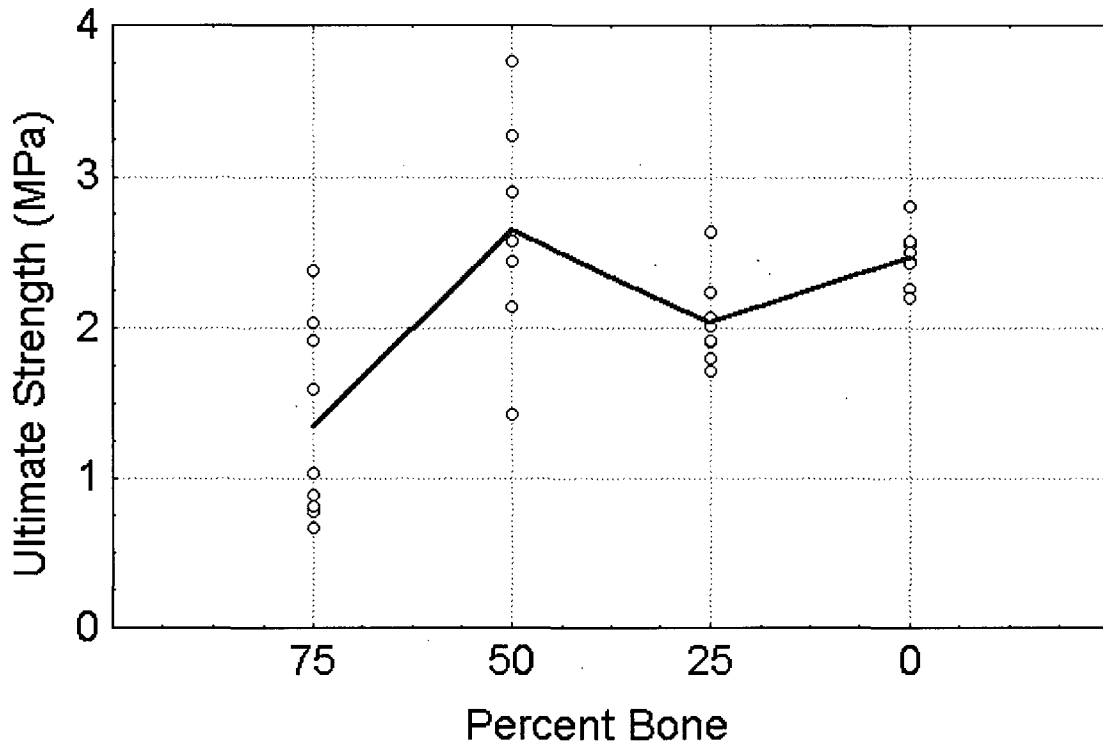
**Figure 3.5:** Ultimate strength of specimens in uniaxial compression. Composition (% bone) had a significant effect on strength (p<0.0001). The solid line connects the group means.

| Bone Fraction | Specimens | Strength, MPa* |
|---|---|---|
| 75% | 9 | 1.35 (0.21) |
| 50% | 7 | 2.65 (0.29) |
| 25% | 8 | 2.03 (0.10) |
| 0% | 8 | 2.47 (0.07) |

**Table 3.1:** Ultimate compressive strength values for each composition. There was no difference between 0% and 50% bone compositions, but the other two were significantly lower (p<0.0005). *Mean (SE).

Student Newman-Keuls (SNK) post-hoc tests revealed that significant differences across specimen composition were due to lower strengths for both 25% and 75% bone compared to both 0% and 50% (p<0.0005). SNK p-values for all comparisons can be found in Appendix C, along with complete statistical results for all other properties examined.

The elastic modulus (Figure 3.6) showed larger differences as well as a more obvious trend. As expected, the stiffness of the samples increased greatly with decreasing bone

content. Bone volume fraction had a statistically significant effect on the modulus (p<0.0001, ANOVA), with every decrease in bone fraction creating a significantly stiffer material (p<0.04, SNK post-hoc). Batch-batch variability was statistically significant, affecting specimens of 0% and 50% bone (p<0.02, SNK post-hoc), although differences across composition were comparatively large and not hidden by this. Modulus values for each specimen composition are given in Table 3.2.
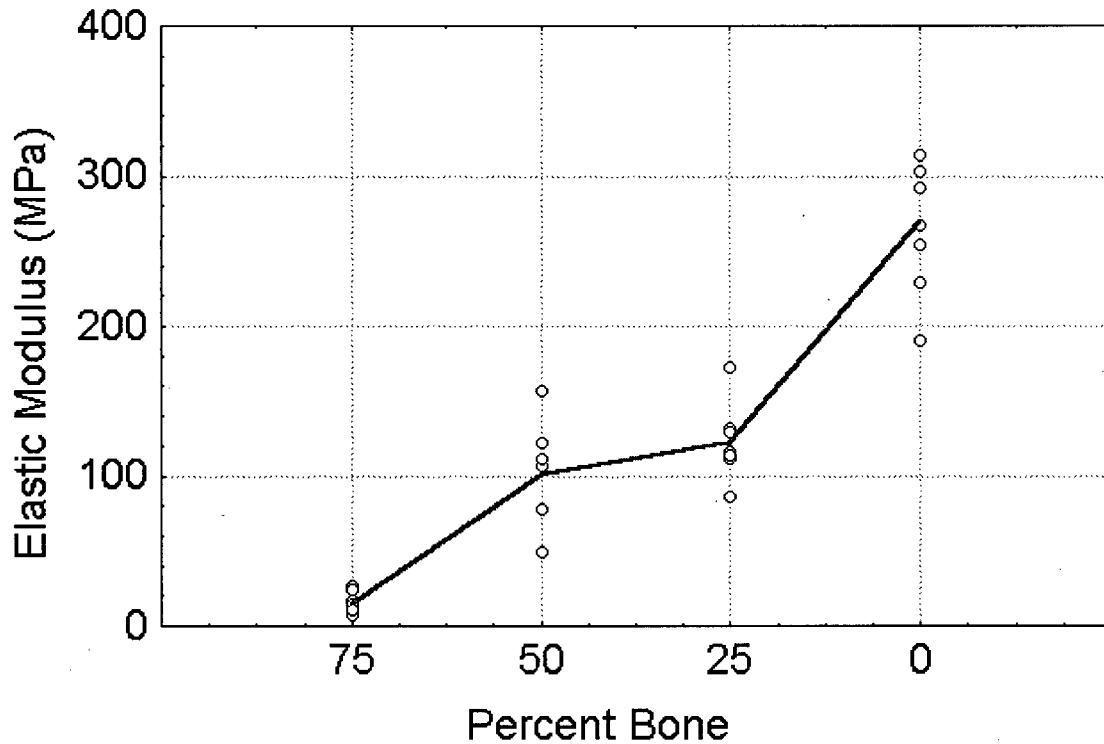


**Figure 3.6:** Changes in specimen modulus due to bone fraction. ANOVA indicated a significant effect of composition (p<0.0001).

| Bone Fraction | Specimens | Modulus, MPa* |
|---|---|---|
| 75% | 9 | 14.7 (2.3) |
| 50% | 7 | 100 (13) |
| 25% | 8 | 122 (8.8) |
| 0% | 8 | 269 (15) |

**Table 3.2:** Effect of composition on elastic modulus. Post-hoc tests indicated significant differences between every group (p<0.03). *Mean (SE).

Strain to failure also showed large differences across composition, with an obvious decreasing trend as bone fraction decreased (see Figure 3.7). Again, bone fraction had a significant effect (p<0.0001); all comparisons between individual groups were also significantly different (p<0.01, SNK post-hoc). Variation between batches was significant only for specimens of 75% bone (p<0.004), although the difference was much smaller than variation due to composition, as can be seen in Figure 3.7 and Table 3.3.
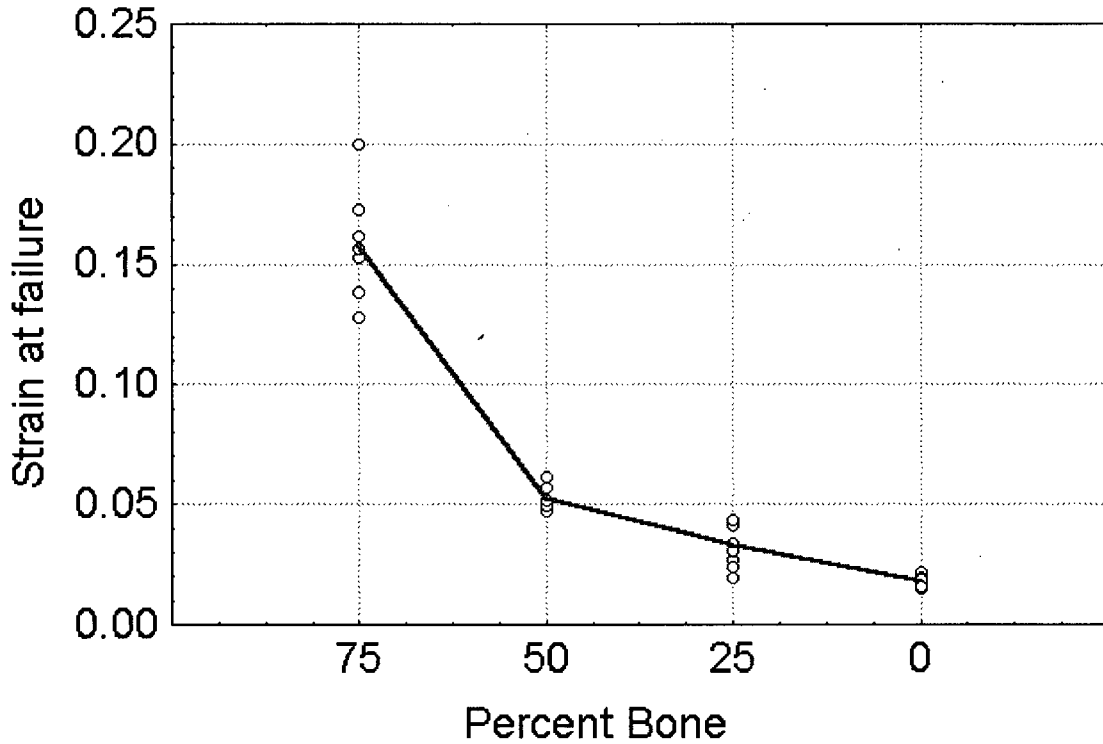


**Figure 3.7:** Effect of bone content on the ultimate strain. Each step decrease in bone volume decreased the strain-to-failure (p<0.01; SNK post-hoc).

| Bone Fraction | Specimens | Ultimate strain, m/m* |
|---------------|-----------|------------------------|
| 75% | 9 | 0.158 (0.007) |
| 50% | 7 | 0.053 (0.002) |
| 25% | 8 | 0.033 (0.003) |
| 0% | 8 | 0.018 (8.7e-4) |

**Table 3.3:** Ultimate strain values for different bone fractions. Variability was small and all between-groups comparisons were significantly different (p<0.009, SNK post-hoc). *Mean (SE).

Since the strength was not greatly affected by bone content, strain energy showed the same trend as ultimate strain i.e. decreasing strain energy for decreasing bone percentage, indicating higher ductility for specimens of high bone fraction (see Figure 3.8, Table 3.4). There was a significant difference between the strain energy that each composition could absorb as the bone content was decreased (p<0.02; SNK post-hoc), except between specimens of 25% and 0% bone. Similar to the other properties, batch had an effect on strain energy, with significant differences for specimens of 50% and 75% bone.
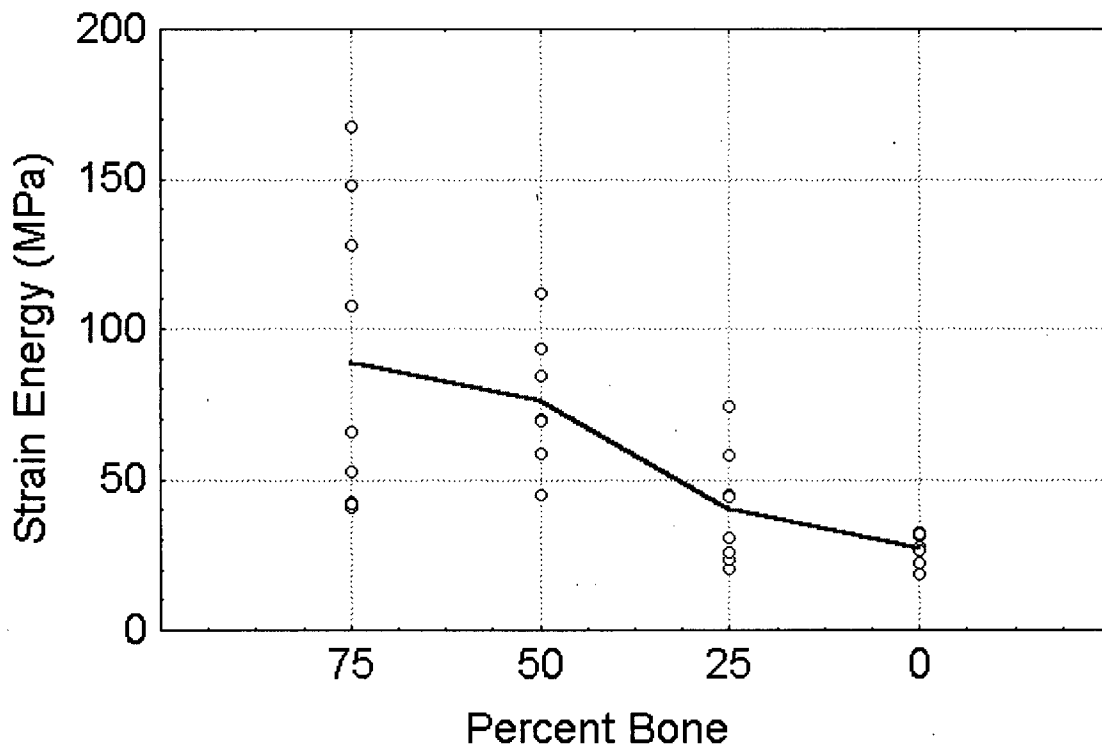


**Figure 3.8:** Effect of bone fraction on strain energy stored in the specimens at failure. Strain energy showed a significant decrease with step decreases in bone fraction from 75% to 25% bone (p<0.02). There was no difference between 25% and 0% bone specimens (p=0.1).

| Bone Fraction | Specimens | Strain Energy, MPa* |
|---|---|---|
| 75% | 9 | 88.4 (16.7) |
| 50% | 7 | 76.3 (8.5) |
| 25% | 8 | 40.1 (6.7) |
| 0% | 8 | 27.1 (1.7) |

**Table 3.4:** Strain energy values at failure for different bone fractions. Each step decrease in bone fraction down to 25% produced a significant decrease in strain energy absorbed before failure (p<0.02, SNK post-hoc). There was no difference between 0% and 25% bone. *Mean (SE).

47

### 3.3.2 Tension

Like the compressive strength, the ultimate tensile strength did not show an obvious trend with bone volume, as shown in Figure 3.9. However, the bone:cement ratio did have a significant effect ($p<0.0001$). This is due to a higher tensile strength of the 50% bone specimens ($p=0.0002$, SNK post-hoc) and lower strength of 75% bone specimens ($p<0.005$, SNK post-hoc) compared to the other two compositions. Batches exhibited different tensile strengths for 50% ($p=0.01$) and 75% ($p=0.04$) bone specimens, but differences were small compared to variation due to composition. Note that specimen strength for all compositions is much lower in tension than compression, roughly 17% to 25%, as would be expected for a ceramic. Data for each composition are shown in Table 3.5.
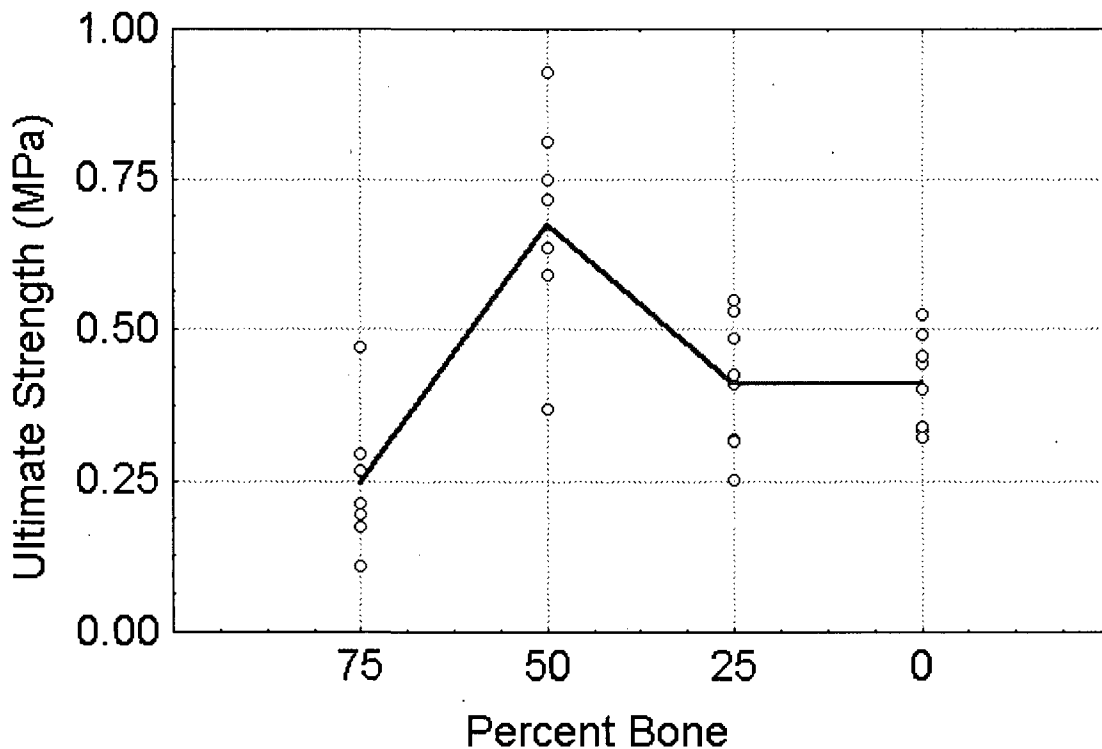


**Figure 3.9:** Effect of bone:cement ratio on diametral tensile strength. Bone fraction had a significant effect ($p<0.0001$); 50% bone specimens were stronger ($p=0.0002$) and 75% bone specimens were weaker ($p=0.0002$) compared to 25% and 0% bone specimens.

| Bone Fraction | Specimens | Strength, MPa* |
|---|---|---|
| 75% | 7 | 0.25 (0.04) |
| 50% | 8 | 0.67 (0.06) |
| 25% | 8 | 0.41 (0.04) |
| 0% | 8 | 0.41 (0.03) |

**Table 3.5:** Diametral tension strength values for different compositions. Strength was highest for 50% bone and lowest for 75% bone. There was no difference between 0% and 25% bone. *Mean (SE).

### 3.3.3 Shear

The ultimate strength of the specimens in simple shear is shown in Table 3.6. Difficulties were encountered with this testing method, and only a small number of specimens were successfully tested. The most significant problem arose from mounting the specimens in the test grips: tolerances were such that any material between the grips could cause them to bind, creating large friction forces. As such, the validity of these results is questionable, but measured values are presented for completeness.

| Bone Fraction | Specimens | Strength, MPa* |
|---|---|---|
| 75% | - | - |
| 50% | 3 | 3.36 (0.52) |
| 25% | 8 | 1.89 (0.25) |
| 0% | 5 | 0.98 (0.09) |

**Table 3.6:** Ultimate strength values for different compositions in simple shear. Results may not be valid due to testing difficulties. *Mean (SE).

### 3.3.4 Failure criteria

Comparison of composite specimen strength with bone graft particulate strength may be done using the Coulomb-Mohr failure theory. This theory can be used for materials that behave differently under tension and compression, and allows comparison of particulate soil-like materials (bone particles) with solid, concrete-like materials (composites). Failure envelopes for the different compositions were constructed as described in Section 2.4, and are shown below. Normally shear strength is also used to construct the failure envelopes, but was omitted due to testing difficulties. Also shown for comparison, is the

failure envelope of bone graft particles, obtained by Brewster et al. (1999). Since 'safe' stress states lie to the left of the failure envelopes, Figure 3.10 indicates that addition of cement expands the safe stress states compared to bone graft alone. Note that the shear stress intercept, known as the cohesion coefficient in soil mechanics, has been greatly increased by the addition of cement, indicating that the material is better able to resist shear stresses. Extension of the failure envelope beyond the point of contact with the Mohr's circle is not appropriate, but has been done for clarity.
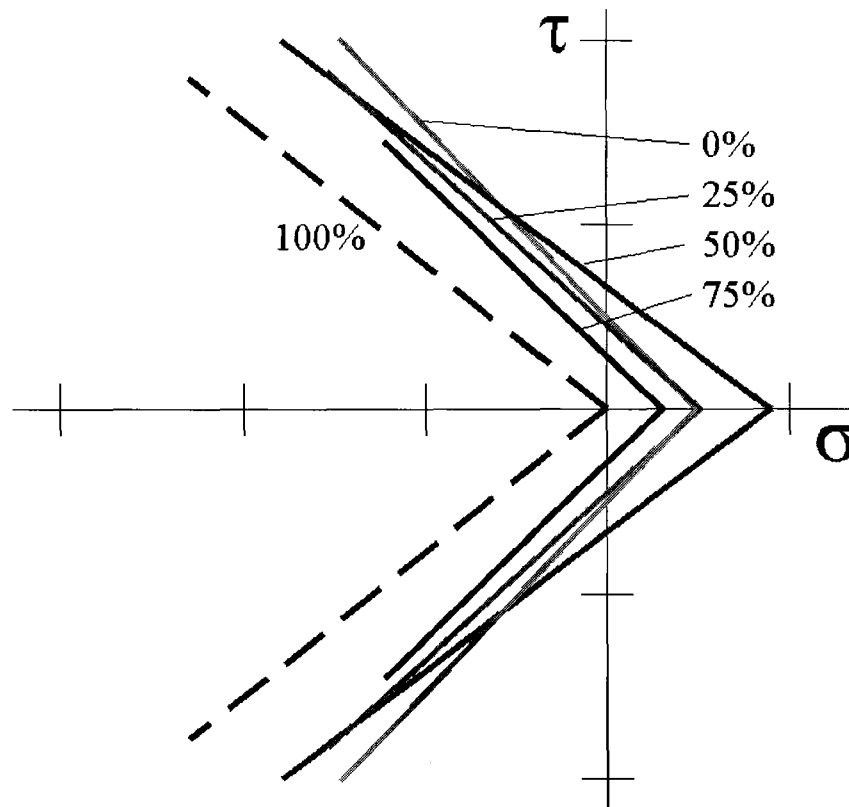


**Figure 3.10:** Coulomb-Mohr failure envelopes from uniaxial tests. Addition of cement to bone particles (solid lines, bone fractions indicated) expands the failure envelope compared to bone particles alone (dashed line, from Brewster et al. (1999)). Tick marks on axes indicate 1 MPa.

Parameters of the failure envelopes, as defined in soil mechanics theory and equation 2.5, are given in Table 3.7. The standard errors of the parameters, the cohesion coefficient and angle of internal friction, were estimated by constructing failure envelopes based on strengths one standard deviation above and below the mean. The deviation from the parameter mean was divided by $\sqrt{n}$ to give the standard error, and is shown Table 3.7.

| Bone Fraction | Cohesion, c (kPa) | Internal Friction, $\phi$ |
|---|---|---|
| 100%* | 6 | 38° |
| 75% | 287 (48) | 44° (0.1°) |
| 50% | 667 (64) | 37° (0.9°) |
| 25% | 457 (33) | 42° (2.6°) |
| 0% | 505 (66) | 46° (2.3°) |

**Table 3.7:** Failure envelope parameters from uniaxial testing. Addition of cement improves the cohesion without large changes in internal friction. * From Brewster et al. (1999).

ANOVA for the four compositions tested in this thesis indicated there was no significant difference in the cohesion coefficient (p=0.23), although this may be due to large variability of the cohesion estimates. ANOVA did indicate a significant difference between the angle of internal friction (p=0.009), due to a lower value for 50% bone (p<0.01, SNK post-hoc) compared to every other composition. No other between-groups comparisons were significant (p>0.05).

Addition of 25% cement (i.e. 75% bone) produces close to a 50-fold increase in cohesion. Compared to the parameters for bone particles alone obtained by Brewster et al. (1999), every composition had a higher cohesion coefficient (p<0.003, with Bonferoni correction for multiple comparisons). Compositions of 0%, 25% and 75% had significantly higher angles of internal friction (p<0.02, Bonferoni), and 50% showed a lower angle of internal friction (p=0.02, Bonferoni). The lower angle for the 50% bone specimens was mainly due to the higher tensile strength.

### 3.3.5 Confined Compression

Confined compression testing showed similar trends as in uniaxial compression testing: addition of cement to bone particles resulted in a large increase in the stiffness of the specimens. Figure 3.11 shows the average behaviour of the specimens at each composition; for each composition, the average stress was calculated for each strain increment of 0.001, and is plotted below.

The strange behaviour of each of the pure cement specimens seen at 40 to 45 MPa (see Appendix B) was due to extrusion of the cement from the top of the mould.
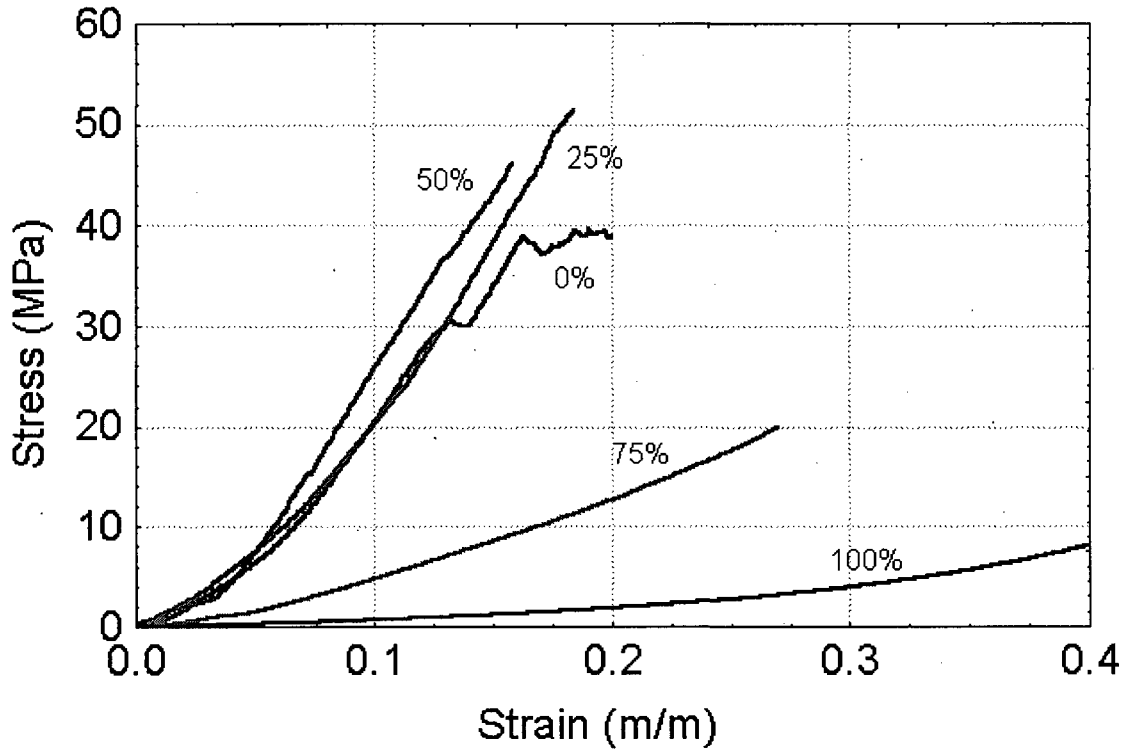
**Figure 3.11:** Average stress-strain behaviour of confined compression test specimens. Specimens of high bone volume exhibited strain-hardening throughout the test whereas specimens of low bone volume tended to show some yielding at high stresses.

Specimens often displayed a yielding-type behaviour at low strain levels i.e. below about 3MPa, depending on the composition. An example of this low strain-level behaviour, from a specimen of 50% bone, is shown in Figure 3.12. This yielding occurs at levels similar to that of uniaxial compressive failure, although the modulus before this and the strain level are lower than the corresponding uniaxial values. Following this yield, the specimens increased in stiffness as the material was compacted.
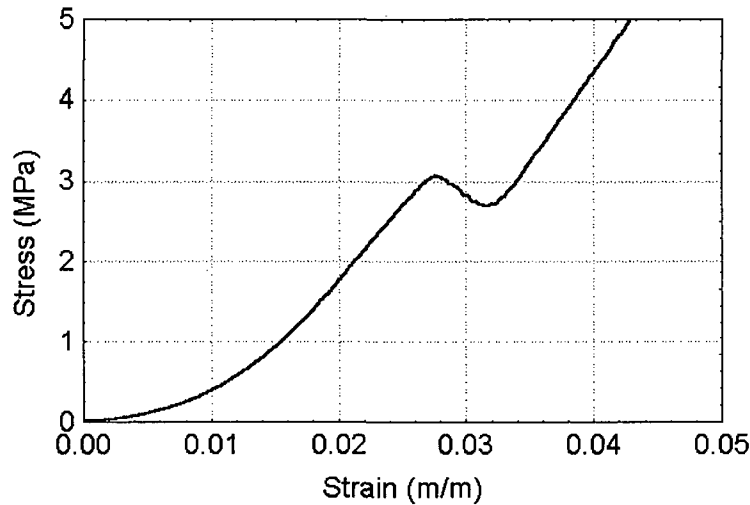
**Figure 3.12:** Low strain-level behaviour of confined compression specimen. This 50% bone specimen exhibited a yield-type phenomenon at approximately the uniaxial compressive strength. If the cement shrinks during setting, initial loading would be uniaxial compression until the specimen expands to fill the mould.

Stress and modulus values were calculated at 5% strain intervals up to 15% strain. The effect of bone volume on stress is shown in Figure 3.13 for the three strain levels. Note that for low bone fractions (0%, 25% and 50%), a higher stress level is required to achieve the same deformation compared to high bone fractions (75% and 100%). Bone fraction had a significant effect on the stress at 5% strain ($p<0.002$, Kruskal-Wallis). This was due to the lower stress level in the pure bone particle specimens compared to 75% bone specimens ($p=0.04$). Although differences between 50% and 75% bone specimens appear large, they were not significant, probably due to low specimen numbers and variability. The median and range of the stress levels at 5% strain are shown in Table 3.8. Values for higher strain levels were not analysed statistically and are not shown in the table, but showed similar trends.
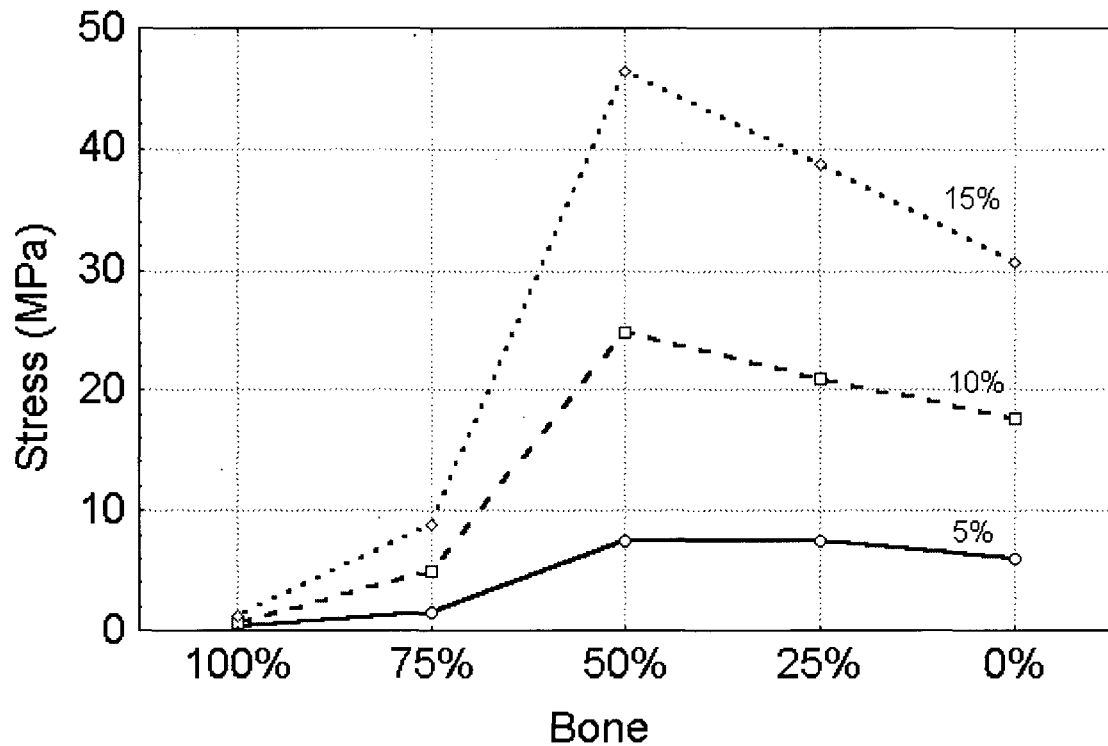
**Figure 3.13:** Median stress levels in confined compression specimens at 5%, 10% and 15% strain. Specimens of low bone volumes had higher stress levels than specimens of high bone volume, for each strain level.

| Bone Fraction | Specimens | Stress, MPa* |
|---|---|---|
| 100% | 6 | 0.25 (0.1-0.42) |
| 75% | 4 | 1.5  (1.4-1.8) |
| 50% | 4 | 7.5  (6.8-8.1) |
| 25% | 4 | 7.6  (6.8-8.6) |
| 0% | 4 | 6.0  (4.5-9.2) |

**Table 3.8:** Stress values at 5% strain from confined compression testing. Bone volume had a significant effect due to low stresses in 100% vs 75% bone specimens (p<0.04, Mann-Whitney with Bonferoni correction). *Median (range)

The modulus of the specimens at different strain levels showed a trend similar to stress, as shown in Figure 3.14. Note that the modulus continued to increase as the strain increased, indicating strain hardening. This was especially true for specimens of high

bone fraction (see Figure 3.11 and individual stress-strain curves in Appendix B), which did not show a large increase in stiffness until well beyond 25% strain.
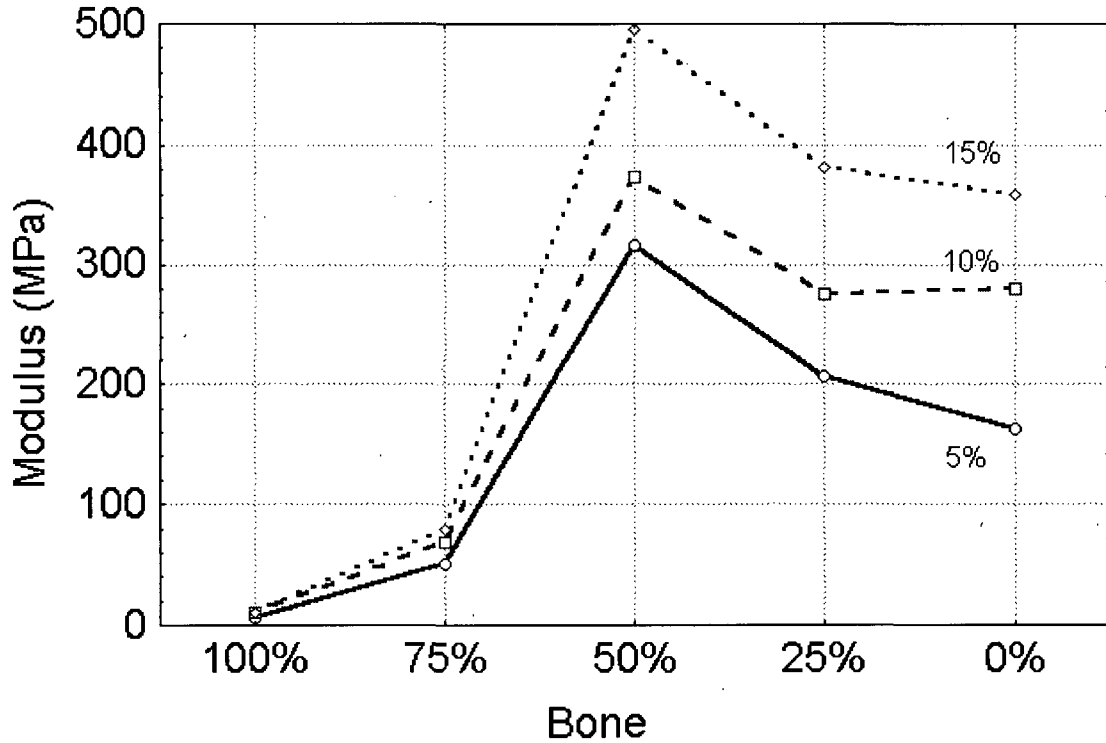


**Figure 3.14:** Median specimen modulus in confined compression at 5%, 10% and 15% strain. Specimens of low bone volumes had higher stiffness than specimens of high bone volume, for each strain level. Most specimens, especially for high bone fractions, showed further increasing stiffness beyond 15% strain.

Values for the modulus at 5% strain are shown in Table 3.9. A Kruskal-Wallis test indicated bone fraction had a significant effect on modulus at 5% strain (p<0.007). This was due to a lower modulus of the 100% bone specimens compared to the 75% bone specimens.

| Bone Fraction | Specimens | Modulus (MPa)* |
|---|---|---|
| 100% | 6 | 6.0    (4.4-7.1) |
| 75% | 4 | 50.8 (50.1-53.2) |
| 50% | 4 | 316   (288-357) |
| 25% | 4 | 206   (163-218) |
| 0% | 4 | 163   (115-310) |

**Table 3.9:** Confined compression modulus at 5% strain. Bone fraction had a significant effect due to lower stiffness of 100% vs. 75% bone compositions. *Median (range)

At very high strain levels, some specimens showed yielding behaviour while others continued to strain-harden. This occurred for all four specimens of pure cement, two specimens of 25% bone and one specimen of 50% bone. Thus there seems to be a higher incidence of yielding at low bone fractions, although this trend could not be statistically analysed due to low specimen numbers.

# 4.0 Discussion

The effects of bone particle fraction on handling characteristics and material properties have been determined in this thesis. Problems encountered during testing and limitations of the test results will be discussed in each of the following sections before discussion of the actual results and their meaning.

## 4.1 Bone Particle Size

Sieve analysis showed that the pneumatic bone mill produced a range of particle sizes with roughly equal amounts of sizes down to 1 mm. Only a small amount of particles finer than 1mm were produced. A large amount of particles larger than 4mm were produced, but were discarded.

Sieving was performed by hand for a constant time, which may have been insufficient to allow complete passage of the particles. This may occur because larger particles, which are trapped by a particular sieve, block the passage of smaller particles. However, the quantity of bone chips in each batch was relatively small, and this effect should be negligible. It was noted that some very small bone chips stuck to the mesh, probably due to static charges, which would result in an underestimation of the quantity of very small particles. An attempt was made to brush these particles into the next sieve of smaller mesh so that they would pass through all appropriate sieves. These particles were generally very small, and were probably finer than #30 mesh so their cumulative mass was small and would not lead to large errors in the mass distribution.

Some of the femurs used in this study came from donors whose spines had low bone mineral density values, indicating the presence of osteoporosis. Brewster et al. (1999) showed that osteoporotic femoral heads resulted in a lower quantity of bone particles, but did not affect the size distribution or the mechanical properties of the morsellized bone under shear loading.

The size distribution of bone particles used in this study was similar to that of Brewster et al. (1999). Figure 4.1 below shows the pooled data of all particles used in this study, compared to data from more recent work of the same group (Dunlop, 2001). Note that in both series, small and very small particles are lacking compared to the theoretically ideal

Fuller's curve for spherical particles, shown on the right. However, distribution of particle sizes obtained in this thesis are close to the log-linear curve, which is used for irregular particles (Brewster, 1999), also shown in Figure 4.1, right. In this study, the lack of small and very small particles is partly due to discarding the particles that passed through the #30 sieve. The curves indicate that, as a soil, morsellized allograft does not have optimum shear strength, but is close. Brewster et al. (1999) addressed this problem by adding bioactive glass particles to the bone particles to create a better graded material, and theoretically improve the shear strength. Under no impaction, the bone-bioglass mixture performed approximately the same as bone particles alone in terms of cohesion and angle of internal friction. However, the shear strength of the mixture improved more than bone after compaction of the specimens.
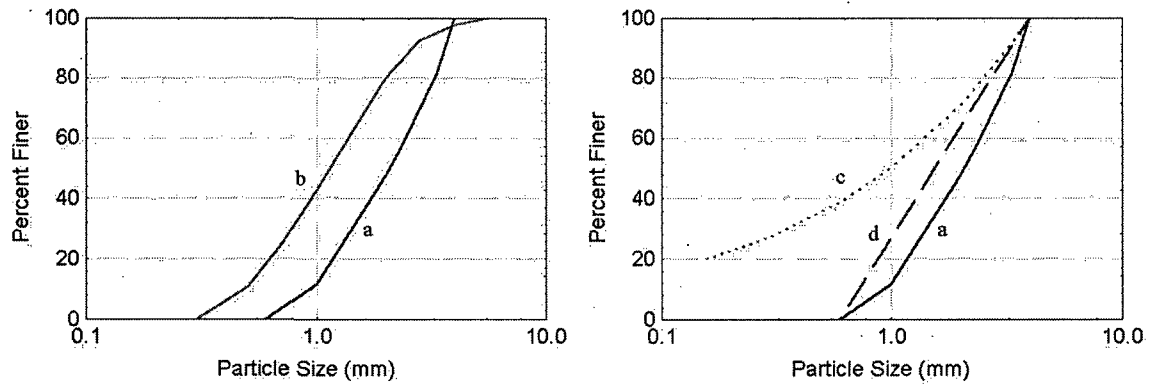


**Figure 4.1:** Sieve analysis of morsellized bone. The distribution of particles obtained in this thesis (a, left and right) is similar to that obtained by Dunlop (2001; b, left), although a narrower range of particles was used. Compared to Fuller's curve (c, right), the bone chips lacked small and very small particles. Compared to the log-linear curve (d, right), the size distribution is close to optimal for irregular particles.

The optimal particle size distribution in concrete is less clear, as there are many 'standard' grading curves (see Neville (1995) for some examples). Fuller's curve is sometimes employed since it gives a theoretical distribution for optimal density of spherical particles. However, in practice, gradings based on empirical findings for specific particle size ranges are used. One such example is shown in Figure 4.2.
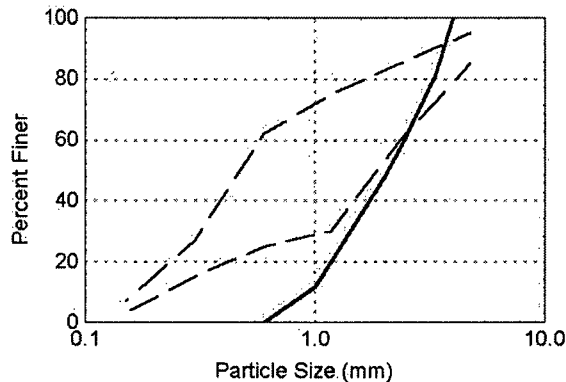
**Figure 4.2:** Aggregate grading for concrete. The dashed lines show the minimum and maximum particle size distribution based on the US Bureau for Reclamation (Neville, 1995). The distribution obtained in this thesis lacks in smaller size particles compared to this grading standard.

## 4.2 Flow Characteristics

Apparent viscosity measurements worked well for PMMA and pure calcium phosphate cement. Addition of the bone particles produced a very large increase in apparent viscosity, and beyond 25% bone was impossible to measure due to negligible flow.

Volume flow was measured by displacement of the LVDT and using the area of the reservoir. The volume in equation 2.1 is the volume of material extruded from the capillary. The two were equated by assuming constant density and mass conservation in the flow from reservoir to capillary. Ideally the amount extruded would be measured directly, but the short duration of the time steps used in the calculations and small volume of material used in the test made this procedure difficult. Volume flow measurement from reservoir diameter and plunger displacement resulted in less uncertainty.

The viscosity calculation assumes a fully developed, laminar flow of a Newtonian fluid. The presence of the bone particles would violate these assumptions, thus the measured viscosity is the apparent viscosity. It is not known whether the calcium phosphate paste is a Newtonian fluid, so corrections may be necessary to determine complete viscosity characteristics. PMMA has been shown to be pseudoplastic i.e. non-Newtonian (Dunne, 1998; Krause, 1982), so corrections should be made to the apparent viscosity to completely describe the fluid. This is only necessary if comparisons are to be made at different shear rates. Thus the apparent viscosity reported in this thesis is only valid for the experimental shear rate. Since the main purpose was to examine the behaviour of different materials, and the shear rates remained constant in all tests, comparisons of the

different materials are valid for the experimental shear rates. Although the apparent viscosities would change for different shear rates (e.g. in pseudoplastic materials, viscosity decreases with increasing shear rate), the relative flow characteristics of the different materials would not change.

The dimensions of the rheometer used in this study were taken from Liu et al. (1987), which is similar to ASTM Standard D3835. All dimensions are within the ranges specified by the Standard, except the ratio of reservoir:capillary diameters. The Standard specifies a range of 3 to 15 for this ratio, and corrections are recommended for ratios larger than 15. The ratio used in this study was 25/9.5 = 2.6, slightly below the specification, so correction factors should not be necessary.

The capillary length:diameter ratio was 5.8, which is within the range specified in the Standard. Equation 2.1 assumes that the applied stress is completely balanced by the shear stress in the capillary so that:

$$p = \tau \left( \frac{2L}{r} \right)$$

However, entrance and elasticity effects will increase the pressure drop across the capillary. This can be corrected by mathematically increasing the L/r ratio. Philipoff and Gaskins (1958) derived an equation for the corrected shear stress:

$$p = \tau_{CORR} \left( \frac{2L}{r} + 2n + s \right) = 2\tau_{CORR} \left( \frac{L}{r} + n + \frac{s}{2} \right)$$

where n accounts for flow development at the capillary entrance and s is related to the elastic strain. Thus the relative error from neglecting the correction term (n + s/2) decreases with increasing L/r. The correction term decreases with decreasing shear rate (Philipoff, 1958) in an apparent power-law relationship, although data is scarce. Data for polyethylene was presented by Philipoff and Gaskins (1958). Assuming PMMA behaves similarly, extrapolation of the polyethylene data to the shear rate used results in a correction term (n + s/2) ≈ 0.4. For the L/r = 11.6 used in this thesis, the resulting error is about 4%, and was neglected.

The measured viscosity for PMMA compares well with previous studies. Krause et al. (1982) performed an extensive parametric study of the non-Newtonian flow of PMMA,

examining seven brands at four shear rates. Viscosity values from this thesis, Krause et al. (1982) and two other studies are shown in Table 4.1. All values are at three minutes following the start of mixing, with the experimental shear rate below. The bottom row is the viscosity value corrected to the shear rate used by Krause et al. (1982). A power index of 0.6 was used for data from this thesis (Krause, 1982); Dunne and Orr (1998) reported a value of 0.25 which was used to adjust their data; Liu et al. (1987) did not report a value, so a value of 0.6 for Zimmer cement was used (Krause, 1982).

| Study: | Present | Dunne and Orr (1998) | Liu et al. (1987) | Krause et al. (1982) |
|---|---|---|---|---|
| Viscosity (Pa·s) | 2811 | 7145 | 46400 | 221 |
| Shear rate (s$^{-1}$) | 0.25 | 0.24* | 0.046 | 97.4 |
| Adjusted viscosity (Pa·s) | 258 | 81.5 | 2169 | 221±34 |

**Table 4.1:** Survey of viscosity of PMMA bone cement. The last line is the viscosity adjusted for the flow rate used by Krause et al. *Shear rate was not reported, but calculated from the data presented.

The viscosity found in this thesis compares well with data from Krause et al. (1982) for Simplex P cement (p=0.6). It is not clear what type of cement was tested by Dunne and Orr (1998), but the above adjusted viscosity value is close to that of two cements studied by Krause et al. (1982). Liu et al. (1987) tested Zimmer PMMA, and the adjusted value is much higher than that reported by Krause et al. (1982) for the same cement (79.1 Pa·s). The reason for this is not clear, although the procedure used by Liu et al. (1987) is not well described. It is possible that the assumption of a constant power index over the wide range of shear rates involved is not valid.

It should also be noted that Krause et al. (1982) reported that their rheometer overestimated the viscosity by about 6% compared to a reference fluid, and adjusted their viscosity calculations by mathematically increasing the capillary length. This step was omitted in this thesis, but would bring the values closer to agreement.

Addition of bone particles to the cement may have two effects that would increase the viscosity: 1) The largest particles were 4 mm, which is almost half the diameter of the capillary. During testing, if several large particles approached the capillary entrance

simultaneously, they could block the entrance, impeding flow; 2) The bone particles were dry and would attract water, decreasing the effective water:cement ratio and therefore increasing the viscosity of the cement paste. There was a very large increase in apparent viscosity due to the addition of a small amount of bone particles, and both phenomena may have occurred.

Apparent viscosity of the calcium phosphate cement was slightly higher than PMMA, but increased rapidly after about 30 seconds. This is most likely due to the plunger approaching the bottom of the reservoir. For example, the 'knee' of the force-displacement curve i.e. where the force starts to increase rapidly, occurs when the plunger is approximately 5 mm from the bottom of the reservoir and the paste cannot flow freely into the capillary. PMMA viscosity increases with time due to polymerisation, but the calcium phosphate setting reaction is reported to be very slow at room temperature (Knaack, 2000) and should not affect viscosity. Addition of 25% bone greatly reduced the ability of the paste to flow, although it would probably be easy to use in a typical PMMA hand syringe, which has a much wider opening. Increasing to 50% bone prevented *any* flow through rheometer, although it was still easy to manipulate by hand. It might be possible to inject this through a syringe, but scooping/packing may be necessary. This would be similar to the current impaction allografting procedure, although the impaction forces could be much lower since packing of the particles may not be as critical. The composition of 75% bone behaved like a particulate material, even in its handling phase, and would definitely require packing instead of injection. A simple test with a PMMA hand syringe would confirm this.

As explained above, reported viscosity values are apparent viscosity. Corrections may be necessary to completely determine the flow characteristics of the materials, however the apparent viscosities give a good impression of the relative 'workability' of the materials. Since the force required to extrude the paste is proportional to viscosity and inversely proportional to (capillary radius)$^4$, the large increase in viscosity could be offset by a small increase in the syringe opening.

The particle size distribution produced in the operating room would include larger particles than used in this thesis since larger particles would not be discarded, and it is

doubtful whether a second morsellizing procedure would be performed. This may require a further increase in the syringe opening.

## 4.3 Mechanical Properties

### 4.3.1 Uniaxial Tests

#### 4.3.1.1 Compression

There are several pitfalls that must be acknowledged during platens compression testing. 'End artefacts' are created by friction at the specimen-platen interface which creates complex stress states close to the specimen ends. These multi-axial stresses can cause premature failure of the specimen, resulting in strength values being underestimated (Keaveny, 1997). Preliminary testing with Plaster of Paris specimens showed that specimens often failed near the end, suggesting that this effect was occurring. Addition of a graphite coating and a thin film of silicone lubricant to the platen surfaces eliminated this problem. All specimens used in this study were inspected following failure, and no failures appeared to initiate at specimen ends.

To ensure accurate material properties, the applied force must be properly aligned and coincident with the specimen axis. An inclined force (not parallel to specimen axis) will reduce the axial compressive force compared to the measured force, resulting in an overestimated stress value, while an eccentric force will increase the stress in part of the specimen, causing premature failure (see Figure 4.3). Care was taken to minimize both effects during specimen preparation and test setup. The ends of the specimens were sanded flush with the mould before removal, ensuring flat, parallel ends that were perpendicular to the cylinder axis. Alignment of the lower platen with the base of the test machine was performed with a dial gauge, and point loads were applied through a ceramic ball and upper platen to eliminate bending moments from specimen-platen misalignment. The lower platen was adjusted to within 0.10 mm of parallel over the 25 mm diameter, resulting in a maximum misalignment of 0.2°. This corresponds to a maximum error of less than 0.01% due to angular misalignment of loading and specimen axes. Any shear force due to an inclined applied force was assumed negligible due to the preparation of the platens. More important is coincidence of applied force and specimen axis. For a small radial malposition, $r$, of the specimen relative to the line of force, an

additional stress due to bending will cause premature failure. The actual stress in the specimen cross-section will be underestimated by 100(8r/D) percent by assuming uniform loading. For example, with a specimen diameter of 12 mm, a misalignment of 0.1 mm would result in roughly a 7% error in the strength. Attempts were made to align the specimen axis, platens and loading axis as accurately as possible. Ideally, uniform strain would be verified in each specimen with strain gauges. These errors are small compared to the variability due to specimen composition (see below).
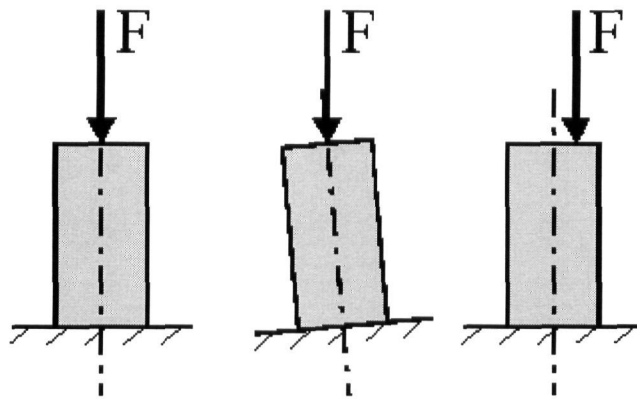


**Figure 4.3:** Specimen alignment errors. Desired loading is shown on the left: the force is parallel to and coincident with the specimen axis. Angular misalignment (middle) results in an overestimate of the axial force in the proportion $\cos\alpha$, where $\alpha$ is the angle of misalignment. Malposition of the force (right) creates bending stresses in the specimen in addition to the uniform compressive stress. The additional stress is $FrD/2I$, where $r$ is the radial misalignment.

It should be noted that the bone particles used in this study were defatted, cleaned and dried. This procedure was performed to facilitate sieving of the particles, and is expected to reduce the variability of measured mechanical properties. This is not done in the current impaction allografting procedure, and exudation of these fluids from the graft under load is thought to be a probable mechanism for graft layer creep (Giesen, 1999; Voor, 2000). However, graft preparation i.e. morsellizing, is done during surgery, and the long defatting and cleaning procedure is not feasible. The consequence of fat and marrow present in graft-cement composites is unknown. The bone-cement interface would not likely be affected since there appears to be no adhesion (see below), although the fluids may displace some of the cement, increasing the porosity and thus decreasing the strength. Additionally, the fat and marrow may interfere with the setting reaction of the calcium phosphate cement, but such chemical analysis and its effect on mechanical properties is beyond the scope of this thesis.

Addition of calcium phosphate cement to the morsellized allograft produced large changes in the material properties. Under compression, the largest changes were seen in the modulus and the strain to failure. As would be expected, higher proportions of cement produced stiffer specimens with lower ductility, and the trends were consistent across the range of compositions tested. There was a smaller change seen in the strength of the material, although the ultimate compressive stress increased with the addition of cement, up to 50% cement, after which it remained roughly constant at about 2.5MPa. The strain energy absorbed by a material before failure is proportional to the product of ultimate strain and ultimate stress. Due to the strong decreasing trend in strain to failure with increasing cement content, the strain energy absorbed before failure also showed a decreasing trend with increasing bone content. The trend, however, was not as strong as for ultimate strain due to the inconsistent relationship between strength and bone content. For homogeneous porous materials there is often a correlation between strength and modulus, since both are related to porosity (Hayes, 1991). In aggregate-cement composite materials the relationship isn't as strong due to the additional possible failure mechanisms (see below). For example, Giaccio and Zerbino (1998) found a weak but significant positive correlation between the modulus and ultimate strength for concrete under compression ($R^2$=0.23, p=0.002). A similar correlation was found in this study when data from all compositions was pooled together ($R^2$=0.34, p<0.0005). It is interesting to note that the modulus increased more rapidly with strength for 50% bone specimens than for 75% bone specimens (p<0.0001). The reason for this is not clear, and may be due to complex relationships between different characteristics of the composites. A hypothesis for this finding is as follows:

- The cement matrix in 75% bone specimens may not have been structurally continuous throughout the specimen, so stiffness was provided mostly by the bone particles, and strength provided by bone particle interlocking and matrix cohesion.

- At 50% bone, specimens were observed to be more continuous regarding the cement. Thus for this composition, strength and stiffness were provided by the cement matrix.

Failure modes of the compression specimens can be broadly classified as three types based on fracture patterns:

- Compressive failure, in which cracks were oriented primarily perpendicular to the loading axis, shown in Figure 4.4, left.

- Tensile failure, in which only a few, large cracks were seen, and were oriented parallel to the loading axis, shown in Figure 4.4, middle. This was caused by 'barrelling' of the specimen, creating tensile hoop strains.

- Shear failure, in which the predominant crack was at 45° to the loading axis, shown in Figure 4.4, right.
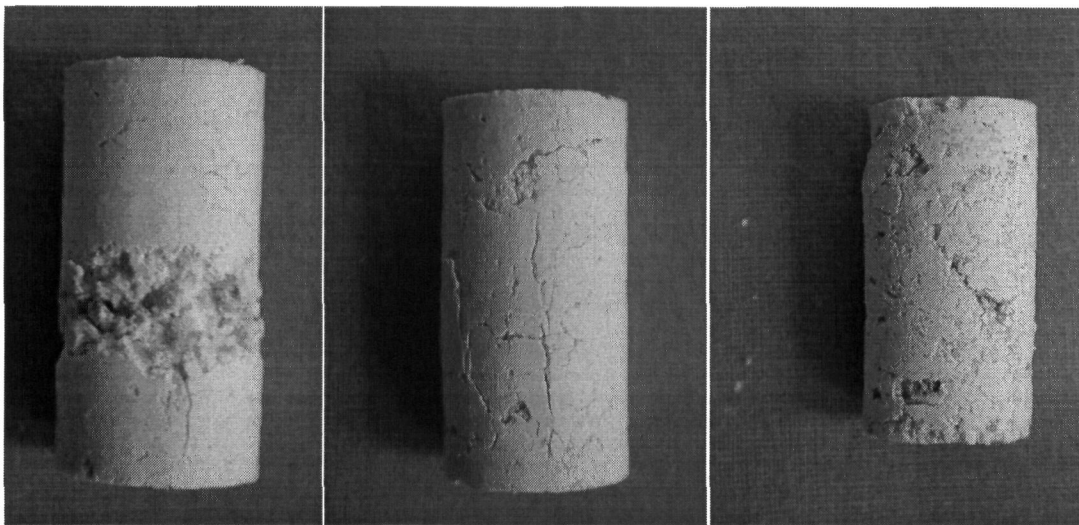


**Figure 4.4:** Compression specimen failures. Failure modes may be classified as compression with mostly transversely-oriented fractures (left); tensile or hoop with mostly axially-oriented cracks (middle); or shear, with a fracture at approximately 45° to the loading axis (right).

There did not seem to be any correlation between failure mode and stress-strain characteristics or mechanical properties, however specimen numbers were limited. Additionally, categorization of some specimens was difficult because cracks appeared to be oriented randomly. Specimens of 75% bone tended to crumble rather than exhibit one of the failure modes described above. This may have been due to discontinuities in the cement. Although this was not verified microscopically, these specimens appeared macroscopically to be a collection of bone particles glued together, whereas at 50% bone and lower, the specimens appeared more like bone particles embedded in a continuous matrix. Since there seems to be no cement-bone adhesion (see below), consequences of cement discontinuities would be to greatly reduce strength and stiffness. This may be the

reason for the large changes seen as cement content increased from 25% to 50%. Additionally, the large variability seen in 75% bone specimens may be due to the quality of packing i.e. elimination of these discontinuities, and 25% cement may be insufficient to achieve this consistently.

Direct comparison to 100% bone is difficult since bone particles are not easily tested under uniaxial compression. However, compressive and tensile properties can be combined to create failure envelopes using the Coulomb-Mohr failure theory, which can also be applied to particulate materials. This will be discussed below.

Some batch-to-batch variability was seen, although these differences tended to be small compared to the effect of bone fraction. Perhaps of clinical significance, however, is that the batch variability tended to be higher for high bone fractions. This suggests that more consistent mechanical properties may be achieved in surgery with a higher cement-bone ratio.

### 4.3.1.2 Tension

Under diametral tension, strength showed a trend similar to compressive strength as cement content increased. The strength increased up to 50% cement, after which it showed a small decline (see Figure 3.9).

Ideally, cylindrical specimens should fracture across the diameter. This occurred for specimens of pure cement, but in specimens containing bone, the fracture surface was not quite as clean, as shown in Figure 4.5. There are two probable locations for crack initiation, either at pores in the matrix, or at the cement-bone interface. As will be explained below, cracks probably initiated at the cement-bone interface, and grew through the matrix. Thus, as bone fraction increases, tensile strength should decrease. However, some of the bone particles may have acted as crack arrestors. Continuation of the crack around the particle would require an increase in energy. It may be that crack arresting occurred significantly more in 50% bone specimens resulting in a higher strength, although this has not been confirmed.
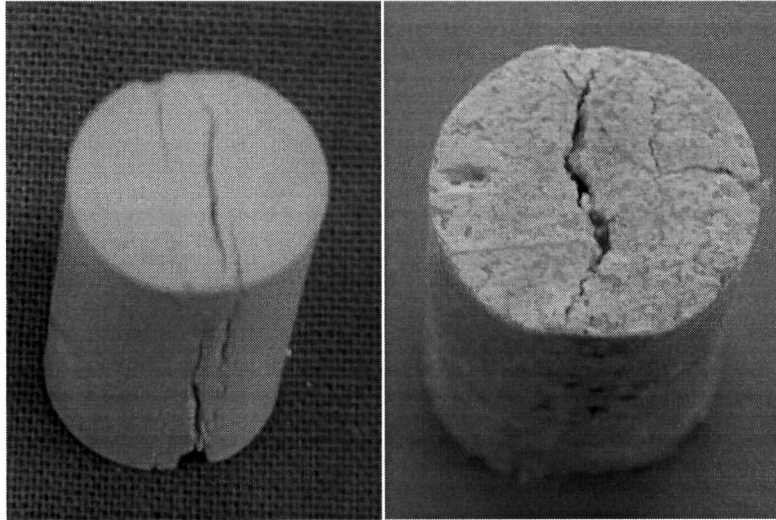
**Figure 4.5:** Tensile testing failure. Pure cement specimens (left) fractured across the diameter. Specimens containing bone particles (right) typically failed across the diameter, although the fracture may have interacted with the bone particles.

Results of 75% bone specimens should be interpreted with caution. While some specimens exhibited definite failure behaviour, others crumbled without any reduction in force. Diametral tension testing is ideal for brittle materials with low tensile:compressive strength ratios so that tension dominates the failure. However, the increased ductility of the 75% bone specimens resulted in a transition from diametral tensile stress, parallel to the lower platen, to a compressive stress perpendicular to the platen. Since the load on the specimen as seen by the load cell is compressive, this transition could not be easily detected. In this case, the strength was defined as the yield stress i.e. where the stress-strain curve softened.

If bone particles alone are assumed to have no tensile strength, then the addition of cement significantly increased the tensile strength ($p<0.0008$; SNK post-hoc) for every composition.

The tensile and compressive strengths of the calcium phosphate cement were low compared to other calcium phosphates. Driessens et al. (1995) studied the compressive and diametral tensile strengths of DCPD, OCP and CDHA cements. They measured strengths of 4.8, 28 and 36 MPa, respectively, in compression, and 1.1, 4.8 and 8.0 MPa, respectively, in tension. The higher strengths may be due to higher crystallinity of the cements tested. Standard deviation of the results ranged from 6% to 11% in compression

and 2% to 27% in tension  This is similar to the variability found in this thesis, 8% for compressive strength and 21% for tensile strength of the pure cement specimens.

Some batch-batch variability in uniaxial tests, especially at high bone concentrations (50% and 75%), suggests that material properties are sensitive to preparation 'skill'.  This also seems to be a problem with the current impaction allografting technique, so adding cement should make the resulting allograft layer properties more uniform from one surgeon to next and one surgery to next (i.e. less inter- and intra-surgeon variability). Giaccio and Zerbino (1998) found the coefficient of variation for concrete to be 4% in compression and 11% in tension.  Variation in this study was much higher: 8 to 47% in compression; 20% to 42% in tension.  This may be due to smaller specimens, higher aggregate volume fraction and larger relative size of the particles used in this study.  Liu et al. (1987) measured the properties of PMMA containing 0 to 30wt% bone particles of 150 to 300 $\mu$m diameter.  They found a coefficient of variation of 2 to 8% for tensile strength and 2 to 16% for the modulus.  The larger particle size used in this study, compared to specimen size, would be expected to increase the specimen variability.  In measurement of material properties, it was assumed that the specimens behaved as a homogeneous material.  Thus particle size and distribution throughout specimen would influence the material properties, and may increase the variability of the results.  X-rays of the specimens were made, but $\alpha$-BSM is very similar to bone mineral, so there was insufficient contrast on x-ray to quantify particle distribution.  Qualitatively, however, there were no abnormalities seen.

The cement-bone composite specimens were weaker and softer than traditional acrylic bone cement, which has ultimate compressive and tensile strengths of 70-100 MPa and 30-50 MPa, respectively, and a modulus of 1.7 to 2.7 GPa (Burke, 1984; Lewis, 1997; Robinson, 1981; Saha, 1984).  These same studies report coefficients of variation for strength of 3 to 9% in compression; 4 to 14% in tension; and 2 to 11% for the modulus, depending on brand and mixing methods.  These are expectedly lower than the coefficients of variation found in this study, since PMMA is a homogeneous material.

### 4.3.1.3 Compression vs. tension

Giaccio and Zerbino (1998) found that splitting tensile strengths varied from 6% to 21% of compressive strength for various different concretes, but the ratio tended to be higher as compressive strength decreased. The ratio of tensile to compressive strength vs. compressive strength for concrete is shown in Figure 4.6 (solid squares). Also shown are the results for specimens in this study (open circles); each data point is calculated from the average tensile and compressive strengths for the four different compositions. It would appear that data from this study fits the general trend shown by Giaccio and Zerbino (1998).
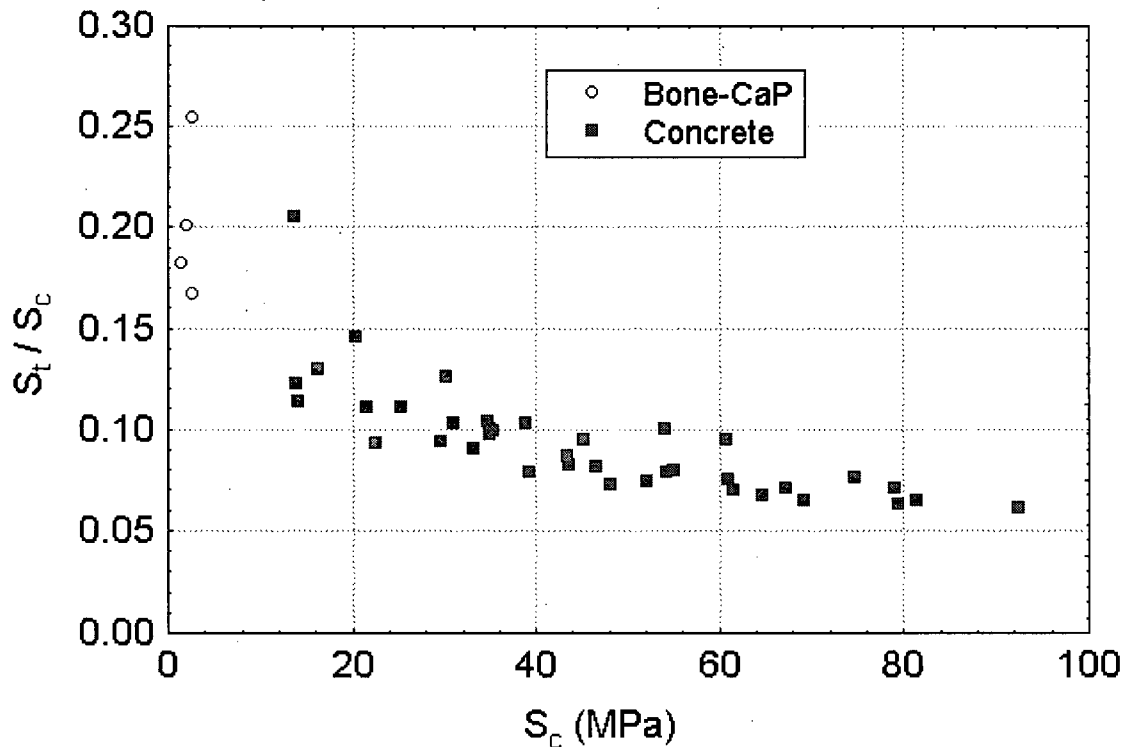


**Figure 4.6:** Relationship between tensile and compressive strengths of concrete (solid squares) and bone-cement specimens (open circles). Shown is the ratio of splitting tensile to compressive strength ($S_t/S_c$) vs. the compressive strength ($S_c$). $S_t/S_c$ tends to be higher for low compressive strength, and extrapolating concrete results (Giaccio, 1998) down to low compressive strengths suggests that data from this study fit the general trend.

### 4.3.1.4 Shear

Significant problems were encountered in the shear testing. This mainly resulted from material being trapped between the two grips. Tolerances of the pieces were such that any intervening material could cause binding, and greatly increase the measured force.

Preliminary torsion tests were done with Plaster of Paris, but gripping the specimens was problematic, and failure often occurred between the specimen and grip. Specimens of high bone content would only make such testing more difficult. For future testing, moulds could be designed that allowed simple shear testing without removal from the mould.

### 4.3.1.5 Failure Mechanisms[2]

Since the composite material studied in this thesis is similar in structure to concrete, it is interesting to compare the characteristics of the two materials. Concrete is generally considered to be a three-phase material: aggregate (gravel, pebbles, sand etc.), cement, and a transition zone in the cement adjacent to aggregate particles. The transition zone forms because thin films of water accumulate around aggregates. This increases the local water-cement ratio, resulting in a zone of weaker material due to larger crystals and the formation of flat $Ca(OH)_2$ crystals that serve as preferred cleavage sites. Although the specimens in this study were not chemically analysed for the presence of a transition zone or crystallographic structure, it is possible that a similar process occurs. The bone particles were initially dry and would attract water, increasing the local water-powder ratio during specimen preparation. An elevated water-powder ratio is known to decrease the compressive strength of α-BSM (Knaack, 2000). Thus it is likely that a transition zone forms during setting of the composite material.

The role of the transition zone in the bone-α-BSM material is probably small, however. Giaccio and Zerbino (1998) showed that in concrete, course aggregate produced the strongest cement-aggregate bond due to the rough surface, thus producing the highest compressive stress. Generally, compressive strength increases with aggregate roughness (i.e. bond strength) until aggregate strength becomes the limiting factor. For smooth-surfaced aggregates, such as gravel, cracks start at the interface and grow through the matrix: Giaccio and Zerbino (1998) found extensive bond failure, with no fractured aggregates. As bond strength increases, more cracks initiate at, and pass through aggregates. It appears that bone chips have a relatively smooth surface like gravel,

---

[2] Failure processes in concretes are from Mehta and Monteiro (1993).

although fractured surfaces are slightly rougher (see Figure 4.7) thus producing stronger bonding with cement.
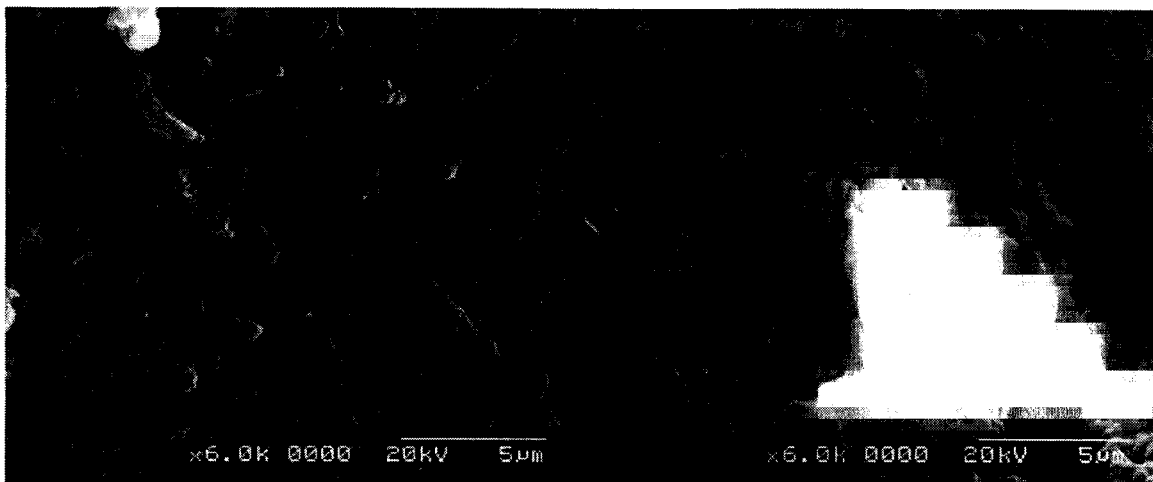


**Figure 4.7:** SEM micrograph of a bone particle surface. The normal surface of a trabecula (left) is smooth. The fracture of trabeculae during morsellization creates a rougher surface (right), which would create better bonding with the cement. The original magnification is the left-most number at the bottom of these and all subsequent images; e.g. in this figure it is 6000x; a length scale is shown in the bottom right corner.

Bone particles and calcium phosphate cement were difficult to differentiate under the scanning electron microscope. However at high magnification (6000x), texture of trabecular surfaces (see Figure 4.7, left) was quite smooth and different from that of fractured calcium phosphate cement, allowing identification of bone particles. Fractured surfaces of bone particles (Figure 4.7, right) were quite similar to the cement, though, so accurate assessment of cement adhesion was impossible under SEM. Figure 4.8 shows a bone particle on the tension test specimen fracture surface. The bone particle was identified at 6000x magnification, as explained above. The particle was delineated by a continuous gap around the entire perimeter, indicating that the entire bone-cement interface had failed. Figure 4.8b is a higher magnification image of the bone-cement interface, showing that there is no adhesion between the cement and bone. There is a fracture evident in the bone particle, but since the cement matrix tensile stresses could not be transferred through the interface to the bone, it is unlikely that this was created during testing. The fracture may have occurred *in vivo*, or more likely during the morsellization process.
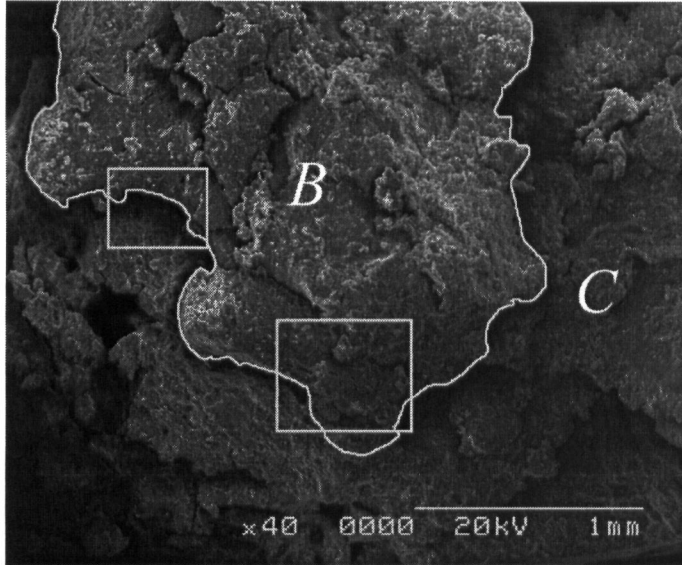
**Figure 4.8a:** Low magnification SEM micrograph of a bone particle on the tensile failure fracture surface. The bone particle (*B*) is embedded in the cement (*C*), however there is no bonding at the interface (rough outlined). The smaller box on the left of the image is enlarged in **Figure 4.8b**, and shows separation of the cement from the bone particle. The larger box is enlarged in **Figure 4.8c** and shows fractures in the bone particle.
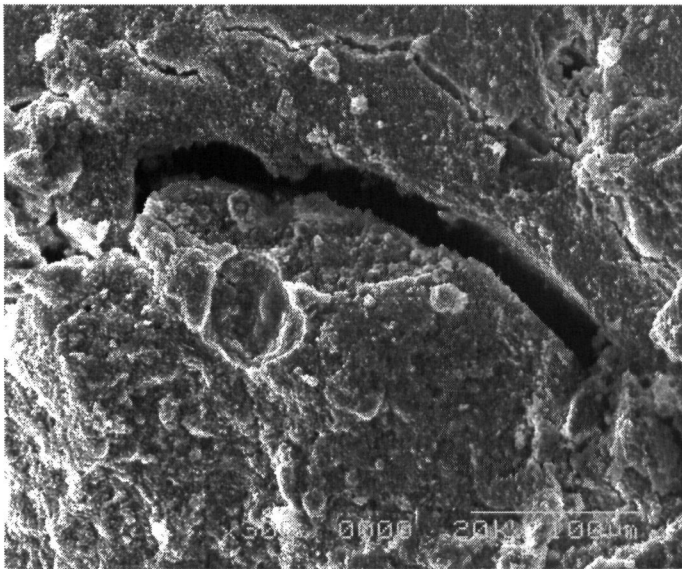


**Figure 4.8b:** Higher magnification of the bone-cement interface. The cement (below gap) has pulled away from the bone particle (above gap) since there is negligbile adhesion, and the interface cannot resist tensile forces.
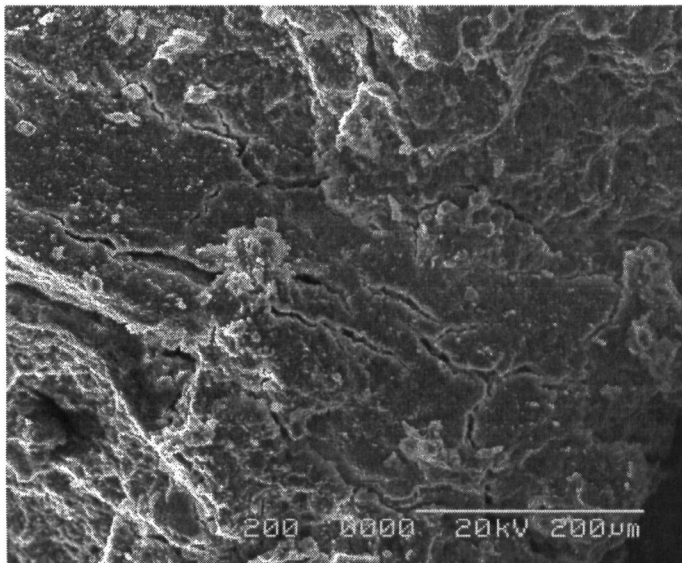


**Figure 4.8c:** Higher magnification of the bone particle. Fractures are evident, and are likely produced by the morsellizing process.

There was no evidence of complete bone particle fracture in the specimens analysed by SEM. It should be noted that in the specimens above, the bone particles appeared to be whole i.e. no corresponding bone fragment could be visually identified on the other side of the fracture surface. Thus the fracture travelled completely around the particle, and the bone-cement interface seems unable to resist tensile stresses. A similar process occurred in axial compression specimens: tensile hoop strains occurred in the cylindrical specimens due to Poisson's effect. This produced an axially oriented crack in many specimens since the calcium phosphate cement is weak in tension. When the crack encountered a bone particle, the fracture path easily went around the particle since the interface has minimal tensile strength, as shown in Figure 4.9.
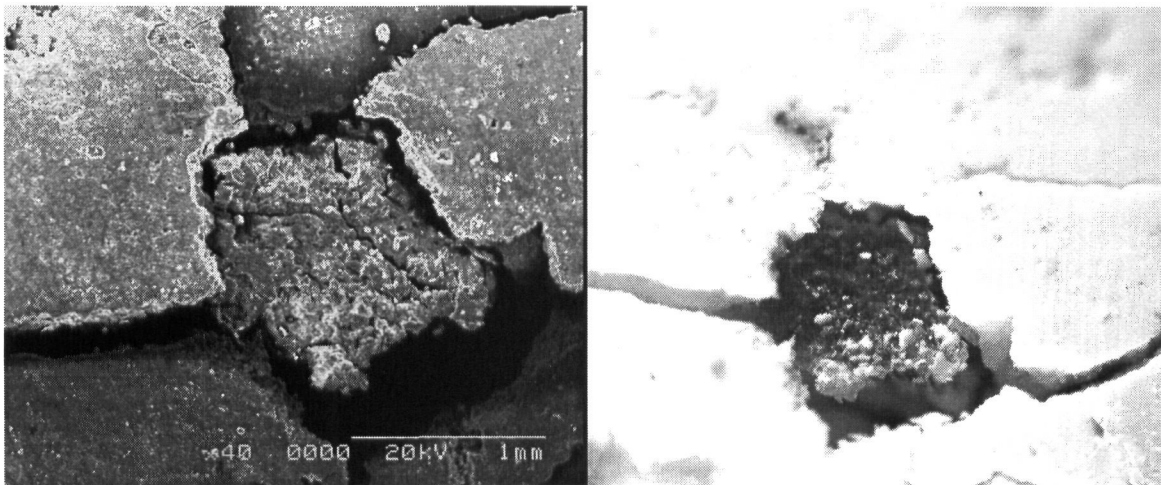


**Figure 4.9:** Path of fracture around a bone particle in compression testing. The SEM micrograph, left, shows an axially-oriented crack on the surface of the specimen travelling around a bone particle. The main crack is oriented horizontally in the picture, which can be seen more clearly under light microscopy (right). There is some adhesion of small calcium phosphate cement fragments to the bone, but failure is mostly at the interface.

Since the bone-cement interface strength appears to be negligible in tension (and probably also in shear), fractures probably initiated at the interface as they do in concretes with smooth-textured aggregates (Giaccio, 1998). It was assumed that this phenomenon dominated the failure process of the specimens in uniaxial testing. In specimens of PMMA containing hydroxyapatite particles, Ishihara et al. (1992) similarly found that the lack of adhesion between hydroxyapatite particles and PMMA limited the compressive and tensile strengths of the composite specimens. When a bonding agent was added, PMMA adhered to the hydroxyapatite particles, and tensile and compressive strength increased.

Porosity of the cement may have also had an effect on the mechanical properties, since strength and stiffness are related to porosity (Liu, 1997; Le Huec, 1995). Liu (1997) showed that for constant porosity, strength and stiffness decreased with macropore size. Under tensile stresses, which may occur in the vicinity of bone particles even in compressive loading, the location of a bone particle would act as a macropore due to the lack of bone-cement bonding. Le Huec et al. (1995) showed that macropores had more influence than micropores on the compressive strength of hydroxyapatite, but the model was limited to two pore sizes, divided by a threshold size of 100μm. The relationship between material properties and cement porosity was not studied in this thesis, although porosity could be adjusted by altering the liquid-powder ratio for the α-BSM. The liquid-powder ratio in this thesis remained constant for all specimens, and was the minimum recommended by the manufacturer.

### 4.3.1.6 Failure criteria

Morsellized bone graft is the current standard for comparison of material properties, since it is used clinically. Since this material behaves like a soil, direct comparison with solid materials is difficult. The Coulomb-Mohr failure theory makes this comparison possible. The theory is appropriate for brittle materials and for materials with different tension and compression strengths, whereas many other common failure theories assume strengths are the same. It was shown that addition of the calcium phosphate cement results in expansion of the failure envelope of morsellized bone graft alone. Since some tensile and shear loading on the graft is expected (see Section 4.4, below), this added resistance to tension and shear may result in significantly lower graft layer subsidence rates.

Mohr-Coulomb theory is not necessarily appropriate for concretes since it tends to overestimate the failure stresses under multiaxial compressive stresses. A more realistic construction of the failure envelope is shown in Figure 4.10. It can be seen that the failure envelope is not a straight line, and under confining compressive stresses, resistance to shear does not increase as rapidly as the theory would predict. However, the theory is convenient and provides a good approximation for low compressive stresses.

Mohr rupture
envelope

Shear

Triaxial
compression

Compression-
tension

Simple uniaxial
compression

Simple uniaxial
tension

$\tau_o$

9

Compression     f          e d       c  b a   Tension
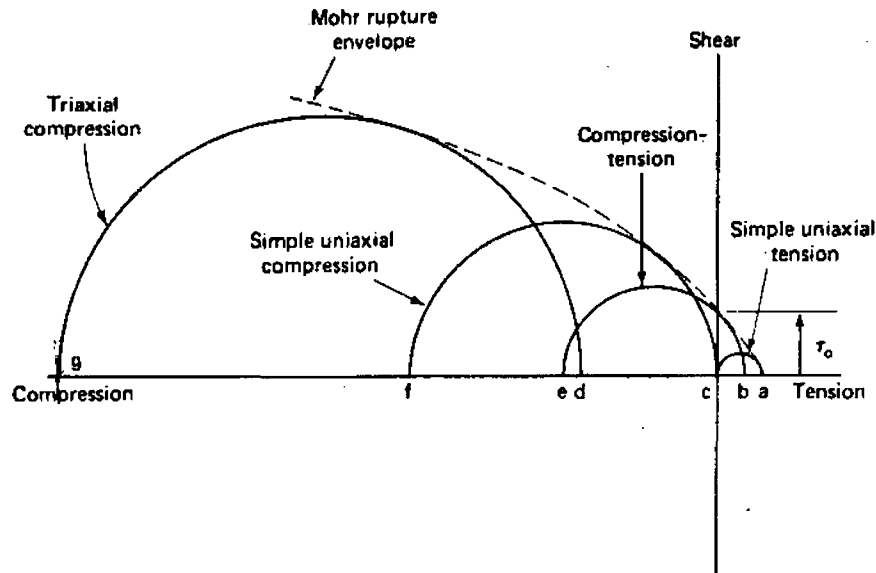
**Figure 4.10:** Modified Coulomb-Mohr failure theory. Increasing multiaxial compressive strengths form a rupture envelope with a decreasing slope. From Mehta and Monteiro (1993).

This study showed a large increase in shear resistance, measured by the cohesion coefficient, due to the addition of calcium phosphate cement. All compositions had significantly higher cohesion compared to bone particles alone, tested by Brewster et al. (1999) ($p<0.003$, Bonferoni). There were large differences in the mean cohesion coefficient between the different compositions, however significant differences may have been hidden by the large variability in the calculated values.

The angle of internal friction was significantly lower for 50% bone specimens compared to the other compositions ($p<0.01$, SNK post-hoc) and compared to bone particles tested by Brewster et al. ($p=0.02$, Bonferoni). This may not have any practical consequences, since at high multiaxial compressive stresses, the Coulomb-Mohr failure criteria overestimates the strength compared to experimental data (Mehta, 1993).

### 4.3.1.7   Confined Compression Tests

Adding up to 50% cement resulted in large increases in the confined modulus at all strain levels. Although the stress and modulus were not statistically analysed at 10% and 15% strain levels, they showed the same trend with bone volume as at 5% strain. Data at higher strains were included in the results to demonstrate the development of these properties with increasing strain.

For some specimens, a decrease in stress was seen at low strain. This occurred in the range of uniaxial compressive stress, suggesting a failure. Up to this point, the specimen was probably in uniaxial compression due to shrinkage during setting. After uniaxial yield, it is fully supported by the confining mould, and starts to behave as fully confined.

It was noted that some specimens showed a yielding behaviour at very high stresses, whereas others continued to strain-harden throughout the test. A decrease from the maximum stress-strain slope was assumed to be an indication of yielding, possibly due to pore collapse. This tended to occur more frequently in specimens of higher cement fraction: all four specimens of 100% cement, two of 75% cement and one of 50% cement behaved this way.

The confined modulus compares well with Voor et al. (2000) for bone particles. Voor et al. (2000) reported a modulus of 8 MPa, although this was at a compressive stress of 1.09 MPa. For 100% bone specimens in this thesis, a similar stress level occurred at 15% strain, for which the confined modulus was $11 \pm 1.5$ MPa.

Giesen et al. (1999) used biphasic theory to determine a confined modulus of $38.7 \pm 13.2$ MPa. This value is *not* the slope of the stress-strain curve; rather it is the ratio of applied stress to equilibrium strain in a creep experiment. Similar calculations from this study yield values of 5.2, 6.7 and 7.9 MPa at 5, 10 and 15% strain levels, although these are probably not fully-relaxed stress states (i.e. equilibrium), and the actual moduli would be lower. The different testing protocol makes the values difficult to compare, especially since Giesen et al. (1999) used preconditioning cycles which would increase the stiffness of the specimens during the test due to particle consolidation.

The low strain rate of this study was chosen to produce quasi-static loading. However, a large decrease in stress was seen when the test stopped, indicating significant stress relaxation. This effect diminished for high cement fractions. Thus the graft material behaviour is strain-rate dependent, so understanding its behaviour requires a range of strain rates to produce fully-relaxed to fully unrelaxed behaviour. *In vivo*, the loading of the graft is expected to be under 'force control'. The hip joint reaction force increases from zero to maximum load (~3xBW) in about 0.3 seconds for young people walking at an average pace (Bergmann, 1993). Elderly patients are likely to walk more slowly and place lower demands on the implant, but this may used as a rough estimate. Thus a

loading or strain rate should be chosen to achieve a maximum value in about 0.3 seconds to understand the *in vivo* load response. Additionally, response to cyclic loading should be studied to evaluate unrecoverable strains (i.e. creep) that would allow implant subsidence.

### 4.3.2 Uniaxial vs. Confined Behaviour

Under confined compression, the composite material was able to withstand very high stresses. In uniaxial compression, pores and particles may create regions of local tensile stresses. Crack extension under tension in a brittle matrix requires very little energy. The addition of confining stress will convert much of the tensile regions to compression, which requires very high energy for crack extension (Mehta, 1993). Thus material failure will require very high stresses. This should be differentiated from clinical failures, which could result from excessive graft layer strains, even though the material doesn't fail.

It is interesting to compare uniaxial vs. confined behaviour with an example. Assuming that shear test results are valid, an average shear modulus of 94 MPa can be calculated for pure cement specimens. Since the uniaxial compressive modulus is known (270 MPa), a Poisson's ratio of $\nu=0.436$ can be calculated.[3] Under confined compression testing, the biaxial stress state gives $\sigma_r = \nu\sigma_a$. One of the pure cement specimens displayed yield-type behaviour (deviation below maximum stiffness) at 35 MPa. A Mohr's circle for this stress state is compared to the Coulomb-Mohr failure envelope in Figure 4.11, assuming $\nu=0.436$. Two other stress states are also plotted, using more reasonable values for Poisson's ratio. Approximate rupture lines in Figure 4.11 (dashed lines) are estimated from the biaxial failure stress state and the failure envelope, and is a more realistic failure criterion (Mehta, 1993).

*In vivo* the graft layer will experience multiaxial stress states, however the degree of confinement will depend on the bone quality of the remaining femur, so the stress state may lie close to the uniaxial condition.

---

[3] This value seems high, especially since a porous material should be compressible. This value will be used for illustrative purposes, as well as values of 0.3, a typical value, and 0.2, for a more compressible material. Ideally this would be determined more directly e.g. with strain gauges.
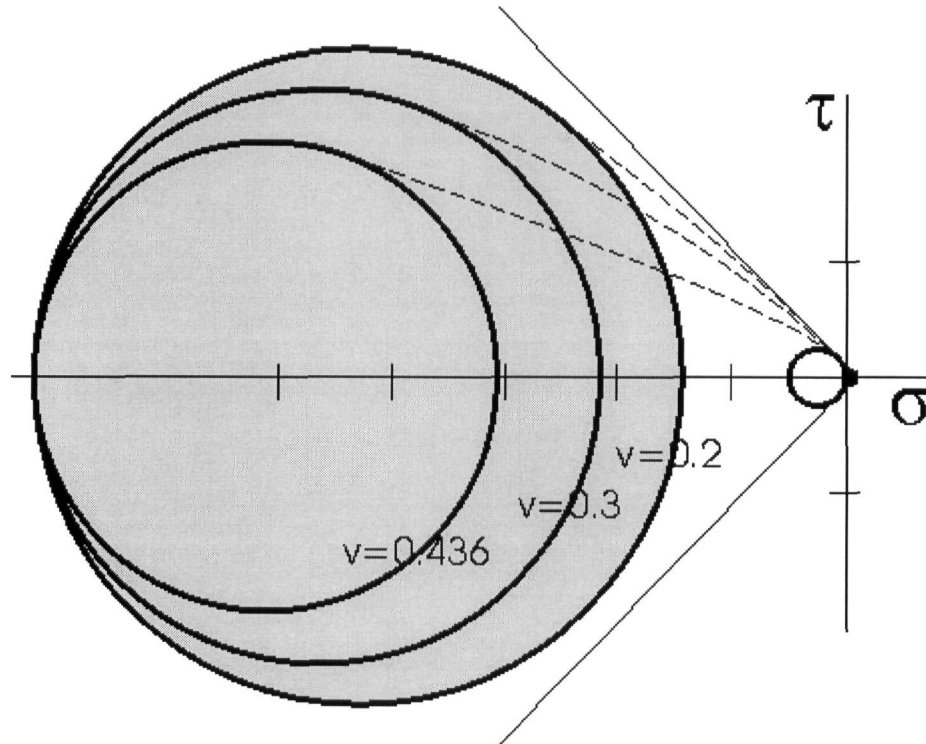
**Figure 4.11:** Mohr-Coulomb rupture diagram for pure cement. The Coulomb-Mohr failure envelope overestimates the failure in a biaxial stress state. Mohr's circles were constructed using values of Poisson's ratio indicated.

## 4.4 *In vivo Stresses*

There have been many studies examining the *in vivo* stress states of implant-PMMA-bone constructs, however most have examined the primary THA scenario. Mechanical studies of the revision THA scenario with bone loss are scarce. These are either finite element models or bench-top tests with strain gauge measurements. A finite element model can be labour-intensive to build, but with modern techniques using CT scans and specialised computer software, the process is simplified. However, once the base-line model has been built, FEA is a very convenient tool for parametric studies. In contrast, bench-top testing requires a lot of preparation work for each test specimen, and specimen variability may hide true differences. Additionally, the simulation of muscles is difficult, although not impossible. Despite these limitations, some investigators have used *in vitro* models because fewer assumptions are necessary, especially regarding interface conditions.

### 4.4.1 Strain gauge studies

Measurement of PMMA and bone strains in an *in vitro* model requires painstaking preparation for each specimen, and often high variability is seen in the results. This discourages many investigators, and there are relatively few such studies. However, two main studies have shed light on strains in the cement surrounding a hip prosthesis. Others have been performed, but mainly as validation of a finite element (FE) model.

Crowninshield and Tolbert (1983) embedded strain gauges in the proximal and distal cement to examine the effect of cement-stem bonding on the cement strains. They found that a fully bonded implant reduced axial, circumferential and radial strains in the proximal cement mantle with little effect distally. Measured strains in the unbonded case ranged from –0.28% to +0.17% and in the bonded case –0.22% to +0.14%. The authors claim this corresponds to maximum stresses of 10 MPa in compression and 6 MPa in tension, although it's not clear how they arrived at these numbers based on their measurements.

O'Connor et al. (1996) performed a more extensive three-part strain gauge study: 1) Axial, circumferential and radial strains were measured in three locations in the medial and three in the lateral cement mantle; 2) axial strains were measured in 37 locations in the lateral and 34 in the medial cement mantle; 3) rosette strain gauges measured the state of strain in the proximal cement. Highest strains were generally in the axial direction, being two- to four-times higher than circumferential and radial strain at the mid- and distal-stem. Axial strains were approximately constant over the length of the implant; average strains on the lateral side were approximately +300 $\mu$-strain whereas medial strains were approximately –400 $\mu$-strain. These strains increased to +1230 $\mu$-strain and –1475 $\mu$-strain at the distal stem tip on the medial and lateral sides, respectively. Failure of the PMMA cement mantle near the distal tip is often seen clinically (Gruen, 1979). Simulated stair climbing showed that proximal cement strains can increase almost three-fold.

In simplified implant models, it has been shown that smooth stems create more tensile hoop strains than rough stems, due to subsidence of the tapered stem into the cement (Manley, 1985; Verdonschot, 1998). Manley et al. (1985) found compressive axial cement strains of roughly 0.6% for both smooth and rough implants; tensile hoop strains

were 0.4% for the smooth stems and 0.2% for rough stems. It was also shown that rough stems produce more cement damage due to abrasive wear (Verdonschot, 1998).

Stolk et al. (2000) measured strains in the PMMA cement mantle and on the surface of a synthetic femur. Maximum and minimum strains in the cement were in the range of +150 to +300 μstrain and –400 to –800 μstrain, respectively, and increased from proximal to distal locations. Results showed good agreement with their FEA model, although better correlation was found with a Lubinus stem vs. a Mueller curved stem. In light of this, it is not known whether the FE model used by Stolk et al. (2000) can be extrapolated to other configurations.

### 4.4.2    Finite Element Studies

Finite element studies have been used extensively to examine stress states in the implant, cement[4] and femur, and to analyse the effect of many different parameters. Studies can be difficult to compare due to different assumptions and model characteristics such as:

1. Cement-stem and cement-bone interface conditions. Interfaces are modelled as either fully bonded, unbonded with friction, or unbonded and frictionless. Obviously stress states will vary depending on the load transfer mechanisms that each interface type can support. This is possibly the most important factor affecting stress patterns around implants (Huiskes, 1998).

2. Loading conditions. A load is applied to the implant, usually corresponding to the magnitude and orientation of the hip joint reaction force as measured by Bergmann et al. (1993) or similar studies. On the femoral side, the hip abductors are sometimes included as a superiorly-directed force on the greater trochanter. The vastus lateralis is rarely included, but can significantly affect the stress state in the femur and cement (Rohlmann, 1983).

3. Specimen geometry. In modern studies, femur models are usually built from CT scans, and implant models are built from the manufacturer's designs. Older studies usually use simplified two-dimensional or symmetrical three-dimensional models. More complex models have shown that stress and strain patterns are generally not

---

[4] For this section, 'cement' refers to PMMA bone cement. The resorbable calcium phosphate cement will be referred to as CPC.

symmetric (Rohlmann, 1983; Verdonschot, 1997b), especially regarding the direction of principal stresses.

Additionally, many studies make assumptions about various conditions in the model, particularly interface conditions, without any validation. Despite these problems, FEA remains a convenient and important tool to study trends in stress states due to parameter variation. One of the early and most complete FE studies was performed by Rohlmann et al. (1983) who examined stresses under various different loading conditions, and validated FE-predicted strains with experimentally-measured strains. This study will be used as the baseline case, and other studies will be introduced to describe the effects of different variables such as stem geometry, interface characteristics, material properties and femoral geometry. This last variable concerns the quality of the femur i.e. the primary versus revision scenario, and is important for the long-term goals of this study since the materials are being developed for use in revision hip arthroplasty.

Rohlmann et al. (1983) examined six loading conditions in a cemented implant-femur construct, three of which have historical and clinical significance. The first scenario is a single load on the implant head, which is used in most experimental studies due to simplicity, and also in many early FE studies. The second is the same load on the implant, balanced by an abductor force. This is by far the most common configuration in FE studies. The third is perhaps the most realistic configuration since it adds the inferiorly-directed force of the vastus lateralis, the so-called 'tension banding' effect. The role of the muscle forces depends on whether an osteotomy of the greater trochanter is performed during the revision surgery, and how it is reattached. This adds considerable complexity to the model, and will be ignored.

Rohlmann et al. (1983) first performed an experimental validation of the model and found that minimum and maximum principal strains on the femoral cortex showed good agreement with FE-predicted strains, as shown in Figure 4.12. There was some disagreement between the two methods, mostly on the anterior aspect of the femur and also proximally.
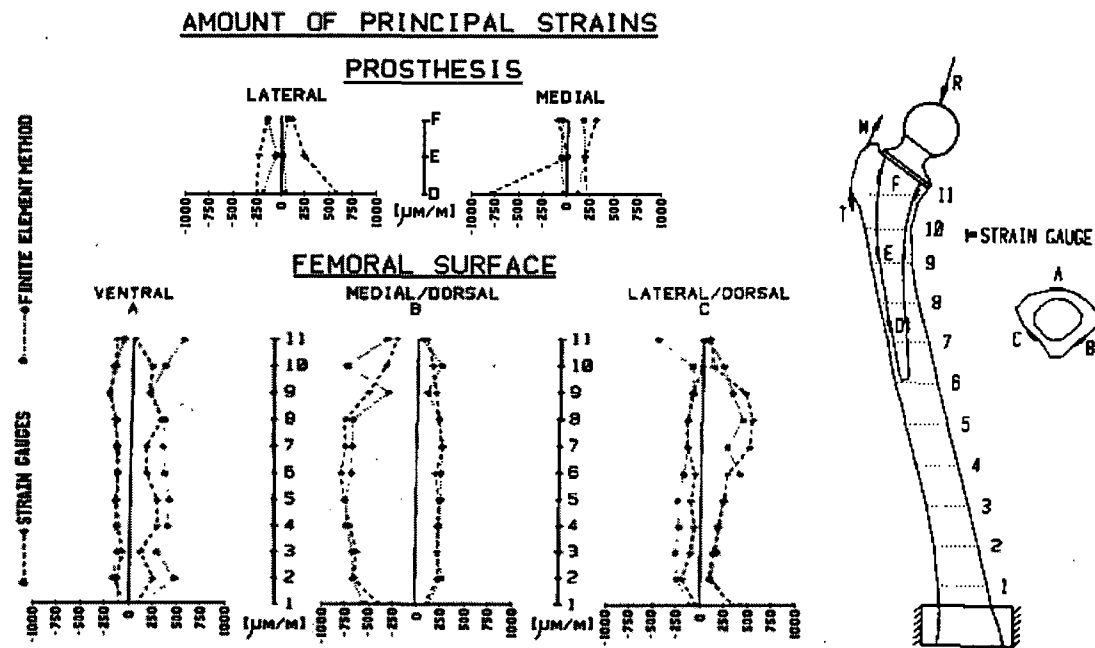
**Figure 4.12:** Comparison of FE-predicted and experimentally measured principal strains. Minimum and maximum principal strains generally agreed quite closely, although some differences were seen, especially anteriorly (gauge A) and superiorly (locations 10 and 11) on the femoral surface. From Rohlmann et al. (1983).

Principal stresses in the femur are shown in Figure 4.13 three of the loading cases reported by Rohlmann et al. (1983). Case 1 consists of a single load on the implant head, and omits all muscle forces. It is probably the most common for configuration bench-top testing since simulated muscle forces can be difficult to apply. Case 2 adds the hip abductors (M) as well as the vastus lateralis (T), the so-called tension-banding effect. Note the large reduction in bending compared to Case 1. Case 3 is presented since it is commonly used in finite element studies. It differs from Case 2 by the omission of the vastus lateralis. Note that Cases 2 and 3 produce similar principal stress profiles, although there is a small increase in bending due to the lack of the vastus lateralis muscle force.
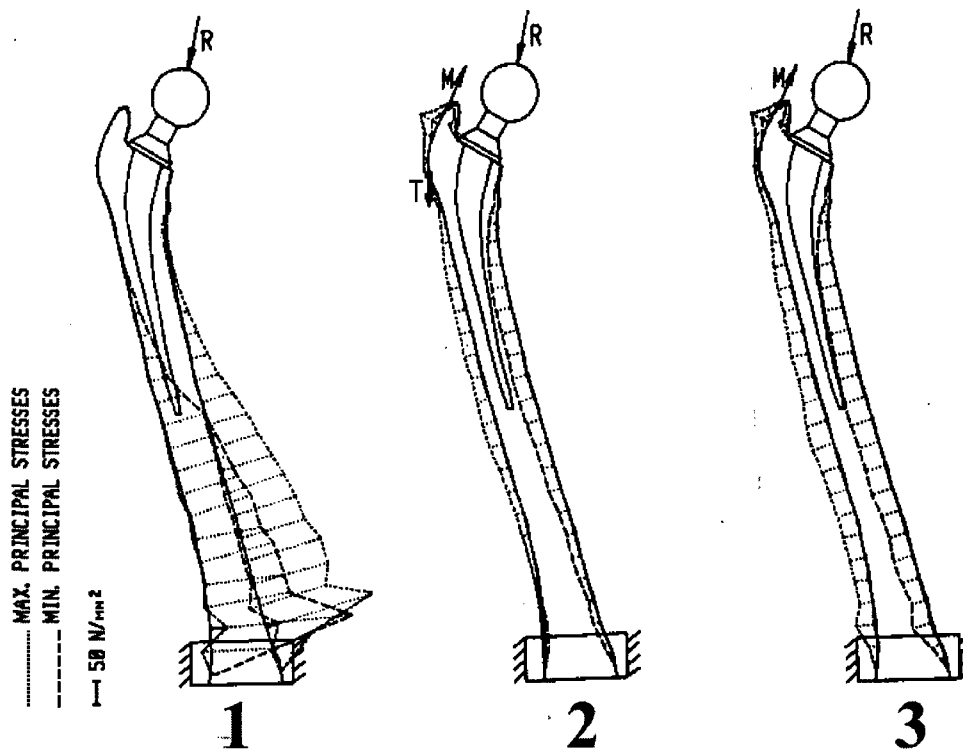
**Figure 4.13:** Principal stresses in a hip implant predicted by finite element modelling for three loading cases. The principal stresses change significantly depending on the loads incorporated in the model. From Rohlmann et al. (1983).

Figure 4.14 shows the cement stresses at the cement-stem interface. This is close to the location of the graft layer in the revision scenario, and may be rough estimates of the expected *in vivo* stress state in the composite graft layer. The principal stresses are relatively low in Case 1, although there is a large increase in both maximum and minimum principal stresses on the lateral side, near the distal tip of the stem. Addition of the muscle forces increases the stresses over the length of the implant with a large compressive stress on the medial side, just above mid-stem.
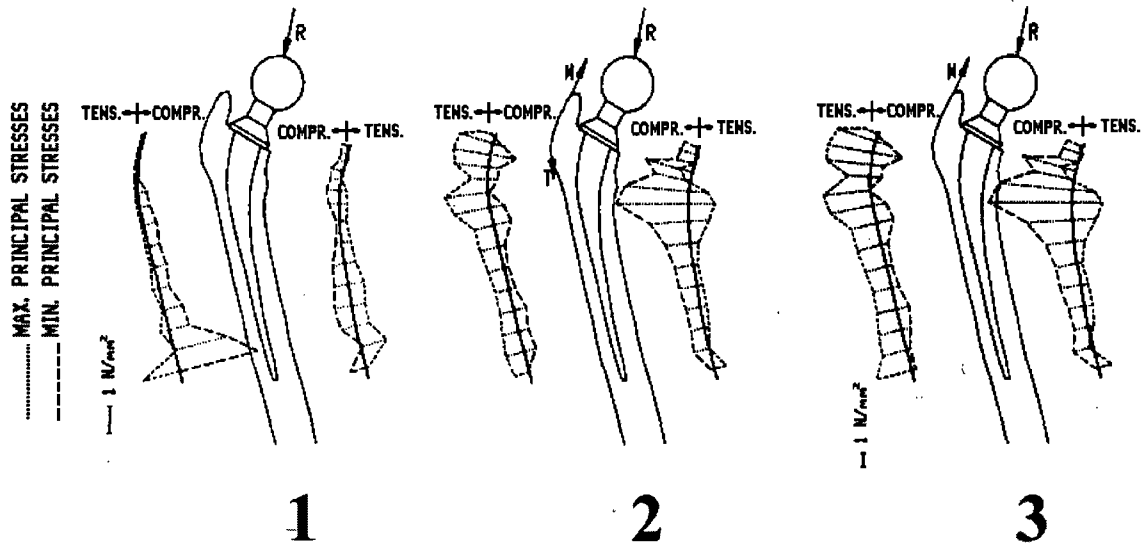
**Figure 4.14:** Cement principal stresses at the cement-stem interface predicted from FEA. Stress distributions can be affected by the loading incorporated in the model. Note that the stress scale is different for Case 3. From Rohlmann et al. (1983).

The graft composite layer is relatively weak in tension and shear, so the critical locations are where the maximum principal stress is largest and in tension, or where the difference between maximum and minimum principal stresses is greatest. There are locations in the cement where the maximum principal stress exceeds the uniaxial tensile stress of the CPC-bone composite in all three loading cases shown in Figure 4.14. An approximate Mohr's circle for the location of maximum principal stress difference is shown in Figure 4.15 along with the Coulomb-Mohr failure envelopes determined in Section 3.3.4.
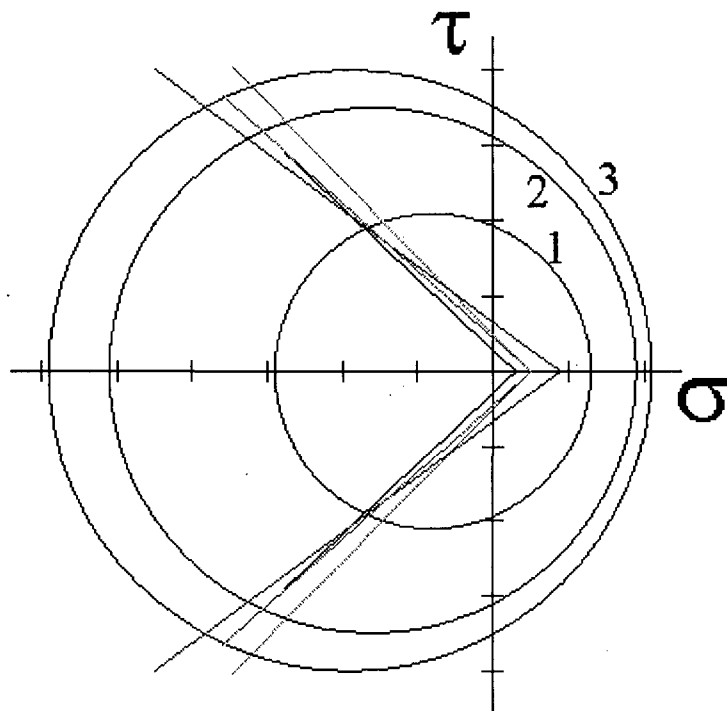
**Figure 4.15:** *In vivo* stress states compared to failure envelopes. Stress states were determined by finite element analysis by Rohlmann et al. (1983) and would cause failure in all compositions tested, represented by the Coulomb-Mohr failure envelopes. Numbers correspond to the loading cases 1, 2 and 3 shown in Figure 4.14. Tick marks on axes indicate 1MPa. Failure envelopes are from Figure 3.10.

Thus it appears that the *in vivo* stresses may cause failure in the graft composite. However, these may not be representative stresses due to different interface conditions and material properties, as will be explained below. Rohlmann et al. (1983) assumed a perfect bond at the cement-stem interface, allowing compressive, tensile and shear stresses. Debonding at the cement-stem interface is thought to be unavoidable (Verdonschot, 1997a; Jasty, 1991), and changes the stresses in the cement because the unbonded interface cannot transmit tension, and shear is limited by friction, and therefore the surface finish of the implant. A simple taper model in Figure 4.16 demonstrates this principle. Note that the interface stresses are largely compressive in the unbonded case.
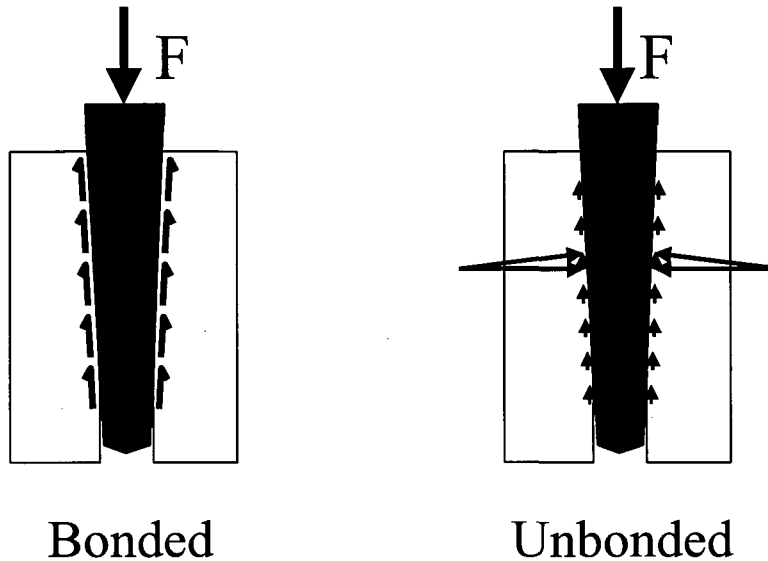
**Figure 4.16:** Stress transfer mechanisms for two different interface conditions. For the bonded case, the applied force is balanced largely by shear stresses at the interface. For the unbonded case, large compressive forces are required to balance the force, and depend on the taper angle. Some shear stresses may also be present, depending on surface roughness. Adapted from Huiskes (1990).

A collarless, polished, tapered stem is the most commonly used design with impaction allografting; six of the eight clinical studies reviewed in Section 1.2.4 used such a design. The polished surface finish prevents bonding at the interface (Crowninshield, 1998) such that tensile stresses cannot be transmitted across the interface (Mann, 1995; Chang, 1998). However, this may have little effect on the cement-bone interface stresses (Chang, 1998; Mann, 1997b), depending on the bonding characteristics at that location.

Most of these studies have examined stresses at the cement-stem interface, since this is often a critical location for primary hip implants. However, some studies have examined stresses at the cement-bone interface, which is closer to the graft layer location. Verdonschot and Huiskes (1996) showed that average tensile, compressive and shear stresses at the cement-bone interface generally increase from the case of bonded cement-stem interface to unbonded with decreasing amounts of friction, as shown in Figure 4.17.
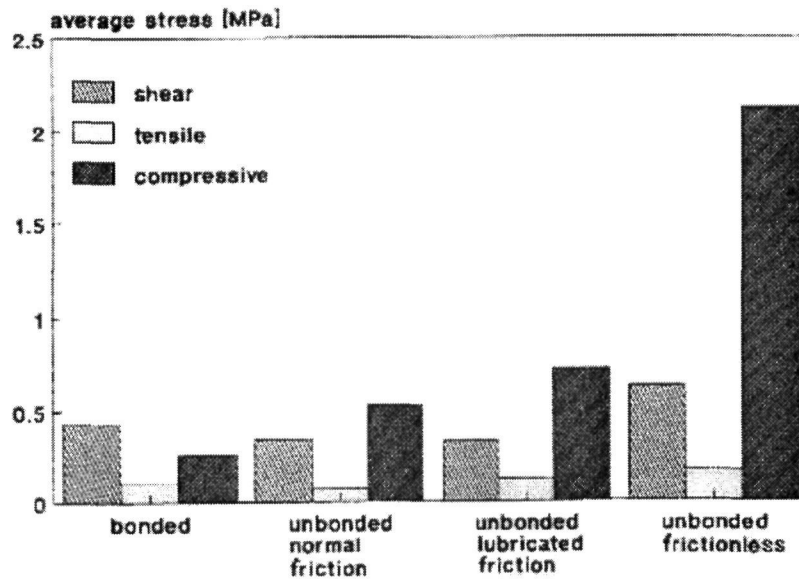
**Figure 4.17:** Stresses at the cement-bone interface for various different cement-stem interface conditions. From Verdonschot and Huiskes (1996).

Debonding does not prevent tensile stresses occurring in the cement, but it does change the orientation of the principal stresses due to altered load transfer mechanisms. Mann et al. (1995) found maximum tensile principal stresses of 5.5MPa for a bonded interface, and was almost normal to the interface. When the interface was modelled as unbonded with friction, maximum tensile stresses were 10.8MPa in the proximal, posterolateral cement mantle, and were oriented mostly circumferentially. This is much greater than the tensile strength of the CPC-bone. Of course, stresses in any material will be limited by the material strength, and stresses will be transferred to other parts of the construct if localized failure occurs. For example, if tensile stresses on the lateral side cause failure in the graft layer, load may be transferred to increase compressive stresses on the medial side.

Additional parameters that have been studied in the primary hip arthroplasty scenario are briefly summarized below.

**Stem geometry**

A distal circular cross-section increased proximal maximum principal stresses as well as proximal interface shear stress (Chang, 1998). A 'flat-sided' stem produced proximal interface shear stresses of 27% to 77% of the values for a 'distal-round' stem. This is

probably due to the decreased resistance to torsion provided by the round cross section, which must be resisted by the proximal region. This was true for both bonded and unbonded interfaces.

Neck length does not have a large influence on cement stresses (Chang, 1998).

Cement principal stresses are mostly unaffected by stem length for lengths above 100 mm (Rohlmann, 1987). For a 70mm stem, maximum and minimum principal stresses increase to +3.5MPa and –5.9MPa, respectively, both on the medial side. The maximum interface shear stress was 3.9 MPa. This was the same model as in Figure 4.13, and can be compared to loading case #3. A further decrease in length to 40mm produced very large increases in the stresses, but this length is unlikely to be used. In contrast, Crowninshield et al. (1980) found a linear decrease of maximum principal stress from 2.5MPa to 2.2MPa as stem length was increased from 100mm to 130mm for a comparable joint load. Minimum principal stress increased from -6.4MPa to -8.1MPa for an increase from 100mm to 110mm, then declined to -6.7MPa for a 130mm stem. The reason for the difference may be due to the simplified symmetric model used in the latter study.

Decreasing the taper angle of the stem increases the cement-bone and cement-stem interface shear and compressive stresses near the distal tip of the stem (Yettram, 1979), although no magnitudes were reported.

**Cement mantle geometry**

Fisher et al. (1997) showed that an increase in cement mantle thickness from 2.4mm to 3.7mm decreases the strains around an implant, especially in the distal region, where reductions were about 50%. Lee et al. (1993) also reported a reduction in distal cement tensile stresses by 50% and shear stresses by 12% due to a similar increase in cement thickness.

**Material properties**

An increase in stem stiffness has been found to decrease cement stresses, especially proximally. An alumina stem (E=400GPa) reduced maximum and minimum principal

stresses by 20% and 33%, compared to cobalt chrome (E=200GPa) (Rohlmann, 1987; Crowninshield, 1980).

Increasing stiffness of the cement increased the stress in the cement by 30% to 44% for increments from 1GPa to 2.3GPa to 4GPa (Rohlmann, 1987). Similar changes were found by Crowninshield et al. (1980), but one study claimed this had little effect (Yettram, 1979).

As a general effect, Huiskes et al. (1985) showed that a soft substrate distributes stresses more uniformly, reducing peak stress. This situation is similar to the graft layer as a substrate 'under' PMMA. Thus the stresses in the composite graft may be less than the stresses reported above.

These studies show that many factors can affect the demands on the cement mantle and the various interfaces. Additionally, strong interactions have been found between some of these variables (Chang, 1998; Mann, 1997b; Huiskes, 1998), so that changes in two parameters may not be additive. To properly understand the expected *in vivo* stresses, a finite element model is required with the appropriate femur, bone graft, cement and stem geometries and material properties. Finite element studies of the revision hip arthroplasty scenario are scarce. One possible reason for this is the apparent randomness of bone loss seen clinically, both in extent and location (Leopold, 2000). One finite element study examined the effect of stem length in a revision arthroplasty model (Mann, 1997a). All cancellous bone was removed from the femur to simulate osteolytic bone loss. The bone-cement interface was modelled as a soft, fibrous-tissue connection. The revision stem, of various lengths, was inserted into the femur, filling the gaps with cement. A summary of the cement mantle maximum principal stresses and cement-bone interface stresses is given in Table 4.2.

| Stem length (mm) | Maximum cement stresses (tension) | | Cement-bone interface stresses | |
|---|---|---|---|---|
| | Proximal (MPa) | Distal (MPa) | Normal (MPa) | Shear (MPa) |
| 140 | 7.1 | 7.9 | | |
| 173 | 5.5 | 10.7 | 0.9 | 6.3 |
| 207 | 5.4 | 9.0 | 1.3 | 4.2 |
| 240 | 5.4 | 8.8 | 1.4 | 3.5 |
| 273 | 5.4 | 8.8 | 1.5 | 3.5 |

**Table 4.2:** Maximum stresses in the revision hip for different stem lengths. For increasing stem length, maximum tensile stresses in the proximal cement decreased; stresses in the distal cement increased slightly, then decreased. Cement-bone interface normal stresses (compression) increased with stem length, whereas shear stresses decreased.

Again, these stresses would cause failure in the composite material, although this would cause the stress patterns to change. Further work with finite element modelling and *in vitro* bench-top testing is required to properly evaluate the CPC-bone composite material. The compressive stresses reported in the various studies are slightly higher than the uniaxial compressive strengths of the different CPC-bone composites tested, but are in the same range. If the graft layer behaves *in vivo* as in the confined compression tests, reported compressive stresses are within tolerable ranges for some of the compositions. For example, the 5.6MPa of compression reported by Rohlmann et al. (1983) would cause average strains in the material ranging from 4.0% to 35% (see Table 4.3). This compaction would allow stem subsidence as shown in Figure 4.18 and Table 4.3, assuming a rigid stem and cement, a taper angle of 10°, and CPC-bone composite layer thickness of 3mm under pure compression.
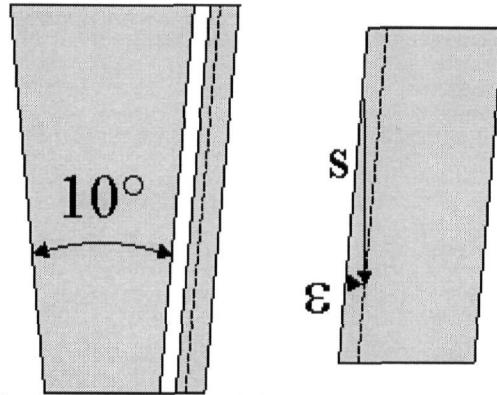
**Figure 4.18:** Subsidence of the implant due to graft layer compaction. Left: a load on the implant (grey taper) and cement (white) transfer stresses to the graft layer, causing it to consolidate to the dashed line. Right: graft layer enlarged; graft is compressed to the dashed line by a strain ε, allowing the stem to subside a distance 's'.

| Bone fraction | Strain @ 5.6MPa | Subsidence (mm) |
|---|---|---|
| 0 | 0.046 | 1.6 |
| 25 | 0.040 | 1.4 |
| 50 | 0.044 | 1.5 |
| 75 | 0.111 | 3.8 |
| 100 | 0.349 | 12 |

**Table 4.3:** Strain of composite material and subsidence of the implant under *in vivo* compressive stress. Minimal subsidence of the implant occurs with compositions of 0% to 50% bone, but greatly increases at high bone fractions.

The high strains shown in Table 4.3 for 75% and 100% are perhaps unrealistic, since load transfer mechanisms are significantly altered, and the implant may find another equilibrium stress state. The shear stress present would also cause subsidence due to graft layer distortion. These subsidence values are considered for trends only, and should be verified in more realistic models.

### 4.5  *Biological Considerations*

Addition of calcium phosphate cement to the graft layer has an unknown effect on the remodelling rates. α-BSM appears to resorb at a rate comparable to bone, but animal studies are required to verify resorption of the composite. α-BSM alone has been tested *in vivo* in both canine and rabbit models. In a canine femoral slot defect, resorption of α-BSM and replacement of host bone compared favourably to autograft (Knaack, 1998).

Only 1.3% of residual cement remained after four weeks. The amount of new bone filling the defect was lower for the cement compared to autograft at four weeks, but there was no difference at 12 weeks. Resorption and bone remodelling was improved by the addition of rhBMP-2, a growth factor that stimulates the differentiation of osteogenic precursor cells into osteoblasts. In a rabbit tibia critical-size defect model, Lee et al. (1999) showed α-BSM alone is replaced by woven bone through the entire thickness of the diaphysis after eight weeks. With the addition of the growth factor, the cement had been completely resorbed with restoration of the natural cortical diaphysis after the same time.

Although Norian SRS has a reported compressive strength much higher than α-BSM, remodelling characteristics do not appear to be as good. Controlled comparisons have not been done, and are unlikely to be performed. However, SRS has been compared to allograft bone in a canine tibial metaphysis defect model (Frankenburg, 1998). Resorption rates were comparable, but slightly lower than allograft. Minimal resorption of the cement occurred after 20 weeks, and more than 25% of the cement remained after 78 weeks. The authors did remark that the cement appeared to resorb faster in areas of cortical bone, where loads are expected to be higher.

Impaction allografting, as it is currently performed, produces a graft layer that may not completely remodel into viable bone (Nelissen, 1995). It is not known whether this would also occur with the composite graft material. However, growth factors may be introduced in the calcium phosphate to promote bone remodelling. Lee et al. (1999) showed that this could be done in a rabbit *in vivo* model, showing marked increase in remodelling rates with rhBMP-2.

### 4.6 Other considerations

Previous studies of impaction allografting, both *in vivo* clinical studies and *in vitro* mechanical testing, have examined the graft layer as a soil. Soils may resist shear forces in two ways: through interlocking of particles, known as cohesion, and by friction. As the shearing force increases, the irregularly shaped particles break, creating a 'shear band' (Craig, 1993). Once the shear band has formed, resistance to shear is by friction alone, and thus relies on normal compressive forces. Fractures in the bone particles could

be seen under SEM, and were attributed to the morsellizing process (see Figure 4.8c). These fractures lower the cohesion of the morsellized allograft because the particles would break apart earlier. Thus the morsellizing process itself appears to limit the shear strength and stiffness of the impacted graft layer. Some investigators have hypothesized that particle fracture also occurred under compressive consolidation testing (Giesen, 1999; Voor, 2000). Thus the fractures that occur during graft morsellizing may predispose the graft layer to early failure. Additionally, consolidation may occur due to particle movement and water, fat or marrow exudation under load. Addition of an interstitial cement may reduce the risk of both of these effects.

The brittleness of the cement is a concern, especially since it is relatively weak compared to bone and many other biomaterials. It may be possible to add other materials to the cement, such as collagen to add strength and toughness (Jew, 2000).

Addition of the calcium phosphate cement to the bone particles created a mouldable material. This should allow the surgeon to easily fill bone defect of any size or shape, and possibly eliminating the large impaction forces associated with the current allografting procedure. While this thesis has concentrated on revision hip arthroplasty, the material may be applicable to other locations such as knee replacement. Further investigation would be required to assess the suitability of the composite graft mechanical properties for such applications.

# 5.0 Conclusions and Future Work

Based on the findings in this thesis, the following conclusions may be made:

- Adding calcium phosphate cement increases the stiffness of the graft layer material, both in confined and unconfined states.

- Increasing cement content up to 50% increased the compressive and tensile strengths. Further increases did not produce large changes. However, batch variability tended to decrease with increasing cement content, indicating preparation skill became less important.

- Low cement fraction gave weaker, more compliant materials; low bone fraction gave stiffer but more brittle materials. A composition of 50% bone appears to be a good compromise, providing good strength and stiffness as well as some ductility.

- The cement paste alone flows like PMMA; thus surgical handling procedures could be similar. Addition of 25% bone allows some flow, although a large bore and opening in a syringe would be required. Higher concentrations of bone would require packing, similar to the current impaction grafting technique. The possibility of reducing the packing forces would reduce the risk of femoral fracture.

- Rough estimates of *in vivo* stresses discussed in the previous chapter suggest the graft composite may have adequate mechanical properties. Further work, including both FEA and more realistic *in vitro* testing is required to confirm this. These tests may include simplified taper models, synthetic femur-implant models and cadaveric femur-implant models.

- Further tests of the graft material should be performed to understand the effect of marrow and other fluids on the mechanical properties of the final, set material.

The biological characteristics of this composite material have not been assessed. There may be interaction between the biological and mechanical characteristics of the composite graft material. In particular, material properties may change during resorption/remodelling of the graft, affecting the stability of the implant over time. Thus *in vivo* animal studies are also required to assess the suitability of this composite graft material for use in revision hip replacement.

# 6.0 References

1. Archibeck, M.J., Jacobs, J.J., Roebuck, K.A., and Glant, T.T.: The Basic Science of Periprosthetic Osteolysis. J.Bone Joint Surg.Am., 82:1478-1489, 2000.

2. Barrack, R.L., Sawhney, J., Hsu, J., and Cofield, R.H.: Cost analysis of revision total hip arthroplasty. A 5-year followup study. Clin Orthop, 369:175-178, 1999.

3. Bauer, T.W. and Muschler, G.F.: Bone graft materials. An overview of the basic science. Clin Orthop, 371:10-27, 2000.

4. Bergmann, G., Graichen, F., and Rohlmann, A.: Hip joint loading during walking and running, measured in two patients. J.Biomech., 26:969-990, 1993.

5. Bergmann, G., Graichen, F., and Rohlmann, A.: Is staircase walking a risk for the fixation of hip implants? J.Biomech., 28:535-553, 1995.

6. Berzins, A., Sumner, D.R., Wasielewski, R.C., and Galante, J.O.: Impacted particulate allograft for femoral revision total hip arthroplasty. In vitro mechanical stability and effects of cement pressurization. J.Arthroplasty, 11:500-506, 1996.

7. Bourne, R.B., Rorabeck, C.H., Skutek, M., Mikkelsen, S., Winemaker, M., and Robertson, D.: The Harris Design-2 total hip replacement fixed with so-called second-generation cementing techniques. A ten to fifteen-year follow-up. J.Bone Joint Surg.Am., 80:1775-1780, 1998.

8. Brand, R.A., Pedersen, D.R., and Friederich, J.A.: The sensitivity of muscle force predictions to changes in physiologic cross-sectional area. J.Biomech., 19:589-596, 1986.

9. Brewster, N.T., Gillespie, W.J., Howie, C.R., Madabhushi, S.P., Usmani, A.S., and Fairbairn, D.R.: Mechanical considerations in impaction bone grafting. J.Bone Joint Surg.Br., 81:118-124, 1999.

10. Brodt, M.D., Swan, C.C., and Brown, T.D.: Mechanical behavior of human morselized cancellous bone in triaxial compression testing. J.Orthop Res., 16:43-49, 1998.

11. Buchholz, H.W. and Heinert, K.: Long-term results of cemented arthroplasty. Analysis of complications fifteen years after operation. Orthop Clin North Am., 19:531-540, 1988.

12. Burke, D.W., Gates, E.I., and Harris, W.H.: Centrifugation as a method of improving tensile and fatigue properties of acrylic bone cement. J.Bone Joint Surg.Am., 66:1265-1273, 1984.

13. Burstein, A.H., Reilly, D.T., and Martens, M.: Aging of bone tissue: mechanical properties. J.Bone Joint Surg.Am., 58:82-86, 1976.

14. Callaghan, J.J., Albright, J.C., Goetz, D.D., Olejniczak, J.P., and Johnston, R.C.: Charnley total hip arthroplasty with cement. Minimum twenty-five-year follow-up. J.Bone Joint Surg.Am., 82:487-497, 2000.

15. Chang, P.B., Mann, K.A., and Bartel, D.L.: Cemented femoral stem performance. Effects of proximal bonding, geometry, and neck length. Clin.Orthop., 355:57-69, 1998.

16. Chapman, M.W., Bucholz, R., and Cornell, C.: Treatment of acute fractures with a collagen-calcium phosphate graft material. A randomized clinical trial. J.Bone Joint Surg.Am., 79:495-502, 1997.

17. Craig, R.F. *Soil Mechanics*. 5th ed., Chapman and Hall, London, 1993.

18. Crowninshield, R.D., Brand, R.A., Johnston, R.C., and Milroy, J.C.: An analysis of femoral component stem design in total hip arthroplasty. J.Bone Joint Surg.Am., 62:68-78, 1980.

19. Crowninshield, R.D., Jennings, J.D., Laurent, M.L., and Maloney, W.J.: Cemented femoral component surface finish mechanics. Clin Orthop, 355:90-102, 1998.

20. Crowninshield, R.D., Johnston, R.C., Andrews, J.G., and Brand, R.A.: A biomechanical investigation of the human hip. J.Biomech., 11:75-85, 1978.

21. Crowninshield, R.D. and Tolbert, J.R.: Cement strain measurement surrounding loose and well-fixed femoral component stems. J.Biomed.Mater.Res., 17:819-828, 1983.

22. Dijkers, R.L.M., Bouma, E.M., van der Meer-Prins, E.M.W., Huysmans, P.E., Taminiau, A.H.M., and Claas, F.H.J.: Human bone allografts can induce T cells with high affinity for donor antigens. J.Bone Joint Surg.Br., 81:538-544, 1999.

23. Dohmae, Y., Bechtold, J.E., Sherman, R.E., Puno, R.M., and Gustilo, R.B.: Reduction in cement-bone interface shear strength between primary and revision arthroplasty. Clin.Orthop., 236:214-220, 1988.

24. Driessens, F.C., Boltong, M.G., Zapatero, M.I., Verbeeck, R.M.H., Bonfield, W., Bermudez, O., Fernandez, E., Ginebra, M.P., and Pliam, N.B.: In vivo behaviour of three calcium phosphate cements and a magnesium phosphate cement. J.Mater.Sci.Mat.Med., 6:272-278, 1995.

25. Duncan, C.P., Masterson, E.L., and Masri, B.A.: Impaction allografting with cement for the management of femoral bone loss. Orthop Clin North Am., 29:297-305, 1998.

26. Dunlop, D. Mechanical and biological aspects of impaction bone grafting in revision hip surgery and the use of a new synthetic bone graft. MD Thesis, University of Edinburgh, 2001.

27. Dunne, N.J. and Orr, J.F.: Flow characteristics of curing polymethyl methacrylate bone cement. Proc.Inst.Mech.Eng.[H.], 212:199-207, 1998.

28. Eldridge, J.D., Smith, E.J., Hubble, M.J., Whitehouse, S.L., and Learmonth, I.D.: Massive early subsidence following femoral impaction grafting. J.Arthroplasty, 12:535-540, 1997.

29. Elting, J.J., Mikhail, W.E., Zicat, B.A., Hubbell, J.C., Lane, L.E., and House, B.: Preliminary report of impaction grafting for exchange femoral arthroplasty. Clin Orthop, 319:159-167, 1995.

30. Enneking, W.F. and Mindell, E.R.: Observations on massive retrieved human allografts. J.Bone Joint Surg.Am., 73:1123-1142, 1991.

31. Fisher, D.A., Tsang, A.C., Paydar, N., Milionis, S., and Turner, C.H.: Cement-mantle thickness affects cement strains in total hip replacement. J.Biomech., 30:1173-1177, 1997.

32. Frankenburg, E.P., Goldstein, S.A., Bauer, T.W., Harris, S.A., and Poser, R.D.: Biomechanical and histological evaluation of a calcium phosphate cement. J.Bone Joint Surg.Am., 80:1112-1124, 1998.

33. Giaccio, G. and Zerbino, R.: Failure mechanism of concrete. Combined effects of course aggregates strength level. Adv Cement Mater, 7:41-48, 1998.

34. Gie, G.A., Linder, L., Ling, R.S., Simon, J.P., Slooff, T.J., and Timperley, A.J.: Impacted cancellous allografts and cement for revision total hip arthroplasty. J.Bone Joint Surg.Br., 75:14-21, 1993.

35. Giesen, E.B., Lamerigts, N.M., Verdonschot, N., Buma, P., Schreurs, B.W., and Huiskes, R.: Mechanical characteristics of impacted morsellised bone grafts used in revision of total hip arthroplasty. J.Bone Joint Surg.Br., 81:1052-1057, 1999.

36. Goldberg, V.M. and Stevenson, S.: Natural history of autografts and allografts. Clin Orthop, 225:7-16, 1987.

37. Grant, J. P. Mapping the structural properties of the lumbosacral vertebral endplateMASc Thesis, University of British Columbia, 2000.

38. Gruen, T.A., McNeice, G.M., and Amstutz, H.C.: "Modes of failure" of cemented stem-type femoral components: a radiographic analysis of loosening. Clin Orthop, 141:17-27, 1979.

39. Haddad, F.S., Garbuz, D., Masri, B.A., and Duncan, C.P.: Structural proximal femoral allografts for failed total hip replacements: A minimum review of five years. J.Bone Joint Surg.Br., 82:830-836, 2000.

40. Hamanishi, C., Kitamoto, K., Ohura, K., Tanaka, S., and Doi, Y.: Self-setting, bioactive, and biodegradable TTCP-DCPD apatite cement. J.Biomed.Mater.Res., 32:383-389, 1996.

41. Hayes, W.C. and Bouxsein, M.L.: Biomechanics of cortical and trabecular bone: Implications for assessment of fracture risk. In Mow, V.C. and Hayes, W.C., (eds.): Basic Orthopaedic Biomechanics. New York, Lippincott-Raven Publishers, 1997, pp. 69-112.

42. Hayes, W.C., Piazza, S.J., and Zysset, P.K.: Biomechanics of fracture risk prediction of the hip and spine by quantitative computed tomography. Radiol.Clin North Am., 29:1-18, 1991.

43. Hedia, H.S., Abdel-Shafi, A.A., and Fouda, N.: Shape optimization of metal backing for cemented acetabular cup. Biomed.Mater Eng., 10:73-82, 2000.

44.  Hench, L.L.:  Bioactive materials: the potential for tissue regeneration.  J.Biomed.Mater.Res., 41:511-518, 1998.

45.  Huiskes, R.:  *The various stress patterns of press-fit, ingrown, and cemented femoral stems.  Clin Orthop,* 261:27-38, 1990.

46.  Huiskes, R., Strens, P.H., van Heck, J., and Slooff, T.J.:  Interface stresses in the resurfaced hip.  Finite element analysis of load transmission in the femoral head.  Acta Orthop Scand., 56:474-478, 1985.

47.  Huiskes, R., Verdonschot, N., and Nivbrant, B.:  Migration, stem shape, and surface finish in cemented total hip arthroplasty.  Clin Orthop, 355:103-112, 1998.

48.  Ikenaga, M., Hardouin, P., Lemaitre, J., Andrianjatovo, H., and Flautre, B.:  Biomechanical characterization of a biodegradable calcium phosphate hydraulic cement: a comparison with porous biphasic calcium phosphate ceramics.  J.Biomed.Mater.Res., 40:139-144, 1998.

49.  Ishihara, K., Arai, H., Nakabayashi, N., Morita, S., and Furuya, K.:  Adhesive bone cement containing hydroxyapatite particle as bone compatible filler.  J.Biomed.Mater Res., 26:937-945, 1992.

50.  Ishikawa, K., Takagi, S., Chow, L.C., and Suzuki, K.:  Reaction of calcium phosphate cements with different amounts of tetracalcium phosphate and dicalcium phosphate anhydrous.  J.Biomed.Mater.Res., 46:504-510, 1999.

51.  Jasty, M., Jiranek, W., and Harris, W.H.:  Acrylic fragmentation in total hip replacements and its biological consequences.  Clin.Orthop., 285:116-128, 1992.

52.  Jasty, M., Maloney, W.J., Bragdon, C.R., O'Connor, D.O., Haire, T., and Harris, W.H.:  The initiation of failure in cemented femoral components of hip arthroplasties.  J.Bone Joint Surg.[Br.], 73:551-558, 1991.

53.  Jensen, S.S., Aaboe, M., Pinholt, E.M., Hjorting-Hansen, E., Melsen, F., and Ruyter, I.E.:  Tissue reaction and material characteristics of four bone substitutes.  Int.J.Oral Maxillofac.Implants., 11:55-66, 1996.

54.  Jew, V. C., Durfee, A., Angle, C., and Dauskardt, R. H.: Enhanced reliability and strength of carbonated apatite bone mineral substitutes with organic reinforcements.  Transactions of Orthopaedic Research Society, 46:681, 2000.

55.  Johnson, K.D., Frierson, K.E., Keller, T.S., Cook, C., Scheinberg, R., Zerwekh, J., Meyers, L., and Sciadini, M.F.:  Porous ceramics as bone graft substitutes in long bone defects: a biomechanical, histological, and radiographic analysis.  J.Orthop Res., 14:351-369, 1996.

56.  Joshi, R.P., Eftekhar, N.S., McMahon, D.J., and Nercessian, O.A.:  Osteolysis after Charnley primary low-friction arthroplasty. A comparison of two matched paired groups.  J.Bone Joint Surg.Br., 80:585-590, 1998.

57. Keaveny, T.M., Pinilla, T.P., Crawford, R.P., Kopperdahl, D.L., and Lou, A.: Systematic and random errors in compression testing of trabecular bone [published erratum appears in J Orthop Res 1999 Jan;17(1):151]. J.Orthop Res., 15:101-110, 1997.

58. Kershaw, C.J., Atkins, R.M., Dodd, C.A., and Bulstrode, C.J.: Revision total hip arthroplasty for aseptic failure. A review of 276 cases. J.Bone Joint Surg.[Br.], 73:564-568, 1991.

59. Personal communication: Knaack, D., Etex Corp.

60. Knaack, D., Goad, M.E., Aiolova, M., Rey, C., Tofighi, A., Chakravarthy, P., and Lee, D.D.: Resorbable calcium phosphate bone substitute. J.Biomed.Mater.Res., 43:399-409, 1998.

61. Knabe, C., Driessens, F.C., Planell, J.A., Gildenhaar, R., Berger, G., Reif, D., Fitzner, R., Radlanski, R.J., and Gross, U.: Evaluation of calcium phosphates and experimental calcium phosphate bone cements using osteogenic cultures. J.Biomed.Mater.Res., 52:498-508, 2000.

62. Krause, W.R., Miller, J., and Ng, P.: The viscosity of acrylic bone cements. J.Biomed.Mater.Res., 16:219-243, 1982.

63. Ladd, A.L. and Pliam, N.B.: Use of bone-graft substitutes in distal radius fractures. J.Am.Acad.Orthop Surg., 7:279-290, 1999.

64. Le Huec, J.C., Schaeverbeke, T., lement, D., aber, J., and e Rebeller, A.: Influence of porosity on the mechanical resistance of hydroxyapatite ceramics under compressive stress. Biomaterials, 16:113-118, 1995.

65. Learmonth, I.D., Hussell, J.G., and Grobler, G.P.: Unpredictable progression of osteolysis following cementless hip arthroplasty. 24 femoral components followed for 6-10 years. Acta Orthop Scand., 67:245-248, 1996.

66. Lee, D.D., Tofighi, A., Aiolova, M., Chakravarthy, P., Catalano, A., Majahad, A., and Knaack, D.: alpha-BSM: a biomimetic bone substitute and drug delivery vehicle. Clin Orthop, 367S:396-405, 1999.

67. Lee, I.Y., Skinner, H.B., and Keyak, J.H.: Effects of variation of cement thickness on bone and cement stress at the tip of a femoral implant. Iowa.Orthop.J., 13:155-9:155-159, 1993.

68. Leopold, S.S., Berger, R.A., Rosenberg, A.G., Jacobs, J.J., Quigley, L.R., and Galante, J.O.: Impaction allografting with cement for revision of the femoral component. A minimum four-year follow-up study with use of a precoated femoral stem. J.Bone Joint Surg.Am., 81:1080-1092, 1999.

69. Leopold, S.S., Jacobs, J.J., and Rosenberg, A.G.: Cancellous allograft in revision total hip arthroplasty. A clinical review. Clin Orthop, 371:86-97, 2000.

70. Leopold, S.S. and Rosenberg, A.G.: Current Status of Impaction Allografting for Revision of a Femoral Component. J.Bone Joint Surg.Am., 81:1337-1345, 1999.

71. Lewis, G., Nyman, J.S., and Trieu, H.H.: Effect of mixing method on selected properties of acrylic bone cement. J.Biomed.Mater.Res., 38:221-228, 1997.

72. Liu, D.M.: Influence of porosity and pore size on the compressive strength of porous hydroxyapatite ceramic. Ceramics International, 23:135-139, 1997.

73. Liu, Y.K., Park, J.B., Njus, G.O., and Stienstra, D.: Bone-particle-impregnated bone cement: an in vitro study. J.Biomed.Mater.Res., 21:247-261, 1987.

74. Livingston, B.J., Chmell, M.J., Spector, M., and Poss, R.: Complications of total hip arthroplasty associated with the use of an acetabular component with a Hylamer liner [see comments]. J.Bone Joint Surg.Am., 79:1529-1538, 1997.

75. Malchau, H., Herberts, P., and Ahnfelt, L.: Prognosis of total hip replacement in Sweden. Follow-up of 92,675 operations performed 1978-1990. Acta Orthop Scand., 64:497-506, 1993.

76. Malkani, A.L., Voor, M.J., Fee, K.A., and Bates, C.S.: Femoral component revision using impacted morsellised cancellous graft. A biomechanical study of implant stability [see comments]. J.Bone Joint Surg.Br., 78:973-978, 1996.

77. Maloney, W.J., Jasty, M., Rosenberg, A., and Harris, W.H.: Bone lysis in well-fixed cemented femoral components. J.Bone Joint Surg.[Br.], 72:966-970, 1990.

78. Manley, M.T., Stern, L.S., and Gurtowski, J.: The load carrying and fatigue properties of the stem-cement interface with smooth and porous coated femoral components. J.Biomed.Mater.Res., 19:563-575, 1985.

79. Mann, K.A., Ayers, D.C., and Damron, T.A.: Effects of stem length on mechanics of the femoral hip component after cemented revision. J.Orthop.Res., 15:62-68, 1997a.

80. Mann, K.A., Bartel, D.L., and Ayers, D.C.: Influence of stem geometry on mechanics of cemented femoral hip components with a proximal bond. J.Orthop.Res., 15:700-706, 1997b.

81. Mann, K.A., Bartel, D.L., Wright, T.M., and Burstein, A.H.: Coulomb frictional interfaces in modeling cemented total hip replacements: a more realistic model. J.Biomech., 28:1067-1078, 1995.

82. Mantell, S.C., Chanda, H., Bechtold, J.E., and Kyle, R.F.: A parametric study of acetabular cup design variables using finite element analysis and statistical design of experiments. J.Biomech.Eng., 120:667-675, 1998.

83. Martin, R.B., Chapman, M.W., Holmes, R.E., Sartoris, D.J., Shors, E.C., Gordon, J.E., Heitter, D.O., Sharkey, N.A., and Zissimos, A.G.: Effects of bone ingrowth on the strength and non-invasive assessment of a coralline hydroxyapatite material. Biomaterials, 10:481-488, 1989.

84. Masterson, E.L. and Duncan, C.P.: Subsidence and the cement mantle in femoral impaction allografting. Orthopedics., 20:821-822, 1997a.

85. Masterson, E.L., Masri, B.A., and Duncan, C.P.: The cement mantle in the Exeter impaction allografting technique. A cause for concern. J.Arthroplasty, 12:759-764, 1997b.

86. Masterson, E.L., Masri, B.A., Duncan, C.P., Rosenberg, A., Cabanela, M., and Gross, M.: The cement mantle in femoral impaction allografting. A comparison of three systems from four centres. J.Bone Joint Surg.Br., 79:908-913, 1997c.

87. Meding, J.B., Ritter, M.A., Keating, E.M., and Faris, P.M.: Impaction bone-grafting before insertion of a femoral stem with cement in revision total hip arthroplasty. A minimum two-year follow-up study. J.Bone Joint Surg.Am., 79:1834-1841, 1997.

88. Mehta, P.K. and Monteiro, P.J.M. *Concrete : structure, properties, and materials.* 2nd ed., Prentice Hall, Englewood Cliffs, NJ, 1993.

89. Mikhail, W.E.M. and Weidenhielm, L.: Impaction grafting with cement. In Sledge, C.B., (ed.): The hip. New York, Lippencott-Raven Publishers, 1998, pp. 335-341.

90. Nelissen, R.G., Bauer, T.W., Weidenhielm, L.R., LeGolvan, D.P., and Mikhail, W.E.: Revision hip arthroplasty with the use of cement and impaction grafting. Histological analysis of four cases. J.Bone Joint Surg.Am., 77:412-422, 1995.

91. Netter, F.H. *Atlas of Human Anatomy.* Novartis Pharmaceuticals Corporation, Summit, NJ, 1997.

92. Neville, A.M. *Properties of Concrete.* 4th ed., Longman Scientific & Technical, New York, 1995.

93. O'Connor, D.O., Burke, D.W., Jasty, M., Sedlacek, R.C., and Harris, W.H.: In vitro measurement of strain in the bone cement surrounding the femoral component of total hip replacements during simulated gait and stair-climbing. J.Orthop.Res., 14:769-777, 1996.

94. Oonishi, H., Kushitani, S., Yasukawa, E., Iwaki, H., Hench, L.L., Wilson, J., Tsuji, E., and Sugihara, T.: Particulate bioglass compared with hydroxyapatite as a bone graft substitute. Clin Orthop, 334:316-325, 1997.

95. Paprosky, W.G., Greidanus, N.V., and Antoniou, J.: Minimum 10-year-results of extensively porous-coated stems in revision hip arthroplasty. Clin Orthop, 369:230-242, 1999.

96. Pauwels, F. *Biomechanics of the Normal and Diseased Hip.* Springer-Verlag, Heidelberg, Germany, 1976.

97. Peltier, L.: The use of plaster of Paris to fill large defects in bone. Am J Surg, 97:311-315, 1959.

98. Philipoff, W. and Gaskins, F.H.: The capillary experiment in rheology. Trans.Soc.Rheol., 2:263-284, 1958.

99. Ragab, A.A., Kraay, M.J., and Goldberg, V.M.: Clinical and radiographic outcomes of total hip arthroplasty with insertion of an anatomically designed femoral component without cement for the treatment of primary osteoarthritis. A study with a minimum of six years of follow-up. J.Bone Joint Surg.Am., 81:210-218, 1999.

100. Reilly, D.T. and Burstein, A.H.: The elastic and ultimate properties of compact bone tissue. J.Biomech., 8:393-405, 1975.

101. Retpen, J.B., Varmarken, J.E., Rock, N.D., and Jensen, J.S.: Unsatisfactory results after repeated revision of hip arthroplasty. 61 cases followed for 5 (1-10) years. Acta Orthop Scand., 63:120-127, 1992.

102. Ritter, M.A. and Campbell, E.D.: Long-term comparison of the Charnley, Muller, and Trapezoidal-28 total hip prostheses. A survival analysis. J.Arthroplasty, 2:299-308, 1987.

103. Roberson, J.R.: Proximal femoral bone loss after total hip arthroplasty. Orthop Clin North Am., 23:291-302, 1992.

104. Robinson, R.P., Wright, T.M., and Burstein, A.H.: Mechanical properties of poly(methyl methacrylate) bone cements. J.Biomed.Mater.Res., 15:203-208, 1981.

105. Rohlmann, A., Mossner, U., Bergmann, G., Hees, G., and Kolbel, R.: Effects of stem design and material properties on stresses in hip endoprostheses. J.Biomed.Eng., 9:77-83, 1987.

106. Rohlmann, A., Mossner, U., Bergmann, G., and Kolbel, R.: Finite-element-analysis and experimental investigation in a femur with hip endoprosthesis. J.Biomech., 16:727-742, 1983.

107. Rohrle, H., Scholten, R., Sigolotto, C., Sollbach, W., and Kellner, H.: Joint forces in the human pelvis-leg skeleton during walking. J.Biomech., 17:409-424, 1984.

108. Saha, S. and Pal, S.: Mechanical properties of bone cement: a review. J.Biomed.Mater.Res., 18:435-462, 1984.

109. Schreurs, B. W. Reconstructive options in revision surgery of failed total hip arthroplastiesPhD Thesis, University of Nijmegen, 1994.

110. Schreurs, B.W., Slooff, T.J., Buma, P., Gardeniers, J.W., and Huiskes, R.: Acetabular reconstruction with impacted morsellised cancellous bone graft and cement. A 10- to 15-year follow-up of 60 revision arthroplasties. J.Bone Joint Surg.Br., 80:391-395, 1998.

111. Silva, M.J., Reed, K.L., Robertson, D.D., Bragdon, C., Harris, W.H., and Maloney, W.J.: Reduced bone stress as predicted by composite beam theory correlates with cortical bone loss following cemented total hip arthroplasty. J.Orthop Res., 17:525-531, 1999.

112. Slooff, T.J., Huiskes, R., van Horn, J., and Lemmens, A.J.: Bone grafting in total hip replacement for acetabular protrusion. Acta Orthop Scand., 55:593-596, 1984.

113. Smith, S.E. and Harris, W.H.: Total hip arthroplasty performed with insertion of the femoral component with cement and the acetabular component without cement. Ten to thirteen-year results. J.Bone Joint Surg.Am., 79:1827-1833, 1997.

114. Stolk, J., Verdonschot, N., Cristofolini, L., Firmati, L., Toni, A., and Huiskes, R.: Strains in composite hip joint reconstructions obtained through FEA and experiments corresponded closely. Transactions of Orthopaedic Research Society, 46:515, 2000.

115. Stromberg, C.N., Herberts, P., and Palmertz, B.: Cemented revision hip arthroplasty. A multicenter 5-9-year study of 204 first revisions for loosening. Acta Orthop Scand., 63:111-119, 1992.

116. Report: Prognosis of Total Hip Replacement The Swedish National Hip Arthroplasty Registry, 2000.

117. Tagil, M., Jeppsson, C., and Aspenberg, P.: Bone graft incorporation. Effects of osteogenic protein-1 and impaction. Clin Orthop, 371:240-245, 2000.

118. Tamura, J., Kitsugi, T., Iida, H., Fujita, H., Nakamura, T., Kokubo, T., and Yoshihara, S.: Bone bonding ability of bioactive bone cements. Clin Orthop, 343:183-191, 1997.

119. Tartora, G.J. and Anagnostakos, N.P. *Principles of Anatomy and Physiology*. 4th, Harper&Row, Publishers, Inc., New York, NY, 1984.

120. Tay, B.K., Patel, V.V., and Bradford, D.S.: Calcium sulfate- and calcium phosphate-based bone substitutes. Mimicry of the mineral phase of bone. Orthop Clin North Am., 30:615-623, 1999.

121. Teitelbaum, S.L.: Bone resorption by osteoclasts. Science, 289:1504-1508, 2000.

122. Tordella, J.P.: Capillary flow of molten polyethylene: A photographic study of melt fracture. Trans.Soc.Rheol., 1:203-212, 1957.

123. Urist, M.R., Silverman, B.F., Buring, K., Dubuc, F.L., and Rosenberg, J.M.: The bone induction principle. Clin Orthop, 53:243-283, 1967.

124. van Biezen, F.C., ten Have, B.L., and Verhaar, J.A.: Impaction bone-grafting of severely defective femora in revision total hip surgery: 21 hips followed for 41-85 months. Acta Orthop Scand, 71:135-142, 2000.

125. Verdonschot, N. and Huiskes, R.: Mechanical effects of stem cement interface characteristics in total hip replacement. Clin.Orthop., 329:326-336, 1996.

126. Verdonschot, N. and Huiskes, R.: Cement debonding process of total hip arthroplasty stems. Clin.Orthop., 336:297-307, 1997a.

127. Verdonschot, N. and Huiskes, R.: The effects of cement-stem debonding in THA on the long-term failure probability of cement. J.Biomech., 30:795-802, 1997b.

128. Verdonschot, N. and Huiskes, R.: Surface roughness of debonded straight-tapered stems in cemented THA reduces subsidence but not cement damage. Biomaterials, 19:1773-1779, 1998.

129. Verdonschot, N., van Hal, C., Schreurs, B. W., Buma, P., and Huiskes, R.: Mechanical characteristics of biomaterial particles used as bone substitutes for morsellized allografts. Transactions of Orthopaedic Research Society, 46:678, 2000.

130. Voor, M.J., Nawab, A., Malkani, A.L., and Ullrich, C.R.: Mechanical properties of compacted morselized cancellous bone graft using one-dimensional consolidation testing. J.Biomech, 33:1683-1688, 2000.

131. Wheeless, C.R. *Wheeless' Textbook of Orthopaedics.* (www.medmedia.com) 1996.

132. Wolff, J. *Das Gesetz der Transformation der Knochen.* Springer-Verlag, Berlin, 1892.

133. Wright, T.M. and Hayes, W.C.: Tensile testing of bone over a wide range of strain rates: effects of strain rate, microstructure and density. Med.Biol.Eng., 14:671-680, 1976.

134. Yettram, A.L. and Wright, K.W.: Biomechanics of the femoral component of total hip prostheses with particular reference to the stress in the bone-cement. J.Biomed.Eng., 1:281-285, 1979.

# Appendix A:

## Design Drawings

24.90

80.0

9.50

88.9

Capillary Rheometer

23.0

24.86
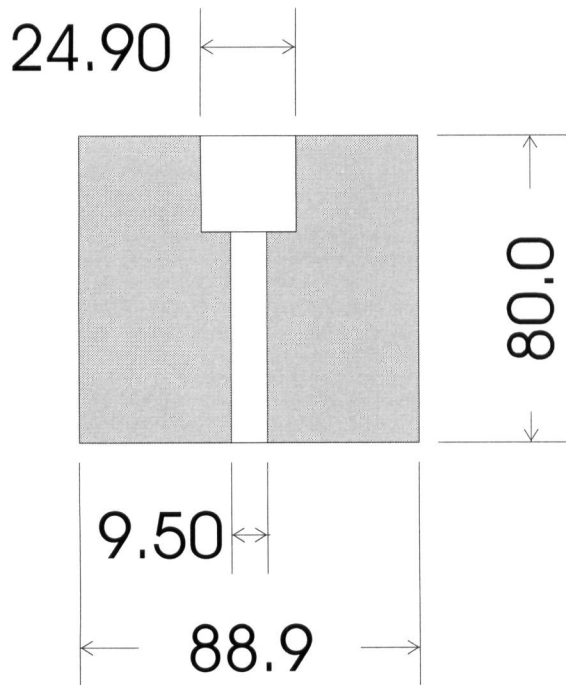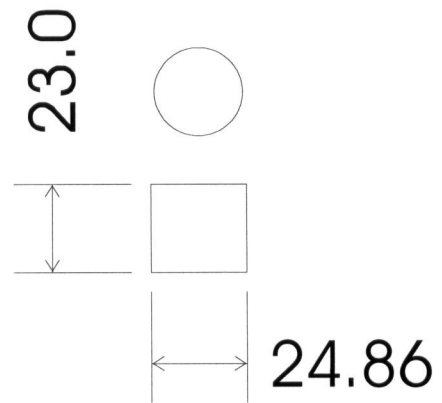
Plunger

All sizes in mm
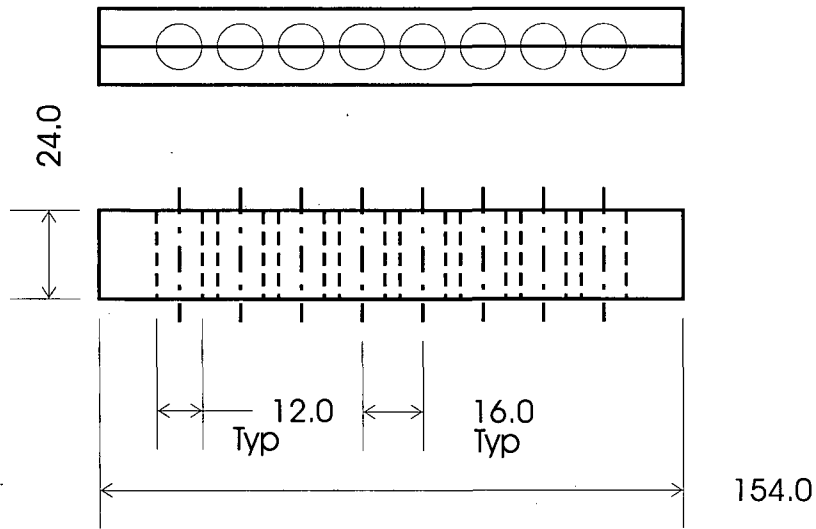
**Specimen moulds**
**from 1/4" aluminum plate**
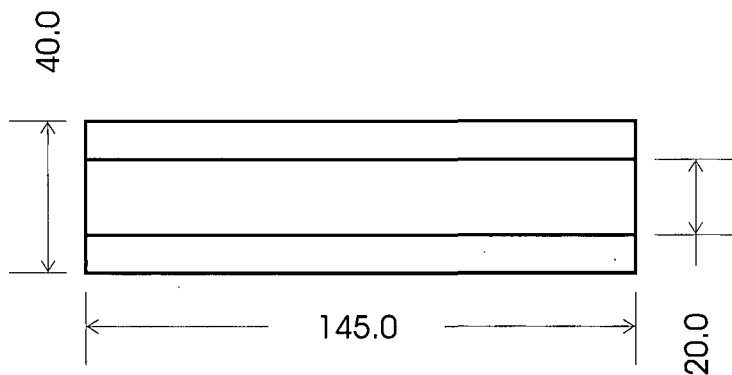


**Clamp for moulds**
**from Delrin**

## All sizes in mm

25.4

25.4

Upper platen

25.4

10.0

19.4

30.0
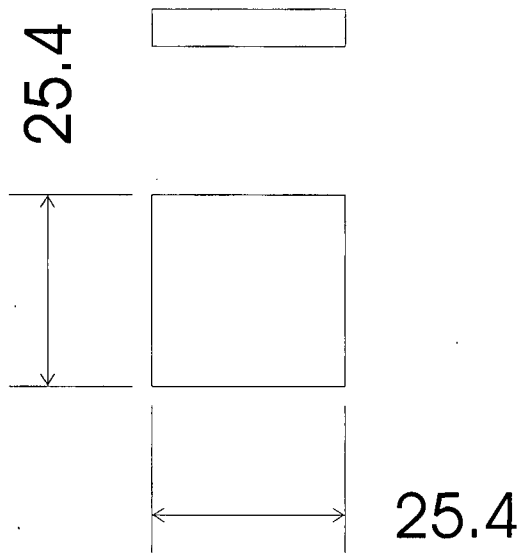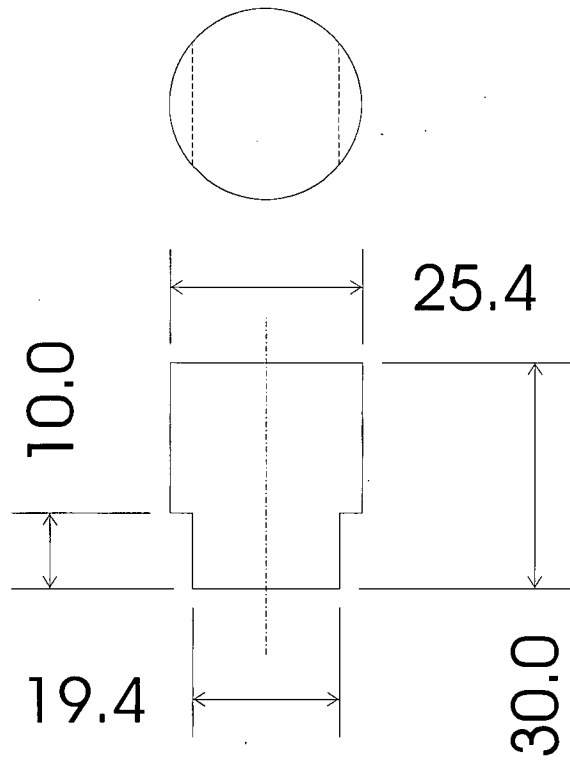
Lower platen

All sizes in mm

# Appendix B:

## Flow and Stress-Strain Graphs

Legend:
- 0bone_1
- 0bone_2
- 25bone_1
- 25bone_2
- 25bone_3
- PMMA_1
- PMMA_2

X-axis: Time (s)

Y-axis: Apparent Viscosity (Pa.s)
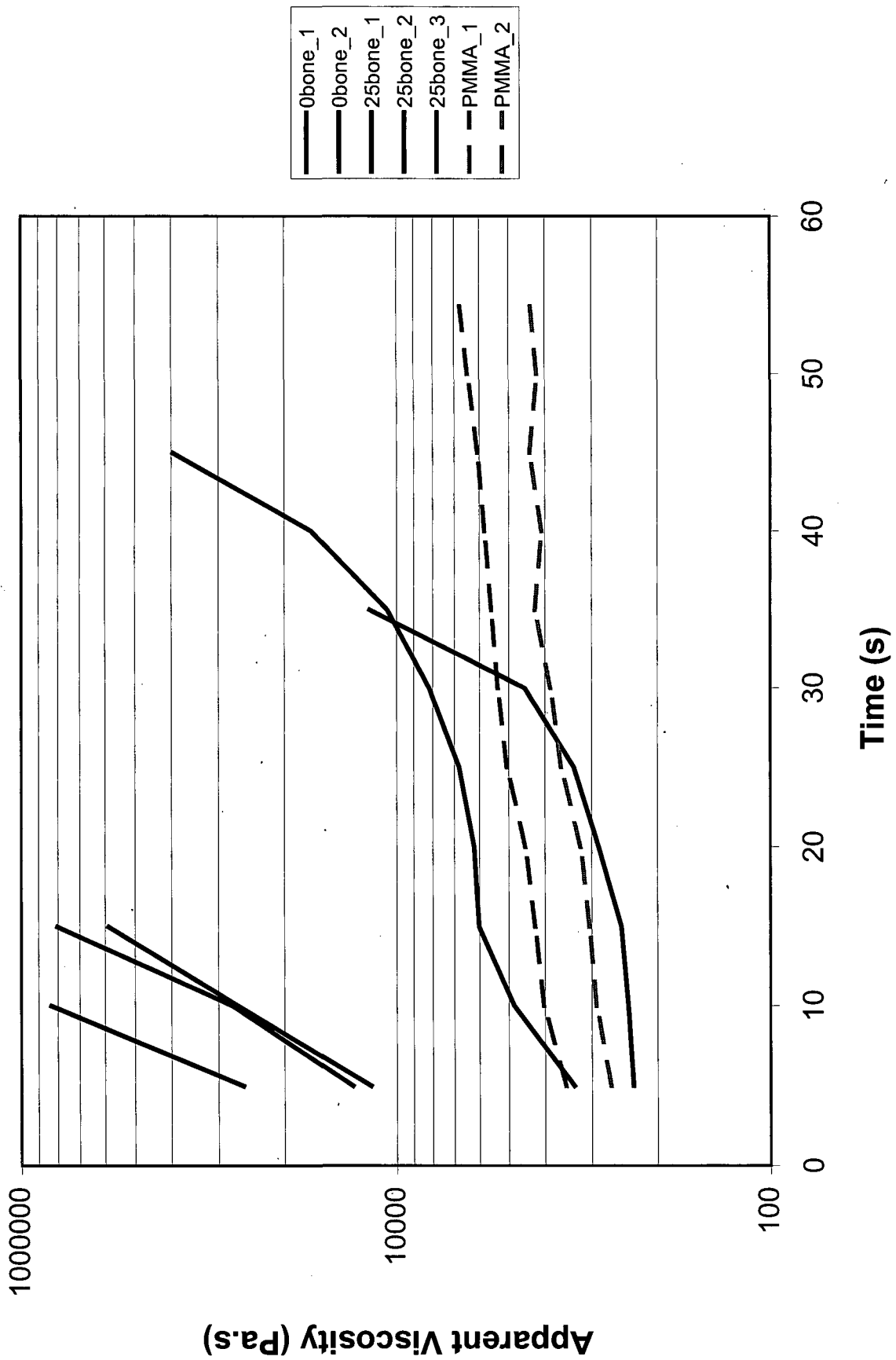
# Uniaxial compression tests: 0% bone
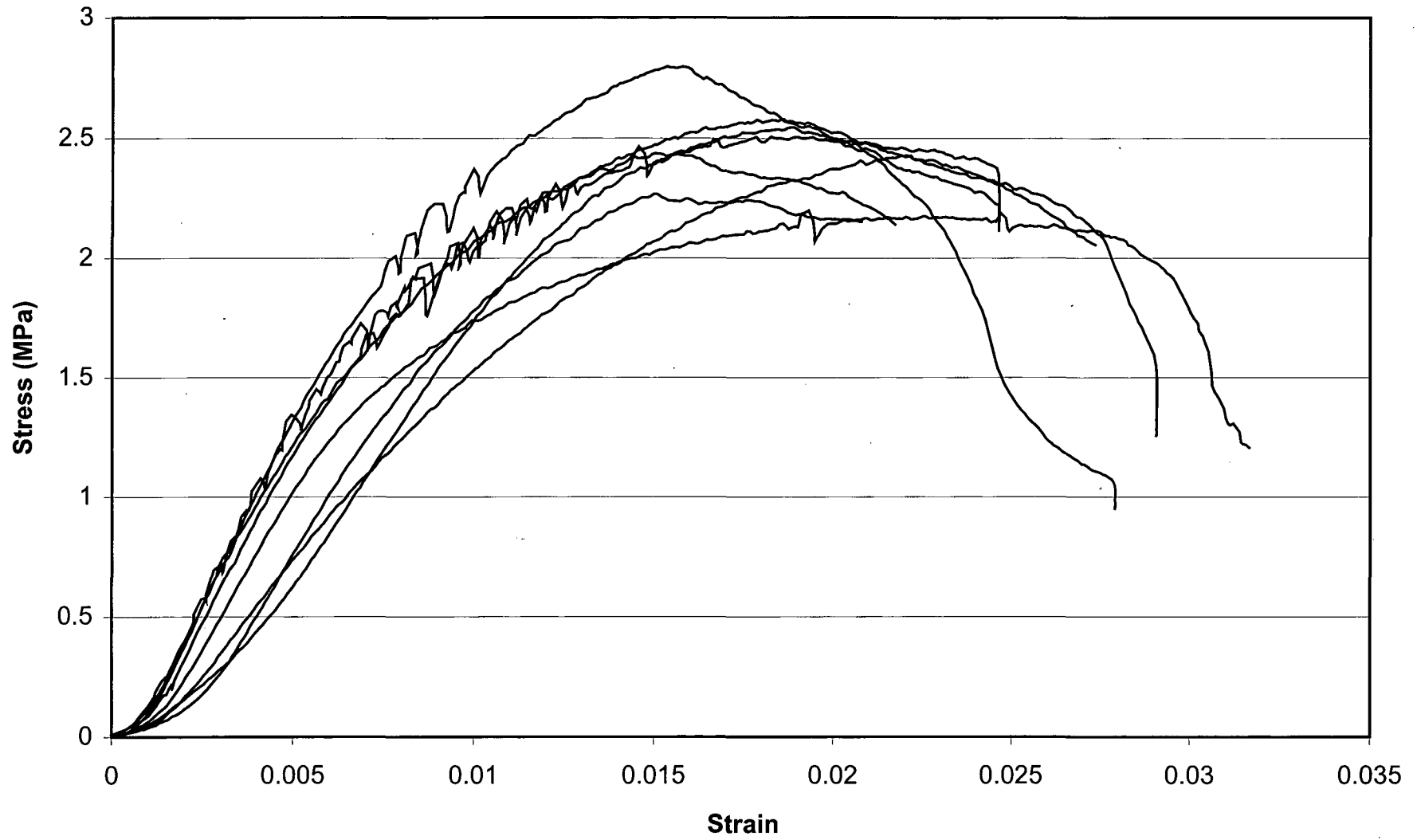
Uniaxial compression tests: 25% bone
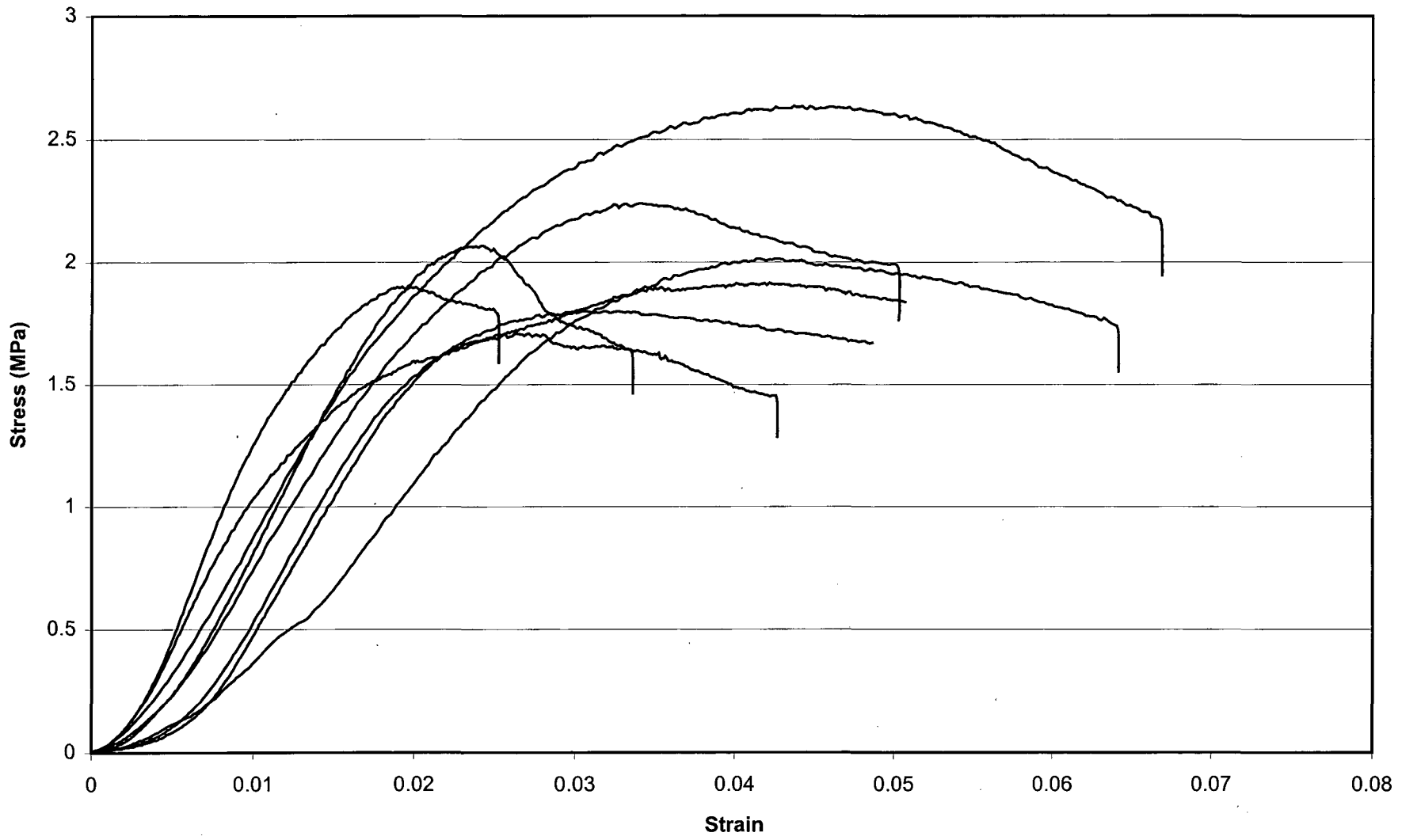
# Uniaxial compression tests: 50% bone
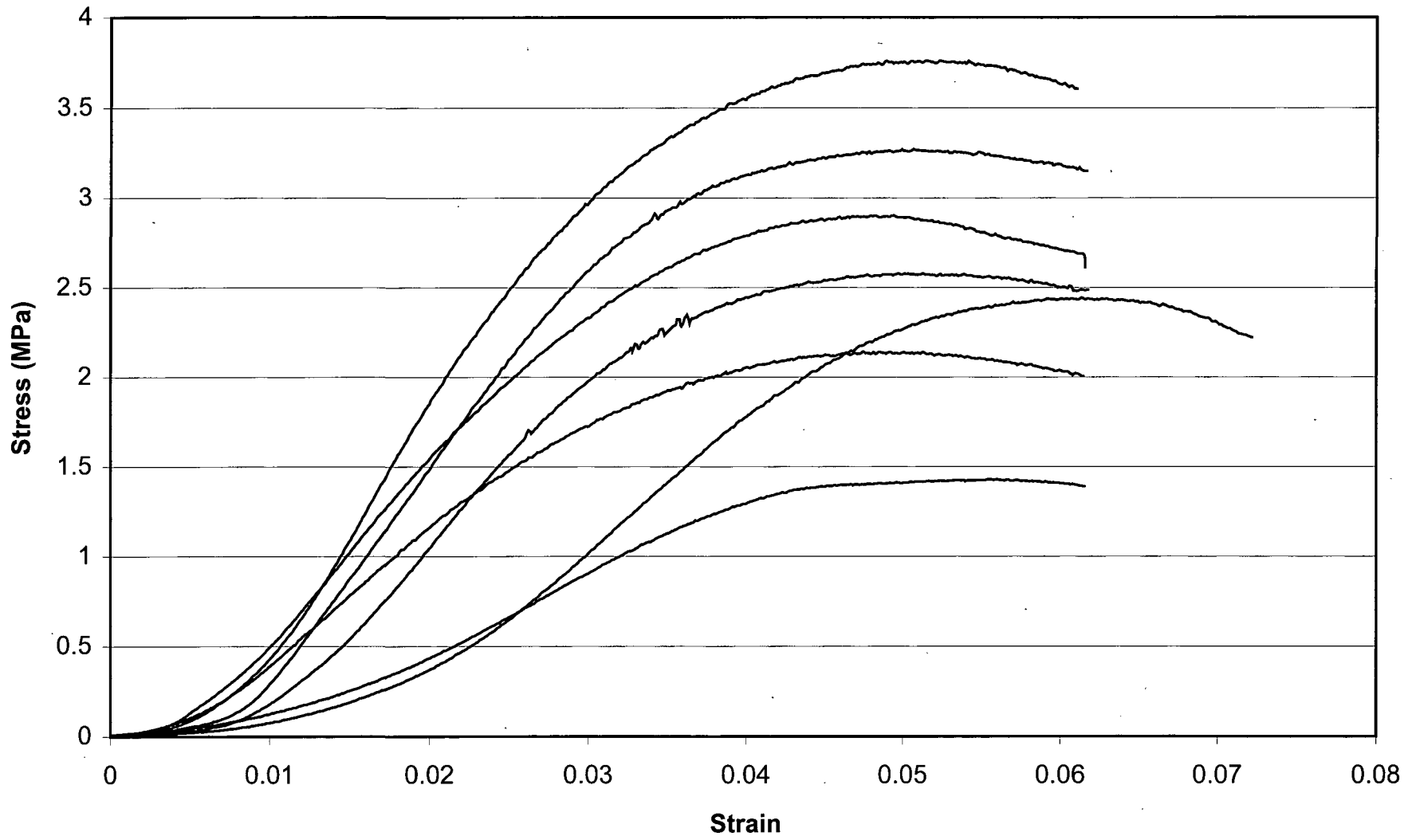
Uniaxial compression tests: 75% bone
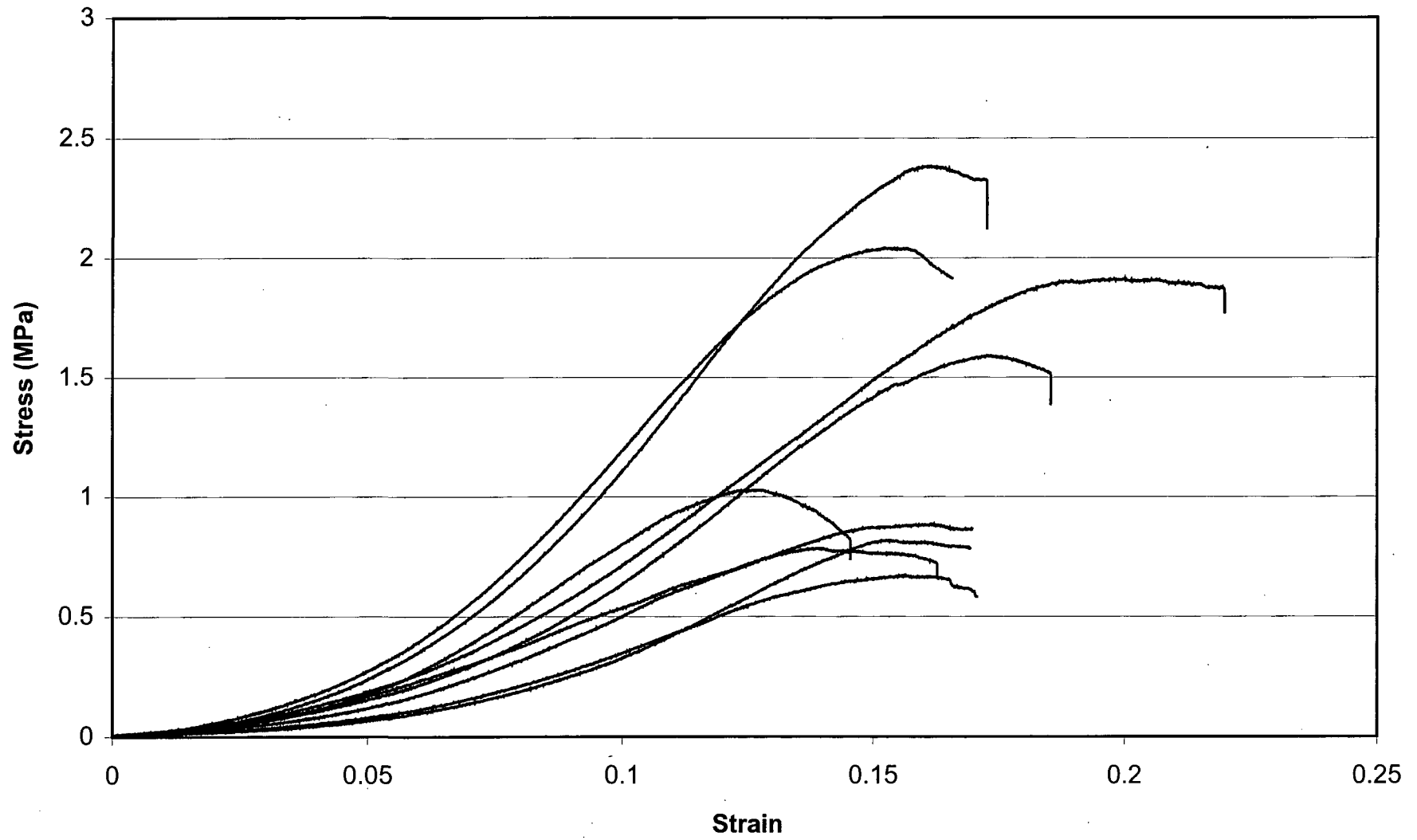
**Confined compression: 0% bone**

Stress (MPa) vs. Strain
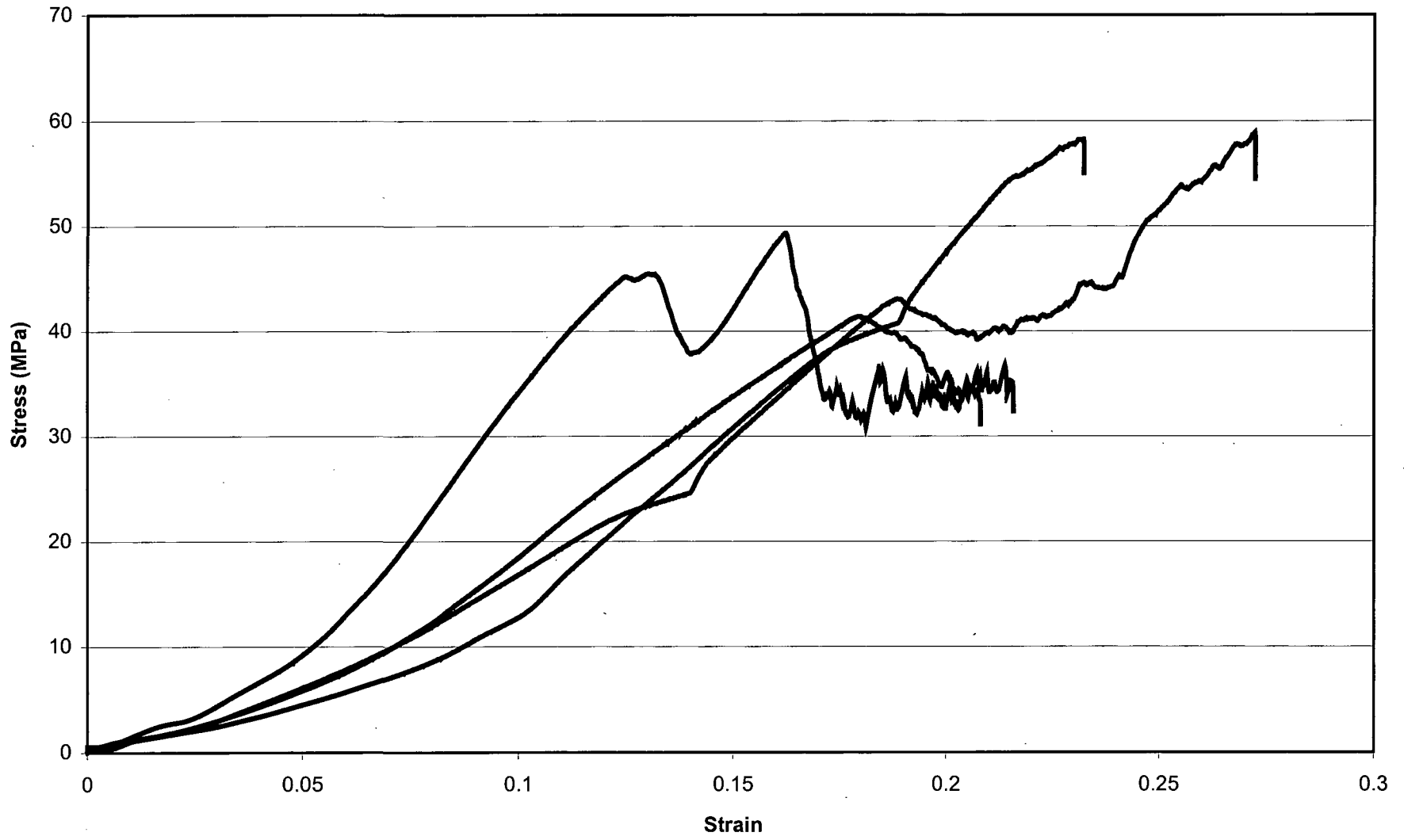
# Confined compression: 25% bone
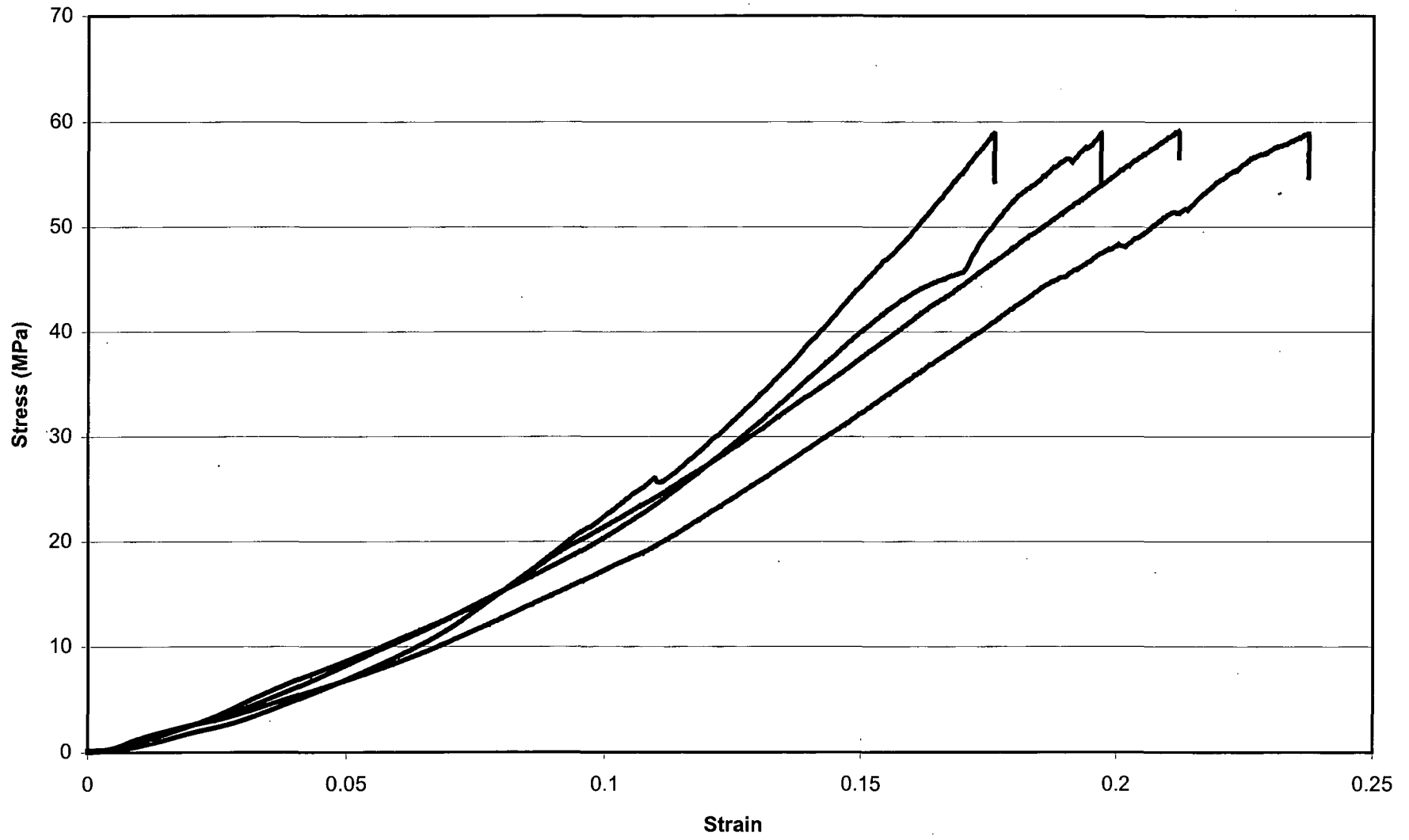
# Confined compression: 50% bone
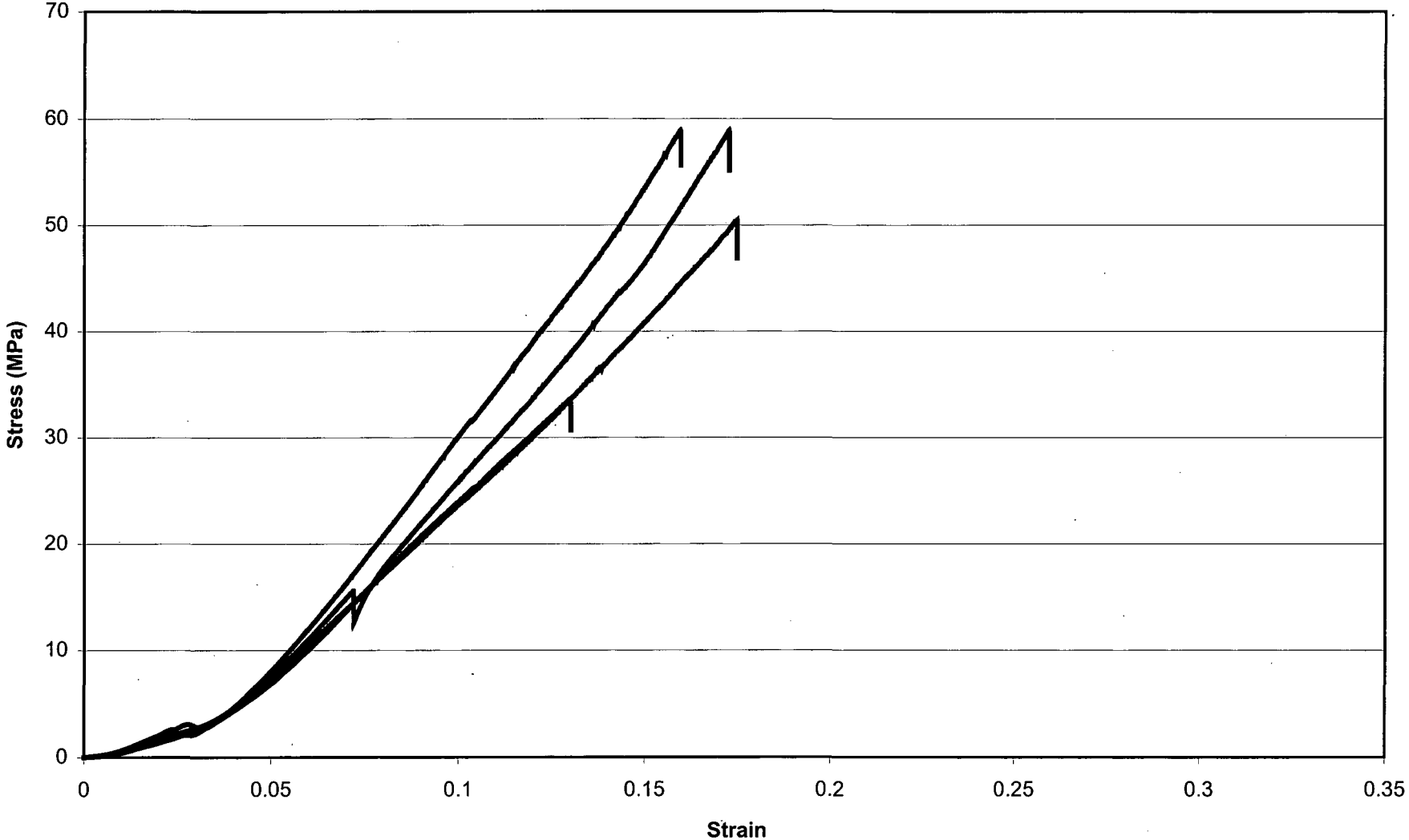
**Confined compression: 75% bone**
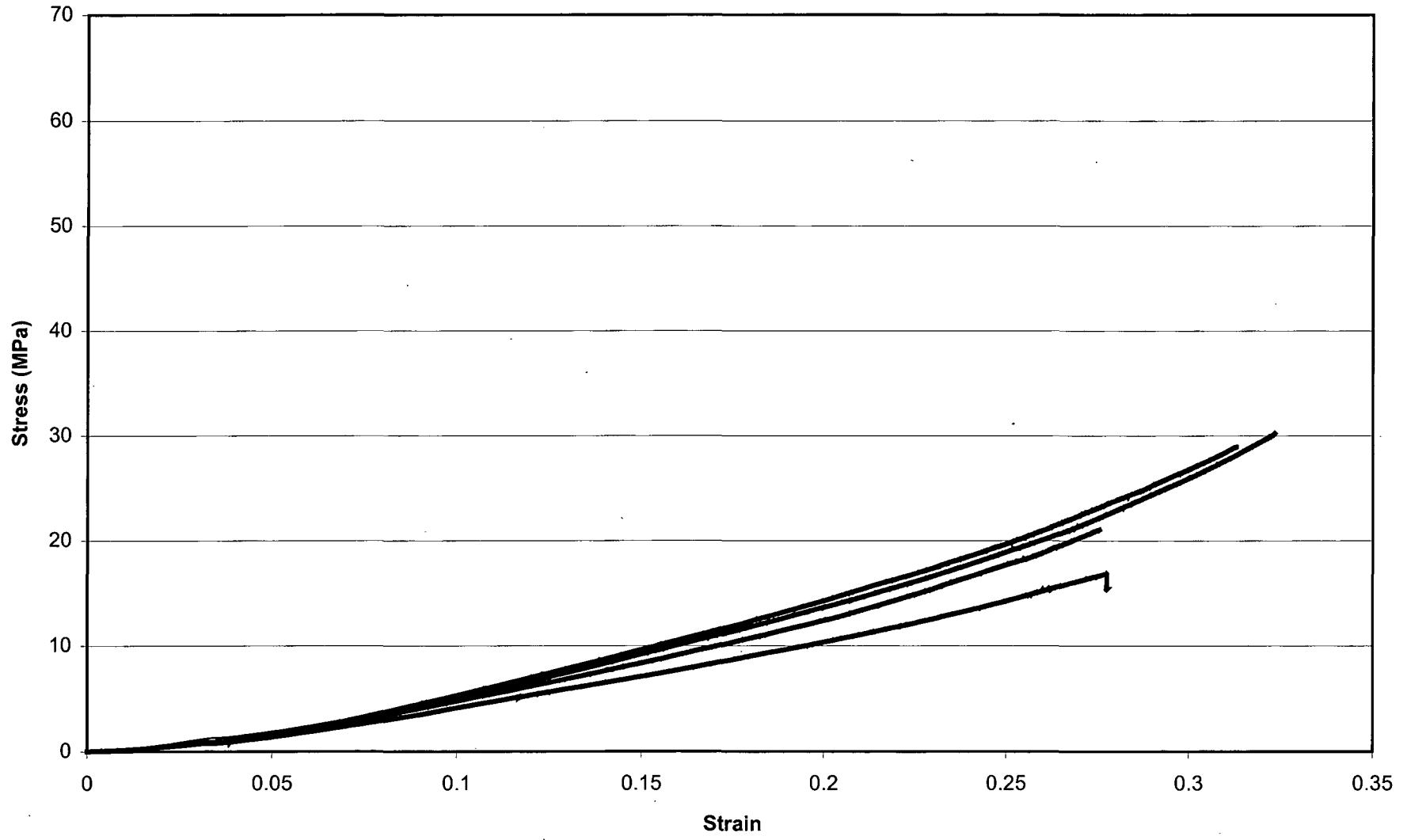
Confined compression: 100% bone
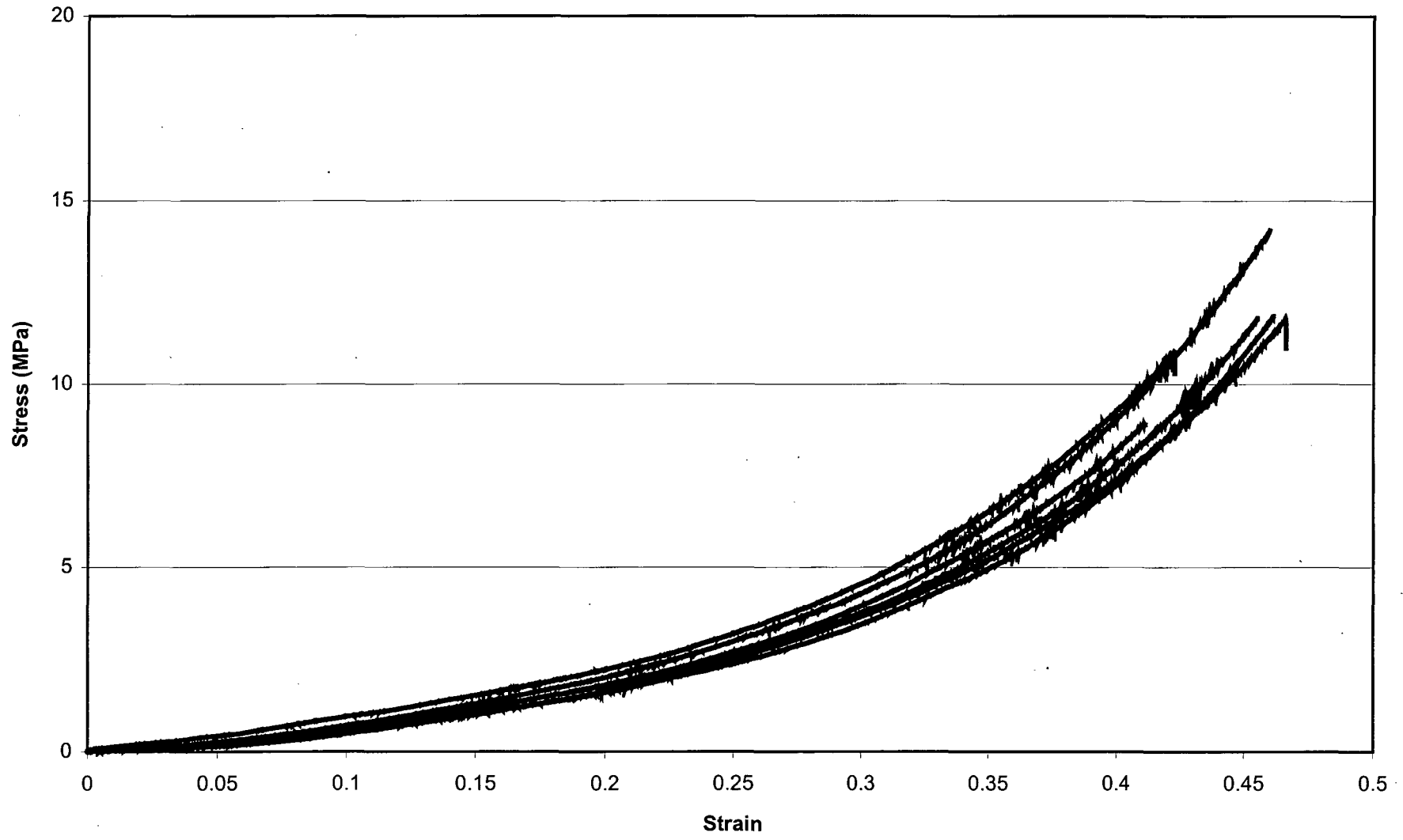
# Appendix C:

## Statistical Results

# Ultimate Stress

Summary of all Effects; design: (compress.sta)
Effect: 1-BONE, 2-BATCH

| | df Effect | MS Effect | df Error | MS Error | F | p-level | |
|---|---|---|---|---|---|---|---|
| 1 | 3 | 2.281607 | 24 | 0.099407 | 22.95219 | **3.125E-07** | Composition has effect |
| 2 | 1 | 0.062134 | 24 | 0.099407 | 0.625046 | 0.4369 | Batch has no effect |
| 12 | 3 | 1.750235 | 24 | 0.099407 | 17.60676 | **2.939E-06** | Batch affects compositions differently (for 50 and 75%) |

Post-hoc test p-values

| Newman-Keuls test; STRENGTH (compress.sta) | | | | |
|---|---|---|---|---|
| Probabilities for Post Hoc Tests | | | | |
| MAIN EFFECT: BONE | | | | |
| Bone: | 0% | 25% | 50% | 75% |
| Group mean: | 2.47 | 2.03 | 2.57 | 1.41 |
| 0% | | **0.0112** | 0.5528 | **0.0001** |
| 25% | | | **0.0073** | **0.0007** |
| 50% | | | | **0.0002** |
| 75% | | | | |

| Batch-batch differences | |
|---|---|
| Bone | p (post-hoc) |
| 0 | 0.6590 |
| 25 | 0.6191 |
| 50 | **0.0005** |
| 75 | **0.0002** |

**Significant p-values in bold**

# Modulus

Summary of all Effects; design: (compress.sta)
Effect: 1-BONE, 2-BATCH

| | df Effect | MS Effect | df Error | MS Error | F | p-level | |
|---|---|---|---|---|---|---|---|
| 1 | 3 | 92931.3 | 24 | 483.7987 | 192.0867 | **6.600E-17** | Composition has effect |
| 2 | 1 | 2480.481 | 24 | 483.7987 | 5.127093 | **0.0329** | Batch has effect |
| 12 | 3 | 3813.398 | 24 | 483.7987 | 7.882199 | **0.0008** | Batch affects compositions differently (for 0% and 50%) |

Post-hoc test p-values

| Newman-Keuls test; MODULUS (compress.sta) | | | | |
|---|---|---|---|---|
| Probabilities for Post Hoc Tests | | | | |
| MAIN EFFECT: BONE | | | | |
| Bone: | 0% | 25% | 50% | 75% |
| Group mean: | 269.1 | 121.7 | 96.4 | 15.3 |
| 0% | | **0.0002** | **0.0001** | **0.0002** |
| 25% | | | **0.0312** | **0.0001** |
| 50% | | | | **0.0002** |
| 75% | | | | |

| Batch-batch differences | |
|---|---|
| Bone | p (post-hoc) |
| 0 | **0.0020** |
| 25 | 0.1723 |
| 50 | **0.0044** |
| 75 | 0.5004 |

**Significant p-values in bold**

# Ultimate Strain

Summary of all Effects; design: (compress.sta)
Effect: 1-BONE, 2-BATCH

| | df Effect | MS Effect | df Error | MS Error | F | p-level | |
|---|---|---|---|---|---|---|---|
| 1 | 3 | 0.035422 | 24 | 0.000108 | 328.1181 | **1.317E-19** | Composition has effect |
| 2 | 1 | 0.000193 | 24 | 0.000108 | 1.790132 | 0.1935 | Batch has no effect |
| 12 | 3 | 0.000428 | 24 | 0.000108 | 3.966979 | **0.0198** | Batch affects compositions differently (for 75%) |

Post-hoc test p-values

| Newman-Keuls test; STRAIN_U (compress.sta) | | | | |
|---|---|---|---|---|
| Probabilities for Post Hoc Tests | | | | |
| MAIN EFFECT: BONE | | | | |
| Bone: | 0% | 25% | 50% | 75% |
| Group mean: | 0.018 | 0.033 | 0.053 | 0.160 |
| 0% | | **0.0084** | **0.0001** | **0.0002** |
| 25% | | | **0.0009** | **0.0001** |
| 50% | | | | **0.0002** |
| 75% | | | | |

| Batch-batch differences | |
|---|---|
| Bone | p (post-hoc) |
| 0 | 0.9829 |
| 25 | 0.2242 |
| 50 | 0.5120 |
| 75 | **0.0033** |

**Significant p-values in bold**

# Strain Energy

Summary of all Effects; design: (compress.sta)
Effect: 1-BONE, 2-BATCH

| | df Effect | MS Effect | df Error | MS Error | F | p-level | |
|---|---|---|---|---|---|---|---|
| 1 | 3 | 7672.698 | 24 | 242.4032 | 31.65263 | **1.653E-08** | Composition has effect |
| 2 | 1 | 655.0889 | 24 | 242.4032 | 2.702476 | 0.1132 | Batch has no effect |
| 12 | 3 | 6224.389 | 24 | 242.4032 | 25.67783 | **1.149E-07** | Batch affects composition differently (for 50% and 75%) |

Post-hoc test p-values

| Newman-Keuls test; STRAIN_E (compress.sta) | | | | |
|---|---|---|---|---|
| Probabilities for Post Hoc Tests | | | | |
| MAIN EFFECT: BONE | | | | |
| Bone: | 0% | 25% | 50% | 75% |
| Group mean: | 27.1 | 40.1 | 74.0 | 93.4 |
| 0% | | 0.1090 | **0.0001** | **0.0002** |
| 25% | | | **0.0004** | **0.0001** |
| 50% | | | | **0.0205** |
| 75% | | | | |

| Batch-batch differences | |
|---|---|
| Bone | p (post-hoc) |
| 0 | 0.7129 |
| 25 | 0.1499 |
| 50 | **0.0084** |
| 75 | **0.0002** |

**Significant p-values in bold**

# Ultimate Stress (Tension)

Summary of all Effects; design: (tension.sta)
Effect: 1-BONE, 2-BATCH

| | df Effect | MS Effect | df Error | MS Error | F | p-level | |
|---|---|---|---|---|---|---|---|
| 1 | 3 | 0.246302 | 23 | 0.009568 | 25.74337 | **1.561E-07** | Composition has effect |
| 2 | 1 | 0.013516 | 23 | 0.009568 | 1.412669 | 0.2467 | Batch has no effect |
| 12 | 3 | 0.054918 | 23 | 0.009568 | 5.740038 | **0.0044** | Batch affects compositions differently (for 50% and 75%) |

Post-hoc test p-values

| Newman-Keuls test; STRENGTH (tension.sta) | | | | |
|---|---|---|---|---|
| Probabilities for Post Hoc Tests | | | | |
| MAIN EFFECT: BONE | | | | |
| Bone: | 0% | 25% | 50% | 75% |
| Group mean: | 0.413 | 0.410 | 0.673 | 0.234 |
| 0% | | 0.9534 | **0.0002** | **0.0043** |
| 25% | 0.9534 | | **0.0002** | **0.0019** |
| 50% | **0.0002** | **0.0002** | | **0.0002** |
| 75% | **0.0043** | **0.0019** | **0.0002** | |

| Batch-batch differences | |
|---|---|
| Bone | p (post-hoc) |
| 0 | 0.4780 |
| 25 | 0.0948 |
| 50 | **0.0102** |
| 75 | **0.0416** |

**Significant p-values in bold**

## Confined Stress: Non-Parametric (5% Strain)

Kruskal-Wallis ANOVA by Ranks (confined.sta)
Independent (grouping) variable: BONE
Kruskal-Wallis test: H ( 4, N= 22) = 17.65613 p = **0.0014**

|  | Code | Valid N | Sum of Ranks |
|---|---|---|---|
| Group 1 | 0 | 4 | 58 |
| Group 2 | 25 | 4 | 71 |
| Group 3 | 50 | 4 | 69 |
| Group 4 | 75 | 4 | 34 |
| Group 5 | 100 | 6 | 21 |

Mann-Whitney U Test (confined.sta)
By variable BONE
Group 1: 0 Group 2: 25

| Compare: | Rank Sum Group 1 | Rank Sum Group 2 | U | Z | p-level | adjusted |
|---|---|---|---|---|---|---|
| 0vs25 | 14 | 22 | 4 | -1.15 | 0.25 | 0.993 |
| 25vs50 | 19 | 17 | 7 | 0.29 | 0.77 | 3.091 |
| 50vs75 | 26 | 10 | 0 | 2.31 | 0.02 | 0.084 |
| 75vs100 | 34 | 21 | 0 | 2.56 | 0.01 | **0.042** |

## Confined Modulus: Non-Parametric (5% Strain)

Kruskal-Wallis ANOVA by Ranks (confined.sta)
Independent (grouping) variable: BONE
Kruskal-Wallis test: H ( 4, N= 22) = 19.15020 p = **0.0007**

|  | Code | Valid N | Sum of Ranks |
|---|---|---|---|
| Group 1 | 0 | 4 | 56 |
| Group 2 | 25 | 4 | 61 |
| Group 3 | 50 | 4 | 81 |
| Group 4 | 75 | 4 | 34 |
| Group 5 | 100 | 6 | 21 |

Mann-Whitney U Test (confined.sta)
By variable BONE
Group 1: 0 Group 2: 25

| Compare: | Rank Sum Group 1 | Rank Sum Group 2 | U | Z | p-level | adjusted |
|---|---|---|---|---|---|---|
| 0vs25 | 15 | 21 | 5 | -0.866 | 0.386 | 1.5459 |
| 25vs50 | 10 | 26 | 0 | -2.309 | 0.021 | 0.0837 |
| 50vs75 | 26 | 10 | 0 | 2.309 | 0.021 | 0.0837 |
| 75vs100 | 34 | 21 | 0 | 2.558 | 0.011 | **0.0421** |

**Significant p-values in bold**